Inaugural-Dissertation zur Erlangung der Doktorwürde

der Tierärztlichen Fakultät

der Ludwig-Maximilians-Universität München

In vivo evaluation of polymeric nanocarriers for targeted gene delivery and novel strategies to overcome chemoresistance

von

Annika Herrmann

aus

Wangen im Allgäu

München 2015

Aus dem Veterinärwissenschaftlichen Department der Tierärztlichen Fakultät

der Ludwig-Maximilians-Universität München

Lehrstuhl für Molekulare Tierzucht und Biotechnologie

Arbeit angefertigt unter der Leitung von: Univ.-Prof. Dr. Eckhard Wolf

Angefertigt an: Fakultät für Chemie und Pharmazie, Lehrstuhl für Pharmazeutische Biotechnologie der Ludwig-Maximilians-Universität München

Mentor: Univ.-Prof. Dr. Ernst Wagner

Gedruckt mit der Genehmigung der Tierärztlichen Fakultät

der Ludwig-Maximilians-Universität München

Dekan:	Univ.-Prof. Dr. Joachim Braun
Berichterstatter:	Univ.-Prof. Dr. Eckhard Wolf
Korreferent:	Univ.-Prof. Dr. Hermann Ammer

Tag der Promotion: 31. Januar 2015

Meiner Familie

Table of contents

I. INTRODUCTION

Cancer is a main cause of disease provoking high morbidity and mortality worldwide. In 2012, 8.2 million cancer-related deaths and estimated 14.1 million new cases arose compared to 7.6 million and 12.7 million in 2008, respectively [1, 2], and the incidence of new cases is even predicted to increase to 22.2 million by 2030 [3]. Treatment options including chemotherapy, radiotherapy, surgery, immunotherapy or hormone therapy often have an insufficient success rate and side effects, therapy resistance and metastasis formation implicate an urgent improvement and further research in cancer therapy. Therefore, two fields of interest, tumor targeted gene delivery and chemoresistance, have been focused and are illustrated in the following.

1. Polymeric nucleic acid carriers for tumor targeted gene delivery

1.1. Nucleic acid therapy

Treatment of diseases caused by genetic alteration is made possible *via* gene therapy. Medicinal nucleic acids offer the possibility to manipulate gene expression in a controlled manner [4] in order to treat genetically-based diseases like monogenetic, infectious, cardiovascular, neurological, ocular and inflammatory disorders or cancer [5], whereas viral vectors have mainly been used as delivery vehicles. These agents can induce gene expression by plasmid DNA (pDNA) resulting in a "gain of function" or trigger gene silencing by antisense oligonucleotides or synthetic small interfering RNA (siRNA) mediating a "loss of function" [4]. Cancer diseases have been focused for gene therapy [5] whereas the major paths to achieve therapeutic effects are silencing of genes responsible for tumor growth, metastasis or cell survival and introduction of genes hampering cellular growth by apoptosis [6, 7]. Remarkable success has already been achieved with gene therapy of patients suffering from hemophilia B [8] or severe combined immunodeficiency (SCID) [9], yet it's still limited therapeutic use so far is based on the inefficient delivery of nucleic acids [10].

Application of naked nucleic acids without a carrier is only rarely effective such as upon intramuscular vaccination or hydrodynamic delivery of naked pDNA [11, 12]. After systemic application nucleic acids face many bottlenecks on the way towards their site of action. In the extracellular environment they have to be protected against enzymatic degradation by nucleases [13], complement activation and unspecific interactions with blood components and matrix

[14]. Once reaching the target tissue nucleic acids have to overcome the cell membrane being internalized into the endosomes [15]. Finally intracellular, they have to escape from the endosomes into the cytosol since these will change later into lysosomes where nucleic acid digestion takes place. siRNA is already on target in the cytosol by incorporation into the RNA-induced silencing complex (RISC) and hence, after separation of the strands, suppresses the gene expression by degrading or blocking translation of target mRNA [16]. For pDNA, further transport to the nucleus is required to mediate gene expression (Figure 1). This illustrates another bottleneck of plasmid delivery because the cellular actin cytoskeleton hinders the translocation of pDNA to the perinuclear region [17, 18]. Moreover, passive nuclear uptake can only occur during cell division in proliferating cells when the nuclear membrane is degraded. In non-dividing cells for particles larger than 9 nm, which therefore cannot pass the membrane *via* passive diffusion, an active nuclear import through the nuclear pore complex (NPC) is necessary which can be achieved with the help of short peptide sequences, called nuclear localization signals (NLS) [19, 20].

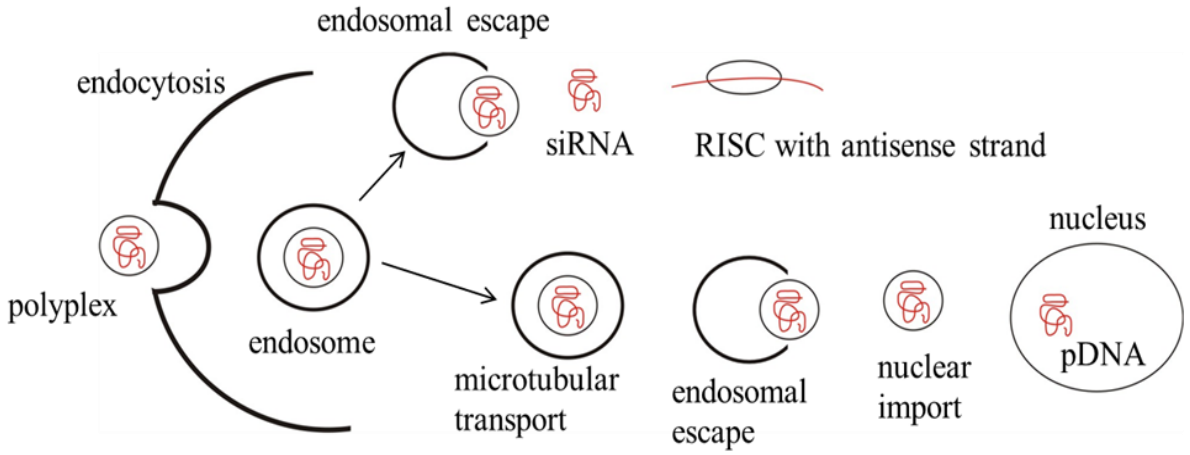

Figure 1: Steps of siRNA and pDNA delivery. Polyplexes are taken up into the tumor cell *via* endocytosis. After escaping the endosome siRNA is released into the cytosol and incorporated into the RISC complex. For successful gene expression from pDNA further transport to the perinuclear region and nuclear import of pDNA is essential.

1.2. Carrier systems for gene delivery

Carriers for gene delivery can generally be classified into viral and non-viral vectors [21]. Viral vectors randomly integrate into the genome and can therefore be used as delivery agents for therapeutic genes. However, their very high transfection efficacy is clouded by safety issues limiting therapeutic use. Viruses can have immunogenic and inflammatory effects hampering

repeated applications. Besides, limited payload capacity and difficulties to produce them in high amounts are further disadvantages of viruses [22]. To conquer these limitations synthetic non-viral carriers have attracted attention as a promising alternative. Carriers synthesized from various natural and synthetic molecules can be tailored to specific needs and mimic functions and surface domains of viruses to avoid unspecific biological interactions and mediate specific targeting of host cells [23]. Especially liposomes [24] and polymers [22, 25] have emerged as promising candidates for gene delivery. The negative charge of the nucleic acid backbone allows electrostatic interactions with the cationic liposomes or polymers which results in condensed complexes also called "lipoplexes" and "polyplexes" [26]. As a result of neutralizing the negative charges, DNA collapses into smaller structures than its free form which is up to µm large in size [27]. The condensation leads to small nanoparticles susceptible for endocytosis [28]. The most widely studied cationic polymers are polypeptides such as polylysine (PLL) [29] or polyethylenimine (PEI) [30, 31] and dendrimers like polyamidoamines (PAMAM) or polypropylenimine (PPI) [32]. Due to its high transfection efficacy based on its good endosomal buffering capacity to enhance endosomal escape, linear polyethylenimine (LPEI) has emerged as gold standard in gene delivery [33]. However, critical drawbacks of these polymers remain such as toxic side effects due to their high molecular weight and cationic charge and a lack of biodegradability [34-36]. Therefore, functional domains, e.g. for shielding, targeting and enhancing endosomal escape can be added to increase safety and transfection efficacy of the polyplexes [23].

1.3. Prospects of endosomal escape

Endosomal escape is a major obstacle in gene delivery. After internalization into endosomes polyplexes have to escape from them since these get acidified and change into lysosomes where degradation takes place. A way to overcome endosomal entrapment is the incorporation of lytic lipid domains such as oleic acids [37, 38], stearic acids [39-41] or cholesterol [42, 43] into the polymeric carrier resulting in hydrophobic interactions between endosomal membrane and polyplexes. Another approach is the incorporation of endosomolytic peptides like hemagglutinin HA2 deriving from the influenza virus [44] or melittin [45]. Cationic polymers such as PEI possess an intrinsic endosomolytic activity [46]. Their unprotonated amine groups can buffer protons which results in chloride and water accumulation in the endosomes leading to osmotic pressure. Triggered by the concomitant increase of positive polymer charges in the endosomes, vesicles lyse consequently and release their content into the cytosol providing an escape mechanism for polyplexes [47], also called "proton sponge effect" [48] with regard to

the absorption of protons like a sponge. Histidines are known to increase this effect because they become cationized upon protonation of their imidazole rings, thus enhancing endosomal buffering capacity. Therefore, the incorporation of histidines as functional domains can improve endosomal escape and hence transfection efficacy [49].

1.4. Targeting of polyplexes towards their site of action

To mediate specific cellular uptake polyplexes have to be directed towards the target tissue. This field of interest can be categorized into active and passive targeting. Passive targeting is occurring due to the enhanced permeability and retention (EPR) effect [50]. This effect is based on the limited blood supply of rapidly growing tumors and the resulting intense angiogenesis leading to fenestrated and leaky blood vessels with reduced lymphatic drainage [51]. Upon systemic administration small molecules can diffuse nonspecifically out of the blood stream into all tissues, whereas macromolecules only pass the leaky endothelium of the tumor and accumulate there due to impaired lymphatic drainage [50, 52]. The other strategy to address tumors is active targeting which is enabled by diverse expression levels of surface receptors in cancer tissues. Commonly addressed receptors are the transferrin receptor [53-56], integrin receptor [57-59], epidermal growth factor (EGF) receptor [60-63] or the folic acid (FA) receptor [64, 65]. Classes of targeting ligands that are able to bind to receptors are antibodies and their fragments [66, 67], glycoproteins [68], peptides [57, 69, 70] and small molecules [71] amongst others. The receptor reviewed in this thesis belongs to the cell surface receptor tyrosine kinases family - the hepatocyte growth factor receptor (HGFR) also named c-Met. It is predominantly expressed in epithelial cells [72] and overexpressed in cancer cells, epithelial-derived tumors and in stromal and interstitial cell-derived tumors like fibro- and other sarcoma types [73]. Upon binding of the natural ligand - hepatocyte growth factor (HGF) - to the receptor mitogenesis, motogenesis and morphogenesis are stimulated, and oncogenesis, tumor progression and aggressive cellular invasiveness are promoted. Possibilities to set anticancer drugs at this signaling pathway are antagonizing of ligand/receptor interactions, inhibition of tyrosine kinase activity and blocking of intracellular interactions [74]. Taking advantage of the c-Met/HGFR overexpression has mostly been limited for *in vivo* imaging and conjugation of an anti-c-Met antibody fragment to doxorubicin so far [75-78] but it has not been applied for targeted gene delivery.

1.5. Dendrimers

Compared to the gold standard in gene delivery, LPEI, with its inherent heterogeneity and cytotoxicity thus limiting its use, dendrimers can be denoted by an advance towards more defined polymers. Their central core molecule is an origin for highly branched symmetrical arms which are covalently coupled. Each additional layer (generation) is added stepwise resulting in a low polydispersity index and well defined size and structure [32]. As transfection efficacy and cytotoxicity of both PAMAM and PPI dendrimers still can be improved several modifications have been carried out for gene delivery such as targeting with folate [79], transferrin [80] and numerous other ligands, hydrophobic modifications with fatty acids [81, 82] or phenylalanine [83], cationization with arginine [84, 85] or histidinylation [86] for improved endosomal escape. Increased molecular weight (Mw) can on the one hand enhance transfection efficacy of the polymers based on low *in vivo* polyplex stability for low Mw compounds [87], but can on the other hand lead to increased cytotoxicity [88]. It is known that environment-triggered biodegradation can solve this problem [27, 89, 90]. The dendrimer reviewed in this thesis was hence built modifying the core of a PPI of the second generation (PPI G2) which has a lower cytotoxicity and moderate pDNA transfer efficacy [91]. An analog molecule to PEI based on the artificial amino acid succinoyl-tetraethylene pentamine (Stp) [92] consisting of increasing numbers of Stp units was attached as octamers *via* disulfide linkages to generate safe carriers with higher Mw (Figure 2).

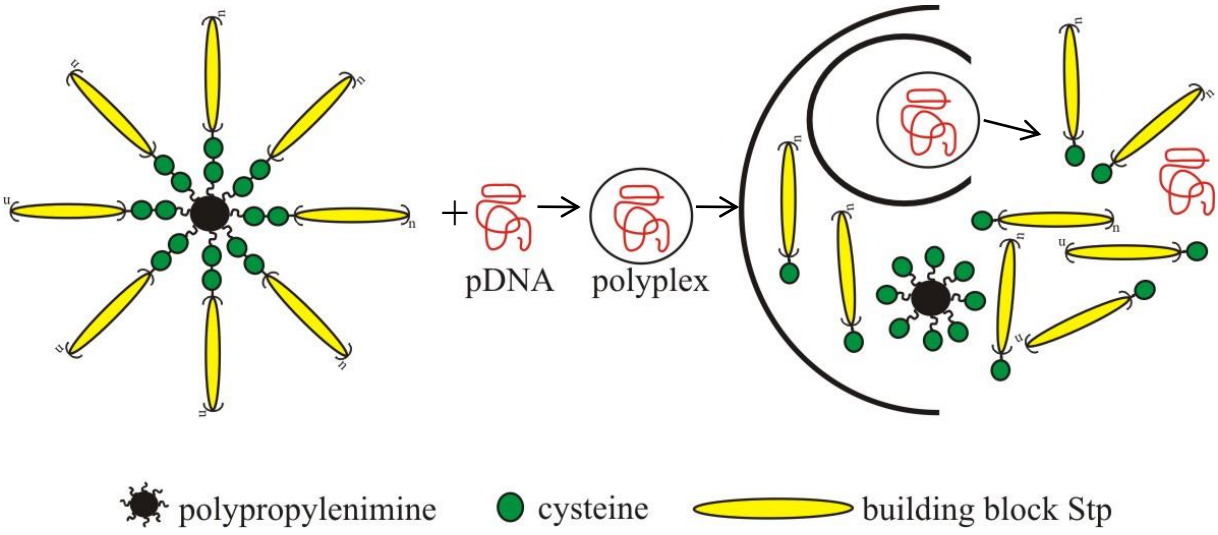

Figure 2: Schematic overview of PPI G2 core linked *via* disulfide linkages to Stp oligomers. Biodegradation takes place in the reducing cytosol environment.

1.6. Precise sequence-defined polymers

Another approach to develop a precise, monodisperse and multifunctional carrier system was illustrated by Hartmann *et al.* They designed well-defined polycationic conjugates with precisely positioned functional moieties for tailor-made features *via* solid-phase synthesis [93]. Schaffert *et al*. developed the method further by introducing novel building blocks [92]. A library of polymers with different topologies and functional domains was hence synthesized for gene delivery [94-97]. Polymers reviewed in this thesis were synthesized according to this method based on a polycationic backbone consisting of repeating units of the artificial amino acids Stp or succinoyl-pentaethylene hexamine (Sph) as building block. Cysteines were incorporated for redox-sensitive polyplex stabilization resulting from disulfide formation and histidines for increased endosomal buffering capacity. Polyethylene glycol (PEG) was attached for surface shielding from unwanted interactions with blood components and the ligand cMBP2 was attached for targeted polymers (Scheme 1).

2. Chemoresistance

Development of chemoresistance is a major drawback in the successful treatment of cancer patients hampering the efficacy of chemotherapeutic drugs. Treatment failure in more than 90% of metastatic cancer patients is believed to be induced by reason of chemoresistance [98]. Circumvention of drug resistance would therefore have a high impact on clinical outcome and survival of patients. On the one hand pharmacological factors such as inefficient tumor drug concentration and on the other hand cellular factors can account for the development of chemoresistance. Manifestation of resistance can be classified into intrinsic, hence existing before the first therapy, and acquired resistance which is developed during chemotherapeutic treatment. The diverse mechanisms leading to cellular resistance include increased drug efflux through ABC (ATP-binding cassette) drug transporters, alterations in drug targets and changes in cellular response such as enhanced repair mechanisms of DNA, stress toleration and evasion of apoptosis pathways [98-100]. Another important mechanism of resistance formation to chemotherapeutic drugs are cancer stem cells (CSCs). These cells within a tumor are protected from chemotherapeutic treatment by ABC transporters as well as to self-renew after chemotherapy and are therefore responsible for relapse [101, 102].

2.1. Metastasis formation and impact of miRNAs

Metastases at distant sites in the body are difficult to treat effectively and remain a major cause of death. Tumor spreading is propelled by a process called epithelial to mesenchymal transition (EMT), a developmental program leading to invasive and migratory properties of cancer cells which dissociate from the primary tumor, invade and exit blood vessels and subsequently cause metastases at distant tissues. For this purpose they undergo mesenchymal to epithelial transition (MET) and reshape into cells with epithelial-like properties [103-105].

microRNAs (miRNAs), small non-coding RNAs of about 22 nucleotide sequences regulating gene expression [106], are a class of molecules that are often up- or downregulated in several types of cancer [107-109]. Based on their target genes they can be classified into tumor suppressor and oncogenic miRNAs [108, 110]. They are known to play a role in the acquisition of chemoresistance as they can modulate the sensitivity of cancer cells upon chemotherapy [111-114]. Additionally, miR-200c has been proposed to regulate EMT through targeting repressors of E-cadherin, an epithelial marker [115, 116], resulting in an increased E-cadherin expression and low migratory capability of cancer cells hence displaying epithelial-like properties [117, 118]. The inhibition of EMT by miR-200c reduces cancer cell migration and invasion thus hampering metastasis formation [119-121]. On the contrary, a loss of miR-200c at the beginning of metastasis induces EMT which results in low E-cadherin and high vimentin levels hence displaying mesenchymal-like properties with an increased migratory capability of cancer cells [115-118, 120].

CSCs show characteristics of cells which have undergone EMT [103] and have also been proposed to be involved in tumor invasion and metastasis formation [101]. Hence, they display crucial targets in cancer therapy.

2.2. Salinomycin

The potassium-ionophore salinomycin (Figure 3) was recently found to selectively target CSCs and to reduce the proportion of CSCs in contrast to the classical chemotherapeutic drug paclitaxel [122]. Salinomycin is a polyether antibiotic isolated from the bacteria *Streptomyces albus* and has been used as an anticoccidial drug in poultry and other livestock [123, 124]. Its anti-cancer mechanisms in diverse cancer types known so far include induction of apoptosis and cell death, interference with ABC transporters and cytoplasmic or mitochondrial K^+ efflux, inhibition of Wnt signaling and oxidative phosphorylation, and differentiation of CSCs [125]. Besides, salinomycin has been proposed to reduce malignant traits in colorectal cancer cells [126] and to inhibit growth and migration of prostate cancer by inducing oxidative stress [127].

Of note, a few clinical pilot studies have shown a partial clinical regression of pretreated therapy-resistant cancers upon treatment with salinomycin [125] which is therefore very promising for further *in vivo* investigations.

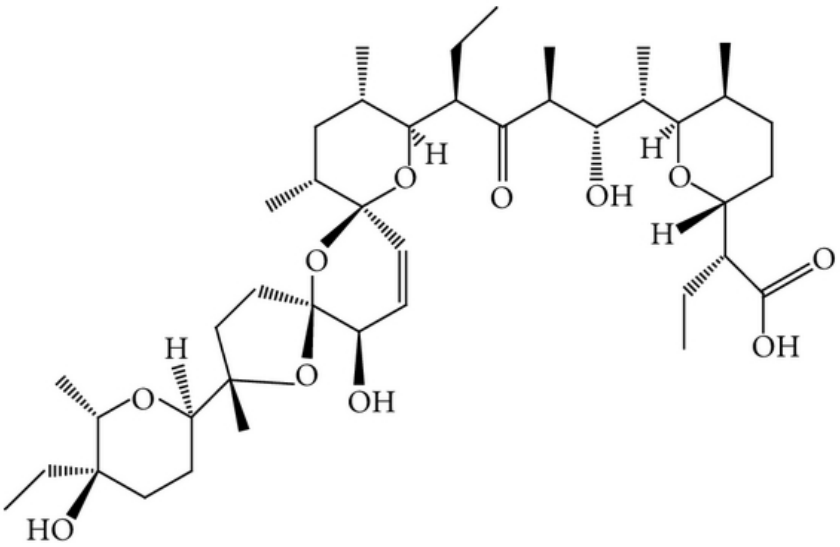

Figure 3: Structural formula of salinomycin.

2.3. Overcoming multiple drug resistance with nanocarriers

Multiple drug resistance (MDR) in cancer is one of the main reasons for chemotherapy failure. MDR is characterized by a broad cross-resistance of cancer cells to structurally different chemotherapeutics after acquiring resistance to an individual drug [128]. Potential mechanisms of MDR in chemotherapy include overexpression of ABC transporters which results in increased drug efflux, CSCs, miRNA regulation, hypoxia induction, efficient repair of DNA damage and epigenetic regulation such as DNA methylation and histone modification. One of the main mediators of MDR represents the overexpression of ABC drug transporters like the well-known permeability glycoprotein (P-glycoprotein), MDR-associated protein1 (MRP1) and breast cancer resistance protein (BCRP) [129]. Several approaches to circumvent MDR such as co-application of P-glycoprotein inhibitors (e.g. verapamil) display poor selectivity for cancer cells hence mediating low therapy efficacy and toxic side effects [130].

Nanoparticle-based drug delivery, a highly investigated field, offers beneficial options concerning specific targeting of cancer cells, increased drug efficacy, lower drug toxicity and improved solubility and stability. Moreover, the intracellular drug concentration in cancer cells is increased because nanosized particles can utilize the EPR effect [130]. Nanoparticles can be

categorized into (1) organic, (2) inorganic and (3) hybrid systems. Organic material systems (e.g. liposomes, emulsions, albumins, etc.) are situated already in clinical stage for cancer chemotherapy as delivery agents for original drugs through improvement of their bioavailability and targeting efficacy [131-133]. Inorganic nanobiomaterials (e.g. magnetic [134], metallic [135], carbon-based nanoparticles [136]) have gained increased attention due to their high thermal/chemical stability, good biocompatibility, resistance to corrosion and easy endowment with structural features and specific properties such as mesoporosity. Yet, a crucial issue to consider remains the low degradability of inorganic materials of which silica is one of the most biocompatible materials due to its endogenous occurrence in bones [131]. A core-shell silica nanoparticle encapsulating a fluorescent dye has already been approved by the FDA for a human stage I clinical trial for molecular imaging of cancer [137]. Organic-inorganic hybrid nanobiomaterials combine advantages of both organic and inorganic materials and can therefore have unique characteristics such as controlled drug release, co-delivery of multiple drugs, etc. [138, 139].

Mesoporous silica nanoparticles (MSN) have been highly investigated for improving chemotherapeutic efficacy, overcoming MDR and inhibiting metastasis formation. In terms of circumventing MDR several strategies have been recognized [140]. Multiple drugs can be co-loaded into MSN such as a classical chemotherapeutic drug together with an ABC transporter inhibitor (e.g. surfactants [141] or siRNA for gene silencing [142, 143]). Moreover, drug efflux can be circumvented by direct intranuclear drug delivery of MSN (e.g. using a cell-penetrating TAT peptide [144]) whereby ABC transporter inhibitors are no longer required. Additionally, a multi-modal combinatorial therapy with MSN combining chemo- with radiotherapy (e.g. MSN encapsulating chemo- and radiotherapeutic agents simultaneously [145]) illustrates another promising strategy.

2.4. Mesoporous silica nanoparticles with pH-responsive polymer coating

MSN display high loading capacity and enable a broad range of inner and outer surface modifications [146]. Several strategies to prevent premature release of MSN exist such as covalent attachment of cargo inside the mesopores [147] or capping of the whole particle [148-151]. Methods to promote drug release are e.g. light irradiation [147, 152, 153] and change of reduction potential [154], temperature [155], or pH [148, 156]. Polymers are highly attractive to coat MSN due to their biocompatibility and tunable properties [157, 158]. pH-responsive polymer coatings take advantage of the pH change during endocytosis as trigger for drug release. The ability of effective pH-responsive MSN coating using polymers was already

demonstrated for poly(acrylic acid) [159] and poly(2-(diethylamino)ethyl methacrylate) [160]. Furthermore, poly(2-vinylpyridine) (PVP) was applied for pH-sensitive functionalization based on the pronounced transition between hydrophobicity and hydrophilicity upon de-/protonation [161]. MSN reviewed in this chapter were functionalized with a pH-responsive cap system using the polymer PVP. At low pH the polymer is protonated and in a hydrophilic state enabling drug molecules to diffuse into and out of MSN. At pH values of 5.5 or higher the polymer is started to be deprotonated, thus converting into a hydrophobic state which results in a collapse of the polymer onto the surface preventing release of the drug molecules (Figure 4). Besides, PEG was attached to the ends of the PVP cap to increase colloidal stability. Furthermore, it enables covalent attachment of a wide variety of functionalities at the outer periphery of the PEG shell such as targeting ligands or dyes. The pores of MSN are about 4 nm and the average particle diameter is 90 nm for unfunctionalized MSN and 200 nm for PVP/PEG modified MSN (Stefan Niedermayer, PhD thesis 2014).

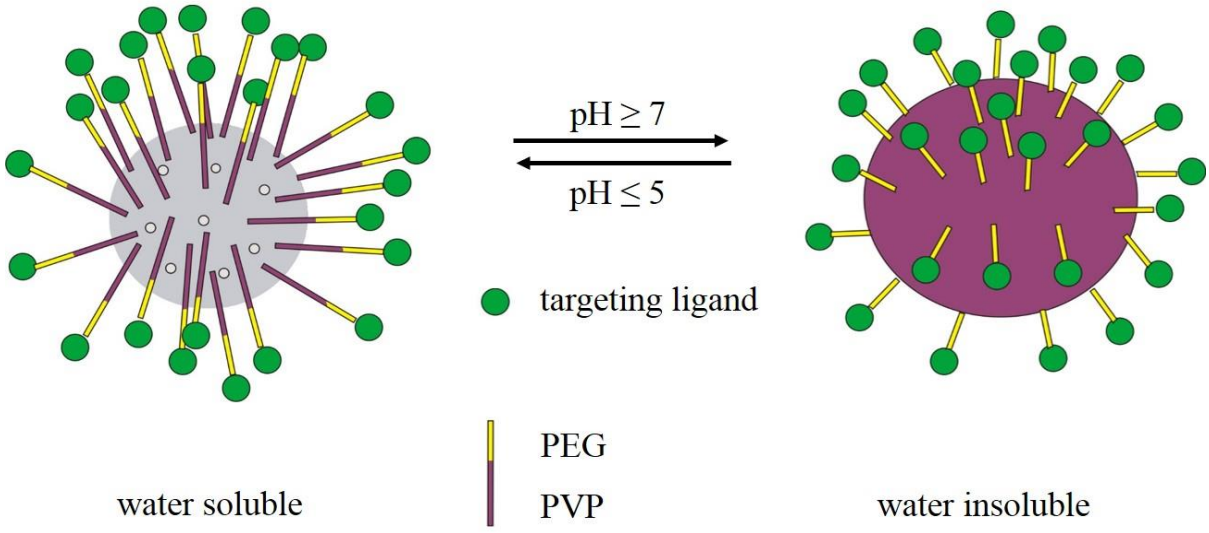

Figure 4: Concept of the pH-responsive polymer coating. The pores can be reversibly uncovered through changes in water solubility of the polymer upon de-/protonation.

3. Aims of the thesis

3.1. Polymeric nucleic acid carriers

The aim of this part of the thesis was to evaluate three synthesized polymeric systems, polypropylenimine (PPI) dendrimers, histidine-containing four-arm polymers and c-Met-directed structures for their gene transfer efficacy *in vivo*. Evaluation should be done in xenograft mouse tumor models by measurement of gene expression after local or systemic administration of pDNA polyplexes.

First, biodegradable polymers with increased molecular weight (Mw) should be compared to lower Mw PPI dendrimers as high Mw is generally associated with enhanced transfection efficacy.

Secondly, four-arm polymers containing histidines should be compared to alanine control polymers because the incorporation of histidines results in enhanced endosomal buffer capacity facilitating endosomal escape, a major bottleneck in gene delivery.

Thirdly, polymers targeted with the c-Met receptor-binding ligand cMBP2 should be evaluated and compared to an alanine control polymer upon local and systemic administration. Additionally, the impact of an enhanced shielding, an increased polycationic part of the polymer and co-addition of non-shielded polymers to improve systemic delivery were to be assessed.

3.2. Chemoresistance

The acquisition of chemoresistance upon treatment with classical anti-cancer drugs and formation of metastasis to secondary tissues still display major drawbacks for the cure of cancer patients. In this part of the thesis two approaches to circumvent these obstacles should be investigated.

First, the polyether antibiotic drug salinomycin, which has been demonstrated to selectively target cancer stem cells and which has therefore been promising to improve cancer therapy, should be analyzed concerning its effect on tumor growth and migration. In a next step, if effective, it was purposed to evaluate its potential as an additive compound to a classical chemotherapeutic drug.

Secondly, loading of chemotherapeutic drugs into nanoparticles has raised hope for improving chemotherapeutic efficacy, overcoming drug resistance and metastasis formation. Since the controlled release displays a critical obstacle in delivery of drugs, synthesized pH-responsive coated mesoporous nanoparticles should be evaluated in terms of biodistribution, biocompatibility and tumor targeting *in vivo*.

II. MATERIALS AND METHODS

1. Materials

1.1. Cell culture

Neuro2A	ATCC (Wesel, Germany)
HuH7 cells	NIBIO (Osaka, Japan) (formerly HSRRB)
4T1-Luc cells	Caliper Life Sciences (Alameda, CA, USA)
MDA MB 231 cells	ATCC (Wesel, Germany)
KB cells	ATCC (Wesel, Germany)
DMEM 1 g/l Glucose medium	Invitrogen (Karlsruhe, Germany)
DMEM 4.5 g/l Glucose medium	Invitrogen (Karlsruhe, Germany)
Ham`s F12 medium	Invitrogen (Karlsruhe, Germany)
RPMI 1640 medium	Invitrogen (Karlsruhe, Germany)
FCS (fetal calf serum)	Invitrogen (Karlsruhe, Germany)
L-alanyl-L-glutamine	Biochrom (Berlin, Germany)
PBS (phosphate buffered saline)	Biochrom (Berlin, Germany)
Trypsin EDTA solution	Biochrom (Berlin, Germany)
Cell culture plates and flasks	TPP (Trasadingen, Switzerland)

1.2. *In vivo* experiments

Isoflurane CP®	CP-Pharma (Burgdorf, Germany)
Bepanthen®	Bayer Vital GmbH (Leverkusen, Germany)
Na-luciferin	Promega (Mannheim, Germany)
Syringes, needles	BD Medical (Heidelberg, Germany)
Multivette (serum tubes)	Sarstedt (Nümbrecht, Germany)
NaCl 0.9 % (isotonic sodiumchloride)	Braun Melsungen AG (Melsungen, Germany)
HBG (HEPES buffered 5% glucose, pH 7.4)	HEPES: Biomol (Hamburg, Germany) Glucose-monohydrate: Merck (Darmstadt, Germany)
Matrigel® Matrix (356231)	Fisher Scientific GmbH (Schwerte, Germany)

1.3. Laboratory animals

1.3.1. NMRI nude mice

Female Rj:NMRI-Foxn1^{nu}/Foxn1^{nu} mice were purchased from Janvier (Le Genest-St-Isle, France). This outbred mouse strain has a mutation in the gene Foxn1 which is affecting thymus development and hair follicle keratinization. Due to the absence of T-lymphocytes mice are immunodeficient and hence used for xenotransplantation. Other immune system cells like B-cells, NK-cells and Macrophages are present. Nudeness enables an ideal experimental setup for bioimaging studies.

1.3.2. BALB/c mice

Female BALB/cByJRj mice were purchased from Janvier (Le Genest-St-Isle, France). These small inbred albino mice are immunocompetent and therefore used in a syngeneic 4T1-tumor model. Furthermore they were used as sentinel animals for health monitoring of the animal facility.

1.3.3. Housing

Laboratory mice were housed inside an air-conditioned room in individually ventilated cages (IVC type II long, Tecniplast) within a 12 h-day-and-night cycle. The maximum occupancy was 5 animals per cage with autoclaved food and water *ad libitum* and weekly change of the bedding. Mice were purchased at an age of 5 weeks and allowed an acclimatization time of at least one week to adapt to the housing conditions. Health monitoring of the animal facility was conducted quarterly according to FELASA recommendations.

All animal experiments were performed according to the guidelines of the German law for protection of animal life. They were approved by the local ethics committee.

1.4. *Ex vivo* experiments

Cell lysis buffer	Promega (Mannheim, Germany)
Lysing Matrix D	MP Biomedicals (Strasbourg, France)
Luciferase assay buffer	Promega (Mannheim, Germany)
Mayer´s haematoxylin solution	Sigma-Aldrich (Steinheim, Germany)
Eosin Y	Sigma-Aldrich (Steinheim, Germany)
Tissue-Tek® Cryomold	Sakura Finetek (Heppenheim, Germany)
Tissue-Tek® O.C.T. Compound	Sakura Finetek (Heppenheim, Germany)
Tissue-Tek® Mega-Cassette	Sakura Finetek (Heppenheim, Germany)

SuperFrost Ultra Plus® slides	Menzel GmbH (Braunschweig, Germany)
DAPI	Sigma-Aldrich (Steinheim, Germany)

1.5. Polymers

PPI conjugates were synthesized by Edith Salcher (PhD thesis 2013, LMU).

Conjugate (Polymer ID)	Sequence	Abbreviation
536	PPI-(C-C-Stp5)8	PPI-Stp5
PPI G2	PPI	-

Three-arm, four-arm and cMBP2-targeted polymers were synthesized by Ulrich Lächelt and Dongsheng He (PhD students, LMU Pharmaceutical Biotechnology).

Conjugate (Polymer ID)	Sequence	Topology
608	AK[AK(A-Sph-A-Sph-A-Sph-AC)2]2	Four-arm; w/o His
606	AK[HK(H-Sph-H-Sph-H-Sph-HC)2]2	Four-arm; with His
442	K[dPEG$_{24}$-HK[H-(Stp-H)$_4$-C]$_2$]-cMBP2	Two-arm; 1 PEG
440	A-dPEG$_{24}$-HK[H-(Stp-H)$_4$-C]$_2$	Two-arm; 1 PEG
694	K[(dPEG$_{24}$)$_2$-HK[H-(Stp-H)$_4$-C]$_2$]-cMBP2	Two-arm; 2 PEG
616	A-(dPEG$_{24}$)$_2$-HK[H-(Stp-H)$_4$-C]$_2$	Two-arm; 2 PEG
677	K[dPEG$_{24}$-K(HK(H-(Sph-H)$_3$-C)$_2$)$_2$]-cMBP2	Four-arm; 1 PEG
678	A-dPEG$_{24}$-K[HK(H-(Sph-H)$_3$-C)$_2$]$_2$	Four-arm; 1 PEG
689	C-H-(Stp-H)$_3$-K-[(H-Stp)$_3$-H-C]$_2$	Three-arm; with His

608/SPH-AC **I)**

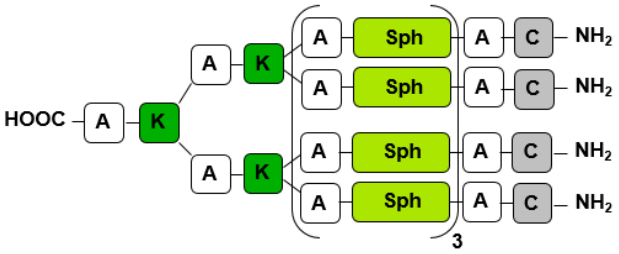

606/SPH-HC **II)**

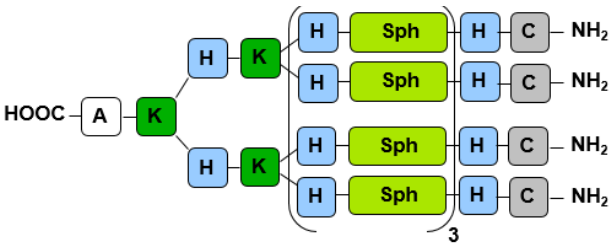

442/cMBP2-1PEG/
440/Ala-1PEG **III)**

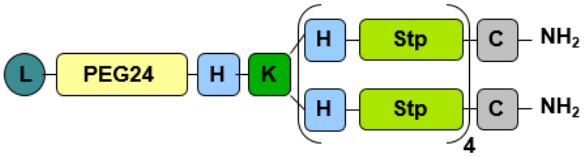

694/cMBP2-2PEG/
616/Ala-2PEG **IV)**

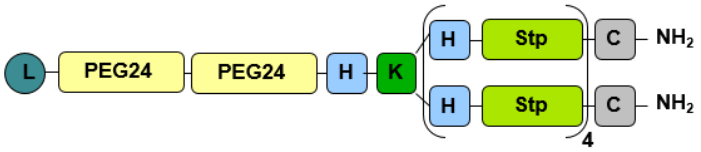

677/cMBP2-1PEG/
678/Ala-1PEG **V)**

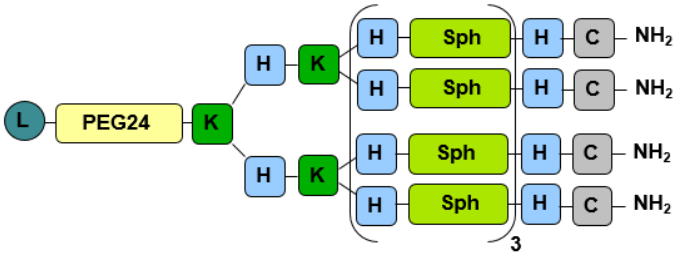

689 **VI)**

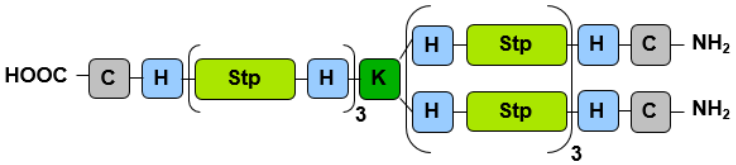

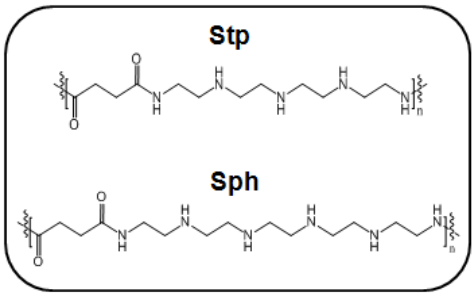

Scheme 1: Schematic overview of the synthesized polymers. A: alanine; K: lysine; H: histidine and C: cysteine represent the α-amino acids in a one-letter-code; L: targeting ligand cMBP2 or the corresponding control alanine.

1.6. pDNA

pCMVLuc	Plasmid Factory (Bielefeld, Germany)

1.7. Chemotherapeutics

Doxorubicin hydrochloride (D1515)	Sigma-Aldrich (Schnelldorf, Germany)
Salinomycin (S6201)	Sigma-Aldrich (Schnelldorf, Germany)

1.8. Mesoporous silica nanoparticles

Mesoporous silica nanoparticles (MSN) were synthesized by Stefan Niedermayer (PhD thesis 2014, LMU) and Stefan Datz (PhD student, LMU Physical Chemistry), both from the group of Prof. Dr. Thomas Bein.

The following types of MSN were applied:

MSN-NH_2

MSN-PVP-PEG-NH_2

MSN-PVP-PEG-NH_2-FA

Cy7 (Cyanine 7 NHS-ester/maleimide)	Lumiprobe, (Hannover, Germany)
ATTO 633 maleimide	ATTO-TEC GmbH (Siegen, Germany)
Calcein	Sigma-Aldrich (Schnelldorf, Germany)

1.9. Instruments

FastPrep®-24 instrument	MP Biomedicals (Solon, USA)
Centro LB 960 luminometer	Berthold Technologies (Bad Wildbad, Germany)
Cordless animal shaver GT 420 ISIS	Aesculap Suhl GmbH (Suhl, Germany)
Caliper DIGI-Met	Preisser (Gammertingen, Germany)
IVIS Lumina	Caliper Life Science (Rüsselsheim, Germany)
Tissue embedding Leica EG1150	Leica Microsystems GmbH (Wetzlar, Germany)
Microtome Leica RM2265	Leica Microsystems GmbH (Wetzlar, Germany)
Paraffin floating bath	MEDAX GmbH & Co. KG (Neumünster, Germany)
Cryostat Leica CM3050 S	Leica Microsystems GmbH (Wetzlar, Germany)
Olympus BX41	Olympus (Hamburg, Germany)
Zeiss Cell Observer SD	Carl Zeiss AG (Göttingen, Germany)

1.10. Software

Graph Pad Prism 5 software	Graph Pad Software (San Diego, USA)
Living Image 3.2	Caliper Life Science (Rüsselsheim, Germany)

2. Methods

2.1. Cell culture

Mouse neuroblastoma cells (Neuro2A) were cultured in Dulbecco´s modified Eagle´s medium (DMEM 1 g/l Glucose). Human hepatocellular carcinoma cells (Huh7) were grown in a 1:1 mixture of Dulbecco´s modified Eagle´s medium and Ham´s F12 medium. Stably luciferase expressing murine breast adenocarcinoma cells (4T1-Luc) were cultured in RPMI 1640 medium. Human breast adenocarcinoma cells (MDA-MB-231) were grown in Dulbecco´s modified Eagle´s medium (DMEM 4.5 g/l Glucose) and human cervix carcinoma cells (KB) were cultured in RPMI 1640 folate free medium at 37 °C in 5 % CO_2 humidified atmosphere. All media were supplemented with 10 % fetal calf serum (FCS) and 4 mM stable glutamine.

2.2. *In vivo* experiments

Laboratory mice were purchased at an age of five weeks and experiments were carried out at 6-8 weeks old mice. Tumor cells for all *in vivo* experiments were cultured as described above. In order to harvest the cells, they were peeled off using trypsin/EDTA solution which was subsequently inactivated with medium. Cells were centrifuged at 1000 rpm for 5 minutes and the cell pellet was resuspended in PBS at the desired final concentration. For experiments using Matrigel® matrix for propagation of human tumors, cells were also resuspended in PBS but diluted with Matrigel® (1:1) prior to injection. Subcutaneous inoculations of cells were carried out with a 1 ml syringe with a 27 gauge needle. Intraperitoneal applications required a 1 ml syringe with a 29 gauge needle and for intravenous and intratumoral injections an insulin syringe (29 gauge) was used. Tumor growth and body weight were monitored every second or third day. Inhalation anesthesia was performed with 2.5 % isoflurane in oxygen and eye lube (Bepanthen®) was used to prevent drying out the cornea.

2.2.1. Systemic luciferase gene transfer with polypropylenimine dendrimers

Neuro2A cells (5 x 10^6 per mouse) in 150 µl PBS were injected subcutaneously into the left flank of 8 female NMRI nude mice. On day 12, after tumor cell inoculation, mice were divided into two groups (n = 4) and polyplex solution was injected into the tail vein. The polyplex solution contained 60 µg pCMVLuc (around 2.5 µg/g body weight) complexed with either **536**/PPI-Stp5 or PPI G2 at N/P (protonatable nitrogens of oligomer/phosphate in the nucleic acid backbone) ratio of 12 in a total volume of 200 µl HBG. After 48 hours all mice were euthanized by cervical dislocation, tumors and organs (lung and liver) were collected and homogenized in cell culture lysis buffer using a tissue and cell homogenizer (FastPrep®-24). The samples were subsequently centrifuged at 3000 g at 4 °C for 10 minutes to separate insoluble cell components. Luciferase activity was determined in the supernatant using a Centro LB 960 luminometer.

2.2.2. Systemic luciferase gene transfer with four-arm polymers with and without histidines

Neuro2A cells (5 x 10^6 per mouse) in 150 µl PBS were injected subcutaneously into the left flank of 10 female NMRI nude mice. On day 12, after tumor cell inoculation, mice were divided into two groups (n = 5) and injected with polyplex solution into the tail vein. The polyplex solution contained 60 µg pCMVLuc (around 2.5 µg/g body weight) complexed with either **608**/SPH-AC or **606**/SPH-HC at N/P 12 in a total volume of 200 µl HBG. After 48 hours all mice were euthanized by cervical dislocation and tumors and organs (lung, liver, spleen, kidney and heart) were collected. Sample preparation was carried out as stated above.

2.2.3. Intratumoral luciferase gene transfer with two-arm c-Met-directed polymers

Huh7 cells (5 x 10^6 per mouse) in 150 µl PBS were inoculated subcutaneously into the left flank of 20 female NMRI nude mice. Approximately 12 days after tumor cell implantation, when tumors reached the adequate size (about 500-700 mm^3), mice were divided into four groups (n = 5), anesthetized with isoflurane and injected with polyplex solution intratumorally. The polyplex solution contained 50 µg pCMVLuc (around 2.5 µg/g body weight) complexed with either two-arm polymer **442**/cMBP2-1PEG, **440**/Ala-1PEG, **694**/cMBP2-2PEG or **616**/Ala-2PEG at N/P 12 in a total volume of 60 µl HBG. After 24 hours all mice were euthanized by

cervical dislocation and tumors were dissected. Sample preparation was carried out as stated above.

2.2.4. Fluorescence imaging after local polyplex administration

Huh7 cells (5 x 10^6 per mouse) in 150 µl PBS were inoculated subcutaneously into the left flank of 4 female NMRI nude mice. Two weeks after tumor cell implantation mice were divided into two groups (n = 2), anesthetized with isoflurane and injected with polyplex solution intratumorally. The polyplex solution contained 50 µg pCMVLuc (20 % labeled with Cy7) complexed with either targeted (**442**/cMBP2-1PEG) or untargeted (**440**/Ala-1PEG) polymers at N/P 12 in a total volume of 60 µl HBG. Near infrared (NIR) fluorescence was measured by a charge-coupled device (CCD) camera immediately after polyplex injection and repeated after 0.25, 0.5, 4, 48 and 72 hours. Efficiency of the fluorescence signals was presented for evaluation with equalized color bar scales for each group. Pictures were taken with medium binning and an exposure time of 30 seconds.

2.2.5. Systemic luciferase gene transfer of initial and modified c-Met-directed polymers

Huh7 cells (5 x 10^6 per mouse) in 150 µl PBS were inoculated subcutaneously into the left flank of 40 female NMRI nude mice. Approximately 12 days after tumor cell implantation, when tumors reached the adequate size (about 500-700 mm^3), mice were divided into eight groups (n = 5) and polyplex solution was injected into the tail vein. The polyplex solution contained 80 µg pCMVLuc (around 4 µg/g body weight) at N/P 12 in a total volume of 200 µl HBG. For this purpose initial two-arm polymers **442**/cMBP2-1PEG and **440**/Ala-1PEG; four-arm polymers **677**/cMBP2-1PEG and **678**/Ala-1PEG and mixtures of the initial two-arm polymers with three-arm **689** or four-arm **606**/SPH-HC were used. After 48 hours all mice were euthanized by cervical dislocation and tumors and organs were dissected. Sample preparation was carried out as stated above.

Quantification by real-time PCR (RT-PCR) was carried out to determine residual amounts of pDNA in tumors. Polyplex solution was injected as described above and mice (n = 3) were sacrificed after 4 hours. Total DNA was isolated according to manufacturer's instructions using peqGOLD guanidinisothiocynate/phenol method (Peqlab, Germany). Quantitative RT-PCR was then performed on a LightCycler 480 system (Roche) using UPL Probe #84 (Roche) and Probes Master (Roche). The following primer sequences were used: reverse primer 5'-CCC CGT AGA AAA GAT CAA AGG-3' and forward primer 5'-GCT GGT AGC GGT GGT TTT

T-3'. The pDNA dilution series were run in parallel to allow the absolute quantification. RT-PCR was performed by Petra Kos (PhD student, LMU Pharmaceutical Biotechnology).

2.2.6. Preliminary dose-finding of doxorubicin

Regarding the effect of doxorubicin on tumor growth and metastasis of 4T1-Luc tumors different dosages were evaluated. Mice were locally shaved and 4T1-Luc cells (1 x 10^6 per mouse) in 50 µl PBS were inoculated into the left next to the last caudal mammary fat pad of 12 female BALB/c mice. 24 hours later mice were randomly divided into four groups (n = 3) and treated with doxorubicin (2 mg/kg, 5 mg/kg and 8 mg/kg) or control (NaCl 0.9 %) every six days for three times. Body weight and tumor growth were determined every second or third day during the experiment. On day 18, after tumor cell inoculation, two mice treated with 8 mg/kg doxorubicin had to be euthanized due to severe weight loss (the third mouse of this group already on day 7). Before euthanasia bioluminescence imaging was performed as described for the other groups. On day 22 the remaining three groups were anesthetized with 2.5 % isoflurane in oxygen and 6 mg Na-luciferin in 100 µl PBS were injected intraperitoneally. After 15 minutes of distribution all mice were euthanized through cervical dislocation, lungs were dissected and bioluminescence imaging was performed by a CCD camera (IVIS Lumina system) with Living Image software 3.2. Photon emission of isolated lungs was measured and images were interpreted with equalized color bar scales. Regions of Interest (ROIs) were defined for quantification and were calculated as photons/second/cm^2 (total flux/area). Bioluminescence imaging was performed with an exposure time of 10 seconds and medium binning.

2.2.7. Effect of salinomycin on tumor growth rate

For evaluating the effect of salinomycin on tumor growth the syngeneic 4T1-Luc mouse model was used in BALB/c mice. Mice were locally shaved and 4T1-Luc cells (2 x 10^6 per mouse) in 150 µl PBS were inoculated subcutaneously into the left flank of 18 female BALB/c mice. Three days after tumor cell injection mice were randomly divided into one treatment (n = 9) and one control group (n = 9). Mice were treated with 5 mg/kg salinomycin (2 mg/ml in dimethyl sulfoxide (DMSO) stock solution was diluted in phosphate buffered saline), control mice were treated with DMSO in phosphate buffered saline. Treatment was carried out on day 3, 6, 8, 10, 13 and 15 after tumor cell inoculation. Tumor growth was measured on day 2, 4, 6, 9, 13 and 17, after tumor cell inoculation, with a caliper using formula a x $b^2/2$ (a = longest side of the tumor; b = widest side vertical to a). Over a period of 17 days the average tumor volumes

of the two groups were compared. On day 17 all mice were euthanized through cervical dislocation and tumors were harvested.

2.2.8. Effect of salinomycin on tumor colonization and migration

The effect of salinomycin on tumor colonization was tested in the syngeneic 4T1-Luc mouse model. 20 female BALB/c mice were randomly divided into two groups (treatment and control) and 4T1-Luc cells (1 x 10^5 per mouse) were injected intravenously *via* tail vein. 24 and 0.5 hours before tumor cell inoculation the treatment group was premedicated intraperitoneally with 5 mg/kg salinomycin (2 mg/ml in DMSO stock solution was diluted in phosphate buffered saline) and the control group with DMSO in phosphate buffered saline. Treatment was repeated on day 3, 6 and 9, after tumor cell injection, and tumor colonization was monitored *via* bioluminescence imaging on day 3, 8 and 13. For this purpose, mice were anesthetized with 2.5 % isoflurane in oxygen and 6 mg Na-luciferin in 100 µl PBS were injected intraperitoneally. After 15 minutes of distribution bioluminescence imaging of anesthetized mice was performed by a CCD camera (IVIS Lumina system) with Living Image software 3.2. Lungs were defined as ROI for quantification and photon emission was calculated as photons/second/cm^2 (total flux/area). Images were interpreted with equalized color bar scales. Bioluminescence imaging was performed with an exposure time of 5 seconds and medium binning. On day 13 mice were euthanized after bioluminescence imaging and organs (lung, brain, spleen, kidneys and liver) were dissected for subsequent *ex vivo* luciferase measurements. Sample preparation was carried out as stated above. One mouse of the control group had to be sacrificed already earlier due to severe medical condition.

2.2.9. Combinatorial treatment of doxorubicin and salinomycin

Regarding the combinatorial effect on tumor growth and metastasis, treatment with doxorubicin and salinomycin was evaluated within one trial in the syngeneic 4T1-Luc mouse model. 4T1-Luc cells (1 x 10^6 per mouse) in 50 µl PBS were inoculated into the left next to last caudal mammary fat pad of 40 female BALB/c mice. 24 hours later mice were randomly divided into four groups (n = 10). The first, the control group, received weekly intravenous injections of 0.9 % NaCl and intraperitoneal injections of DMSO in phosphate buffered saline at the same intervals as the group treated with salinomycin. The second group was weekly treated intravenously with 3.5 mg/kg doxorubicin for three weeks, the third group received 5 mg/kg salinomycin intraperitoneally twice a week on day 4, 6, 11, 13, 18 and 20 and the fourth group was treated with 3.5 mg/kg doxorubicin plus 5 mg/kg salinomycin at the same intervals as

indicated above. Body weight and tumor growth were determined every second or third day. On day 21, after tumor cell inoculation, mice were anesthetized with 2.5 % isoflurane in oxygen and 6 mg Na-luciferin in 100 µl PBS were injected intraperitoneally. After 15 minutes of distribution all mice were euthanized through cervical dislocation, lungs were dissected and bioluminescence imaging was performed by a CCD camera (IVIS Lumina system) with Living Image software 3.2. Photon emission of the isolated lungs was measured and images were interpreted with equalized color bar scales. ROIs were defined for quantification and were calculated as photons/second/cm^2 (total flux/area). Bioluminescence imaging was performed with an exposure time of 10 seconds and medium binning. Tumors and organs were harvested.

2.2.10. Systemic distribution of mesoporous nanoparticles (MSN)

Tumor free NMRI nude mice were anesthetized with 2.5 % isoflurane in oxygen and injected intravenously into the tail vein with a 100 µg (5 mg/kg) dose of Cy7-labeled (covalently linked to amino groups on the surface of MSN) or Cy7-loaded (covalently linked to the inner surface of MSN) functionalized MSN-PVP-PEG-NH_2-FA or unfunctionalized MSN-NH_2 dispersed in 100 µl HEPES buffered glucose (HBG). NIR fluorescence was measured by a CCD camera immediately after injection and was repeated after 0.25, 0.5, 1, 4, 24 and 48 hours. Each trial was performed with three animals per group. Efficiency of the fluorescence signals was presented for evaluation with equalized color bar scales for each group. Pictures were taken with medium binning and an exposure time of 30 seconds.

2.2.11. Clinical chemistry and histopathology after systemic injection of MSN

Tumor free NMRI nude mice (n = 9) were sacrificed through cervical dislocation 48 hours after intravenous injection of pure HBG or a 100 µg (5 mg/kg) dose of functionalized MSN-PVP-PEG-NH_2-FA or unfunctionalized MSN-NH_2 dispersed in 100 µl HBG. Blood was collected in serum tubes and clinical chemistry parameters (alanine transaminase/aspartate transaminase, creatinine levels and blood urea nitrogen) were analyzed. Organs were dissected, fixed in formalin and embedded into paraffin. Organs were cut with a microtome into 4.5 µm slices and stained with eosin and haematoxylin. Results were documented using an Olympus BX41 microscope.

For biocompatibility experiments with increased dosages of MSN, tumor free NMRI nude mice (n = 8) were divided into four groups and injected intravenously with a 1.6 mg (80 mg/kg) or 2

mg (100 mg/kg) dose of functionalized (MSN-PVP-PEG-NH_2-FA) and unfunctionalized (MSN-NH_2) particles. Intravenous administration of MSN was repeated after seven days.

2.2.12. Tumor-targeting after systemic administration of MSN

MDA MB 231 cells (5 x 10^6 per mouse) resuspended in PBS but diluted with Matrigel® (1:1) prior to injection were inoculated subcutaneously into the left flank of 9 female NMRI nude mice. On day 42, after tumor cell implantation, mice were randomly divided into three groups (n = 3) and injected intravenously *via* tail vein with a 100 µg (5 mg/kg) dose of untargeted (MSN-PVP-PEG-NH_2) and folic acid (FA) targeted (MSN-PVP-PEG-NH_2-FA) particles loaded with fluorescent dyes (calcein and covalently linked ATTO 633) dispersed in 100 µl HBG or pure HBG. Mice were sacrificed by cervical dislocation 3 hours after injection, tumors and organs (liver, spleen, kidneys and lungs) were harvested, embedded into TissueTek™ and stored immediately at -20 °C. For preparation of cryosections with a thickness of 5 µm a Leica cryotom was used. Cryosections were dried and fixed with 4 % paraformaldehyde. Nuclei were counterstained with DAPI and results were documented *via* spinning disc microscopy with a Zeiss Cell Observer SD microscope.

2.2.13. Retention of MSN in subcutaneous tumors

KB cells (5 x 10^6 per mouse) in 150 µl PBS were inoculated subcutaneously into the nape of 6 female NMRI nude mice. On day 14, after tumor cell implantation, mice were randomly divided into two groups (n = 3) and injected intratumorally with a 100 µg (5 mg/kg) dose of Cy7-labeled functionalized FA targeted (MSN-PVP-PEG-NH_2-FA) and untargeted (MSN-PVP-PEG-NH_2) MSN dispersed in 50 µl HBG into anesthetized mice. NIR fluorescence was measured by a CCD camera immediately after injection and repeated after 0.25, 0.5, 1, 4, 24, 48, 72, 96, 120, 144 and 168 hours. Fluorescence signals of the tumors were counted as total flux/area and normalized to 0 minutes. Efficiency of the fluorescent signals was presented for evaluation with equalized color bar scales for each group. Pictures were taken with medium binning and an exposure time of 30 seconds.

2.3. Statistical analysis

Results are expressed as mean value ± S.E.M if not indicated elsewise. Statistical analysis was performed with t-test using GraphPadPrism™. P-values < 0.05 were considered as significant.

III. RESULTS

1. Polymeric nucleic acid carriers for tumor targeted gene delivery

Three different polymeric systems, polypropylenimine dendrimers, histidine-containing four-arm polymers and c-Met-directed structures were analyzed for gene transfer *in vivo*. Experiments were performed with Petra Kos (PhD thesis 2014, LMU) in NMRI nude mice.

1.1. *In vivo* characterization of polypropylenimine dendrimers

The polypropylenimine (PPI) core was modified with increasing units (1 - 5 units) of small sequence-defined oligomers based on the oligoamino acid succinoyl-tetraethylene pentamine (Stp). Unmodified low toxic PPI of the second generation (PPI G2) served as a control. pDNA encoding for firefly luciferase was used for transfections to allow measurement of transgene expression *via* bioluminescence. First, *in vitro* transfection efficacy of all synthesized polypropylenimine dendrimers was screened on Neuro2A cells (murine neuroblastoma). Figure 5 shows the efficacy of dendrimers containing increasing numbers of Stp units. Especially PPI conjugates with 3 to 5 repeating Stp units revealed the highest luciferase gene expression with similar levels as the "gold standard" LPEI. In comparison, unmodified PPI G2 showed only moderate efficacy (around 1 log unit below LPEI). According to these results and to its good pDNA binding ability, low cytotoxicity and high endosomal buffering capacity (Petra Kos, PhD thesis 2014, LMU), **536**/PPI-Stp5 was chosen for further *in vivo* characterization.

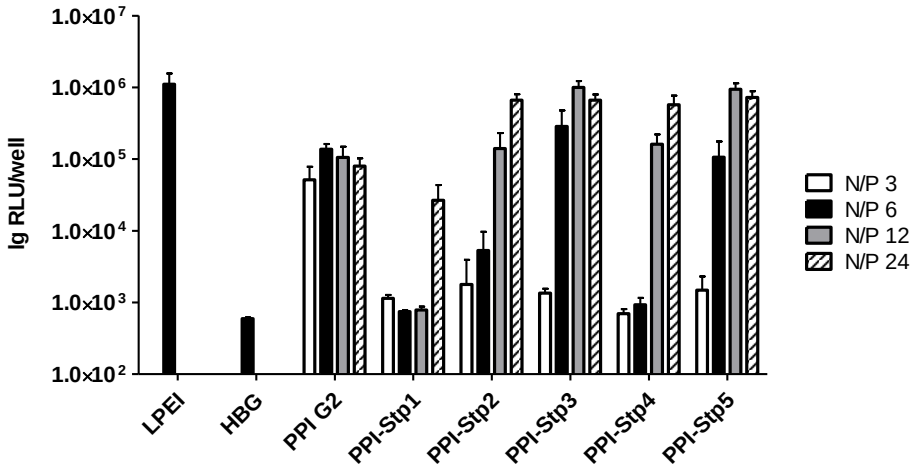

Figure 5: Luciferase gene transfer of polypropylenimine dendrimers with increasing numbers of Stp units at different N/P ratios. The luciferase activity in the cell lysates was analyzed 24 hours after transfection. LPEI was used as a positive control, HBG buffer treated cells served as a background. Data are presented as mean values ± S.D. out of quintuplicate. Data were generated by Petra Kos (PhD thesis 2014, LMU).

To analyze and compare the gene transfer efficacy *in vivo*, **536**/PPI-Stp5 and PPI G2 pDNA polyplexes at N/P 12 containing 60 µg pCMVLuc were injected intravenously in a total volume of 200 µl HBG into the tail vain of mice bearing subcutaneous Neuro2A tumors. After 48 hours mice were sacrificed, tumors and organs (lung and liver) were collected, homogenized in cell culture lysis buffer and subsequently centrifuged. Luciferase activity determined in the supernatant revealed a significant gene expression in tumor, lung and liver (Figure 6). **536**/PPI-Stp5 polyplexes led to a significantly higher gene transfer in Neuro2A tumors compared to PPI G2 polyplexes. In contrast, **536**/PPI-Stp5 polyplexes showed lower luciferase expression in lung and liver than PPI G2 polyplexes.

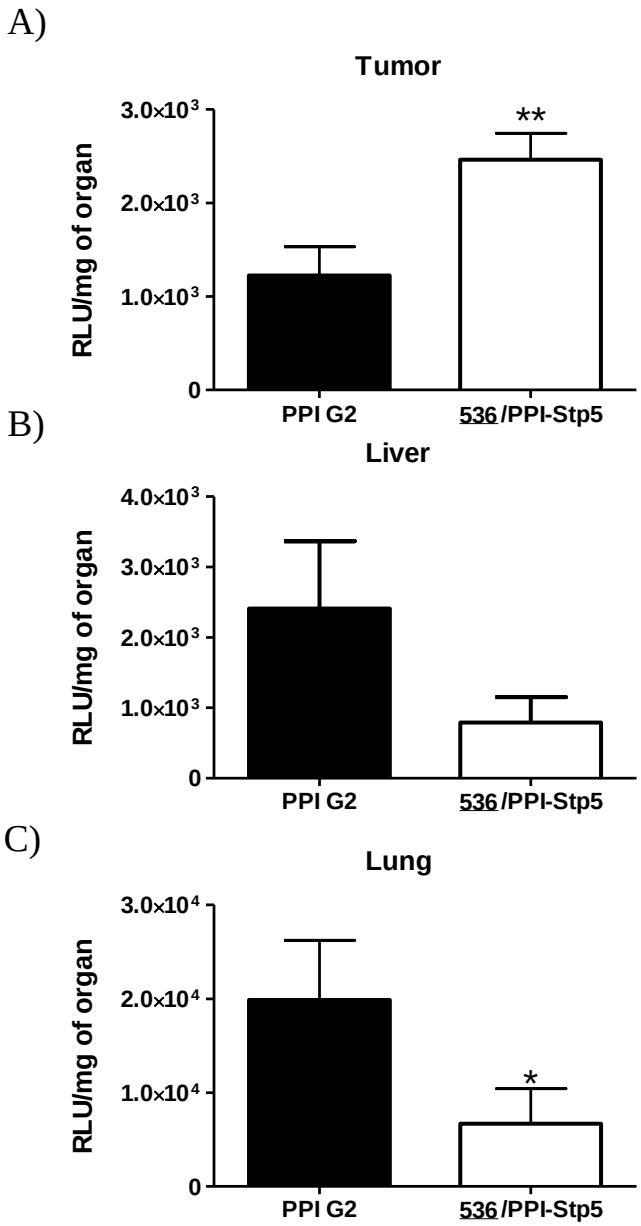

Figure 6: Luciferase gene expression. 48 hours after intravenous administration of PPI G2 and **536**/PPI-Stp5 pDNA polyplexes into Neuro2A tumor bearing mice luciferase gene expression was measured. A) Tumor, B) Liver, C) Lung. Lysis buffer RLU (relative light unit) values were subtracted. Liver weight was around 1.5 g, lung weight around 90 mg and Neuro2A tumor weight 433 ± 134 mg. Represented is the mean ± S.E.M. of four mice per group. Significance of the results was evaluated by t-test (*$p<0.05$; **$p<0.01$).

1.2. Influence of histidines on transgene expression *in vivo*

A critical requirement for efficient gene transfer after cellular uptake remains the escape of polyplexes from endolysosomes. Incorporation of histidines increases the total endolysosomal buffer capacity. Precise four-arm polymers based on the building block succinoyl-pentaethylene hexamine (Sph) containing histidines (**606**/Sph-HC) and the histidine-free analog (**608**/Sph-AC) were thus compared with their luciferase pDNA transfection efficacy. Scheme 1-I+II gives an overview over the structures of the synthesized polymers. First, *in vitro* transfection studies were carried out on Neuro2A tumor cells revealing enhanced gene transfer with histidinylated structures (Figure 7).

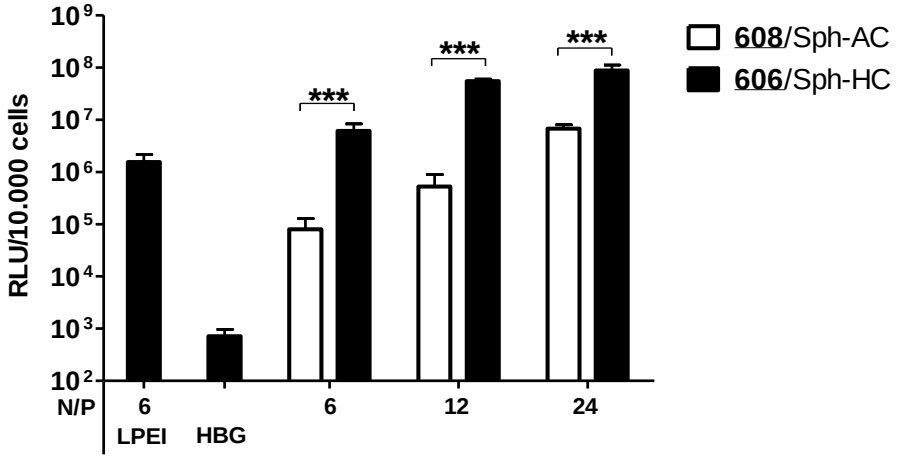

Figure 7: Luciferase pDNA transfection of Neuro2A cells. Comparison of four-arm Sph based polymers containing optionally histidines. The luciferase activity in the cell lysates was analyzed 24 hours after transfection. LPEI was used as a positive control, HBG buffer treated cells served as a background. Data are presented as mean values ± S.D. out of quintuplicate. Data were generated by Petra Kos (PhD thesis 2014, LMU).

Subsequently, mice bearing subcutaneous Neuro2A tumors were injected with **606**/Sph-HC or **608**/Sph-AC pDNA polyplexes at N/P 12 containing 60 µg pCMVLuc intravenously into the tail vein in a total volume of 200 µl HBG. After 48 hours mice were sacrificed, tumors and organs (lung, liver, kidney, spleen and heart) were collected, homogenized in cell culture lysis buffer and subsequently centrifuged. Luciferase activity was determined in the supernatant. Notably, histidine containing **606**/Sph-HC polyplexes mediated highest luciferase transgene expression in the tumor tissue (approximately 20000-fold above lysis buffer background) with tumor expression levels over 32-fold improved over the histidine-free analog **608**/Sph-HC (Figure 8). Both formulations showed low expression levels in lung and heart (approximately

600-800-fold above background) and high transgene expression levels in liver (approximately 3600-7500-fold above background). Furthermore, the histidine containing **606**/Sph-HC formulation also induced considerable gene transfer in spleen and kidney (approximately 2300-2500-fold above background) in contrast to its histidine-free analog **608**/Sph-AC. In summary, **606**/Sph-HC showed 32-fold enhanced activity over **608**/Sph-AC in tumor, 2-fold in liver, 4-fold in spleen and 5-fold in kidney. Aside from these findings, both polyplexes were tolerated quite well and did not mediate any visual sign of acute toxicity.

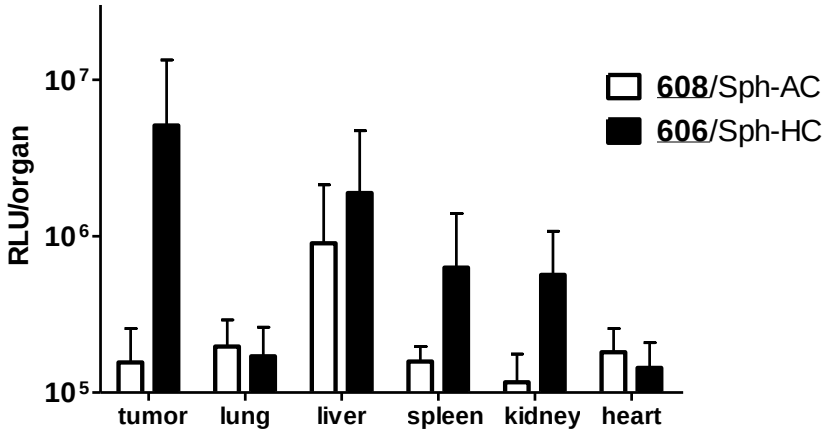

Figure 8: Luciferase gene expression. 48 hours after intravenous administration of pDNA polyplexes with four-arm Sph based polymers containing histidines (**606**/Sph-HC) or alanines (**608**/Sph-AC) into Neuro2A tumor bearing mice luciferase gene expression was measured. Lysis buffer RLU (relative light unit) values were subtracted. Represented is the mean ± S.E.M. of five mice per group.

1.3. Targeted c-Met-directed polyplexes for efficient gene transfer *in vivo*

The goal of active targeting is to enhance specific uptake of particles into cancer cells. Receptor targeted gene delivery with various targeting ligands is enabled through the upregulation of surface receptors in cancer tissues. In the following experiments, the c-Met receptor-binding ligand cMBP2 was evaluated concerning *in vivo* transfection efficacy and compared to a non-targeted alanine control polymer. Petra Kos (PhD thesis 2014, LMU) already demonstrated the successful *in vitro* gene transfer and the absence of receptor activation of cMBP2-targeted polymers. c-Met/HGFR overexpressing hepatocellular carcinoma tumors (Huh7) were utilized as xenograft tumor mouse model in NMRI nude mice.

1.3.1. Intratumoral gene transfer after local administration of c-Met-directed polyplexes

The histidine-enriched two-arm polymer **442**/cMBP2-1PEG with one PEG_{24} (polyethylene glycol) unit (Scheme 1-III) yielded the most auspicious *in vitro* gene transfer (Petra Kos, PhD thesis 2014, LMU) and was therefore selected first for subsequent *in vivo* experiments. Although attachment of a second PEG_{24} unit had not shown a beneficial effect *in vitro*, a shielded analog (**694**/cMBP2-2PEG) with two PEG_{24} units (Scheme 1-IV) was evaluated at the same time, as an additional PEG_{24} chain might be beneficial *in vivo* concerning polyplex biodistribution and ligand accessibility. Anesthetized mice bearing subcutaneous Huh7 tumors were injected intratumorally with polyplexes containing 50 µg pCMVLuc complexed with either **442**/cMBP2-1PEG, **440**/Ala-1PEG, **694**/cMBP2-2PEG or **616**/Ala-2PEG at N/P 12. After 24 hours mice were sacrificed, tumors were collected, homogenized in cell culture lysis buffer and subsequently centrifuged. Luciferase activity was determined in the supernatant and revealed a significant cMBP2 tumor targeting effect of **442**/cMBP2-1PEG polyplexes, with a 15-fold higher gene expression than the alanine control polyplexes **440**/Ala-1PEG (Figure 9-A). A minor gene expression was displayed for polymers with an extra PEG_{24} chain but still revealed a cMBP2 targeting effect of polymer **694**/cMBP2-2PEG (7-fold higher expression) compared to its alanine control **616**/Ala-2PEG.

Due to the fact that luciferase gene transfer studies do not allow a quantification of total plasmid amount in tumors after local administration of polyplexes, quantitative polymerase chain reaction (qPCR) was performed to confirm a cMBP2 targeting effect. According to the luciferase gene transfer experiments, the highest retention of plasmid concentration in the tumor was achieved with the initial cMBP2-targeted two-arm polymer with only one PEG_{24} chain (**442**/cMBP2-1PEG). Compared to its non-targeted alanine control (**440**/Ala-1PEG) the amount of plasmid in tumor was almost 10-fold higher and to the cMBP2-targeted two PEG_{24} unit containing polyplexes (**694**/cMBP2-2PEG) more than 3-fold higher (Figure 9-B).

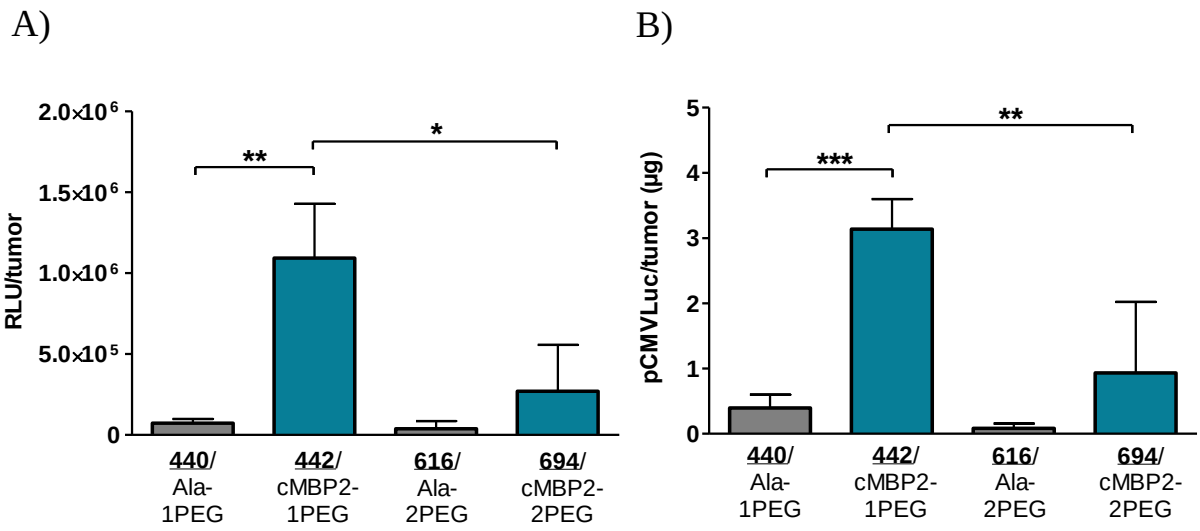

Figure 9: In vivo transfection efficacy. A) Luciferase gene expression 24 hours after intratumoral administration of cMBP2-targeted and alanine control pDNA polyplexes with either one or two PEG_{24} chains into Huh7 tumor bearing mice. Lysis buffer RLU (relative light unit) values were subtracted. Luciferase gene expression is presented as RLU/tumor. The weights of the Huh7 tumors were 387 ± 146 mg. Represented is the mean ± S.E.M. of five mice per group. B) Quantification of luciferase pDNA detected in tumors 24 hours after intratumoral administration of pDNA polyplexes determined with qPCR. Represented is the mean ± S.E.M. of four mice per group. qPCR was performed by Petra Kos (PhD student, LMU Pharmaceutical Biotechnology).
Significance of the results was evaluated by t-test (*p<0.05; **p<0.01; ***p<0.001).

1.3.2. Intratumoral polyplex retention

Based on the first promising intratumoral gene transfer studies which showed a major targeting effect for the two-arm cMBP2 polymer with one PEG_{24} unit (**442**/cMPB2-1PEG) compared to the polymer with 2 PEG_{24} units, it was subsequently chosen for further *in vivo* studies.

To analyze the functionality of the cMBP2-targeted carrier system, its retention effect was compared to its untargeted alanine control polymer (**440**/Ala-1PEG). For this purpose, polyplexes with Cy7-labeled pDNA were injected into subcutaneous Huh7 tumors of anesthetized mice. Analysis was done *via* near infrared (NIR) imaging of the mice immediately after polyplex injection and repeated after 0.25, 0.5, 4, 48 and 72 hours. Figure 10 shows one representative mouse per group.

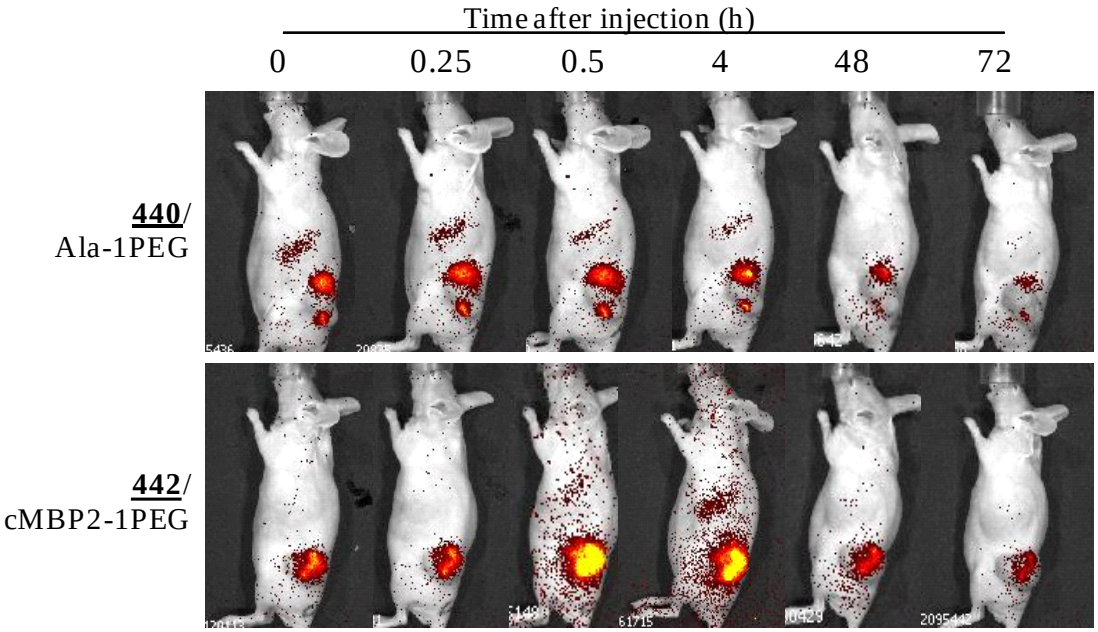

Figure 10: Retention of polyplexes in the tumor tissue. Untargeted polyplexes (top) and targeted polyplexes (bottom) were injected intratumorally and NIR imaging was performed immediately and repeated after 0.25, 0.5, 4, 48 and 72 hours (h). One representative mouse per group is shown. The color scale (efficiency) had a minimum of $2.2e^{-8}$ and a maximum of $1.0e^{-7}$ fluorescent photons/incident excitation photon.

For two-arm targeted (**442**/cMBP2-1PEG) particles a strong fluorescent signal in tumor was visible over 72 hours, being the highest 30 minutes after polyplex injection probably due to the distribution of a high amount of particles in the tumor tissue. In comparison, the non-targeted alanine control particles (**440**/Ala-1PEG) display no Cy7 signal increase in tumor but a decreasing signal after 4 hours representing a weaker retention in the tumor tissue and a shorter persistency than the targeted particles. Importantly, for non-targeted Ala-1PEG particles an immediate liver signal (cranial of the tumor) was observed whereas in case of the targeted cMBP2 particles a liver signal appeared only 30 minutes after polyplex administration.

1.3.3. Systemic gene transfer of c-Met-directed polyplexes after intravenous administration

By reason of the preliminary intratumoral studies which displayed the efficacy of the targeting ligand cMBP2, targeted polyplexes were further analyzed for their systemic delivery potential *in vivo* because of the high impact of this administration route.

1.3.3.1. Initial two-arm polymer

Since the so far tested initial targeted two-arm polymer with one PEG_{24} unit displayed the highest transfection efficacy in the intratumoral gene transfer studies, this polymer was subsequently applied for systemic delivery experiments. Two-arm targeted (**442**/cMBP2-1PEG) and untargeted control polyplexes (**440**/Ala-1PEG) containing an increased amount of pDNA (80 µg pDNA compared to 50 µg in the intratumoral experiments) were injected intravenously into the tail vein of mice bearing subcutaneous Huh7 tumors. Mice were sacrificed two days after administration, tumors and organs (lung and liver) were collected, homogenized in cell culture lysis buffer and subsequently centrifuged. Luciferase activity determined in the supernatant displayed moderate expression levels in tumor and organs but did not reveal any significant targeting effect of the cMBP2-targeted polyplexes over the untargeted control polyplexes (Figure 11).

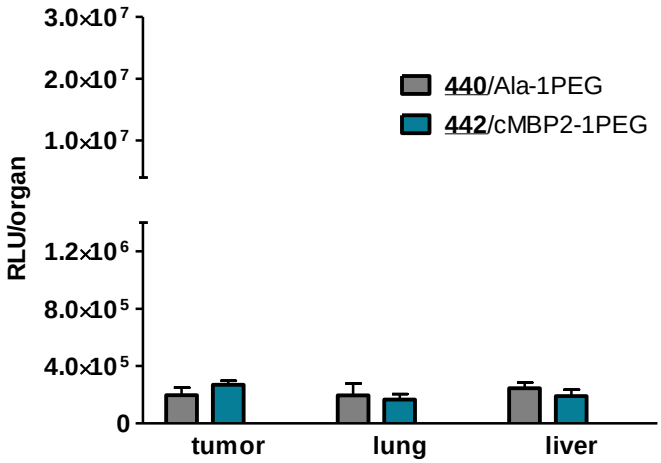

Figure 11: Gene transfer after intravenous administration of the initial two-arm polymer. Gene expression in tumor, lung and liver 48 hours after intravenous administration of **442**/cMBP2-1PEG and **440**/Ala-1PEG pDNA polyplexes into Huh7 tumor bearing mice. Luciferase gene expression is presented as relative light units per organ or tumor (RLU/organ). Lysis buffer RLU values were subtracted. Represented is the mean ± S.E.M. of five mice per group.

1.3.3.2. Polymers with additional polycationic arms

Due to insufficient gene transfer efficacy of the initial two-arm polymer further improvements on polymeric structure of this carrier system were realized. Intratumoral gene transfer experiments already revealed that an increase to an even 2-fold higher PEG content was rather unfavorable hence the opposite direction was taken towards an enhanced dimension of the

polycationic part of the polymers. Although implicating no advantage *in vitro* (Petra Kos, PhD thesis 2014, LMU), polyplexes formed with PEGylated four-arm polymer **677**/cMBP2-1PEG and the untargeted alanine control **678**/Ala-1PEG (Scheme 1-V) were applied for systemic gene transfer studies because they still might be favorable *in vivo*. Polyplexes containing 80 µg pDNA were injected intravenously into the tail vein of mice bearing subcutaneous Huh7 tumors. Mice were sacrificed two days after administration, tumors and organs (lung and liver) were collected, homogenized in cell culture lysis buffer and subsequently centrifuged. Luciferase activity of these polymers with a higher cationic trait determined in the supernatant displayed a significant cMBP2 targeting-dependent luciferase expression in tumor despite only moderate expression levels similar to liver and lung (Figure 12).

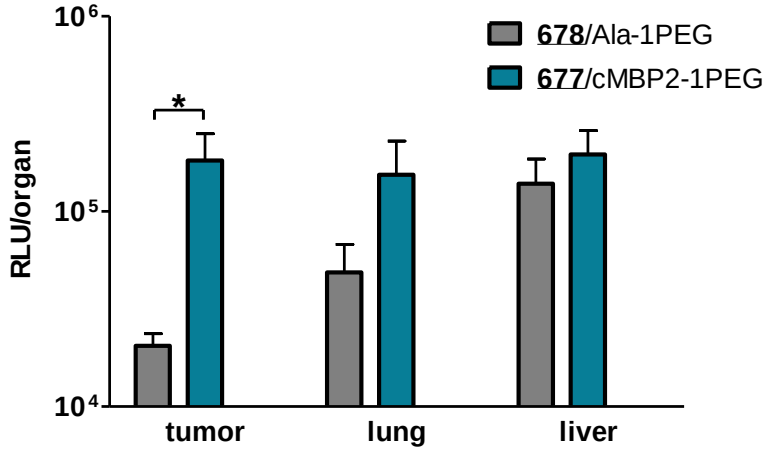

Figure 12: Gene transfer after intravenous administration of polymers with a higher amount of cationic charges. Gene expression in tumor, lung and liver 48 hours after intravenous administration of **677**/cMBP2-1PEG and alanine control **678**/Ala-1PEG pDNA polyplexes into Huh7 tumor bearing mice. Luciferase gene expression is presented as relative light units per organ or tumor (RLU/organ). Lysis buffer RLU values were subtracted. Liver weight was around 1.5 g, lung weight around 210 mg and Huh7 tumor weight 282 ± 197 mg. Represented is the mean ± S.E.M. of five mice per group. Significance of the results was evaluated by t-test (*$p<0.05$).

1.3.3.3. Co-addition of a non-shielded three-arm polymer to the initial two-arm polymer

To further improve transfection efficacy and targeting effect of cMBP2 upon systemic administration, an alternative approach to optimize the polymers was considered. Therefore, a novel three-arm polymer (**689**) without PEG shielding was synthesized (Scheme 1-VI). Due to disulfide-crosslinking of terminal cysteines of the targeted two-arm cMBP2 polymer and the

three-arm polymer stable polyplexes can be formed. Hereupon, this new polymer was mixed in a ratio of 30:70 with the initial cMBP2-targeted two-arm polymer (**442**/cMBP2-1PEG) to reach an N/P ratio of 12. Polyplexes formed with targeted bi-polymeric particles (**442**/cMBP2-1PEG + **689**) or the corresponding untargeted alanine control (**440**/Ala-1PEG + **689**) were applied for systemic gene transfer studies in mice. Polyplexes containing 80 µg pDNA were injected intravenously into the tail vein of mice bearing subcutaneous Huh7 tumors. Mice were sacrificed two days after administration, tumors and organs (lung and liver) were collected, homogenized in cell culture lysis buffer and subsequently centrifuged. In contrast to mono-polymer **442**/cMBP2-1PEG polyplexes (Figure 11), luciferase activity determined in the supernatant revealed a highly increased expression in tumor (Figure 13) for the cMBP2-targeted bi-polymeric particles (**442**/cMBP2-1PEG + **689**). The tumor signal of the non-targeted alanine control polyplexes (**440**/Ala-1PEG + **689**) was exceeded by 22-fold and of the cMBP2-targeted mono-oligomer polyplexes (**442**/cMBP2-1PEG) by 35-fold (Figure 11). The luciferase expression in the organs lung and liver was up to 50-fold lower than in tumor (Figure 13-A). The amount of pDNA accumulating in tumor 4 hours after intravenous injection was determined by qPCR. Administration of cMBP2-targeted polyplexes resulted in an increased pDNA amount in tumor compared to the alanine analogs confirming the cMBP2 targeting effect. According to the luciferase gene transfer experiments, the highest pDNA retention was observed with cMBP2-targeted bi-polymeric particles (**442**/cMBP2-1PEG + **689**) outperforming their alanine analogs 30-fold (Figure 13-B).

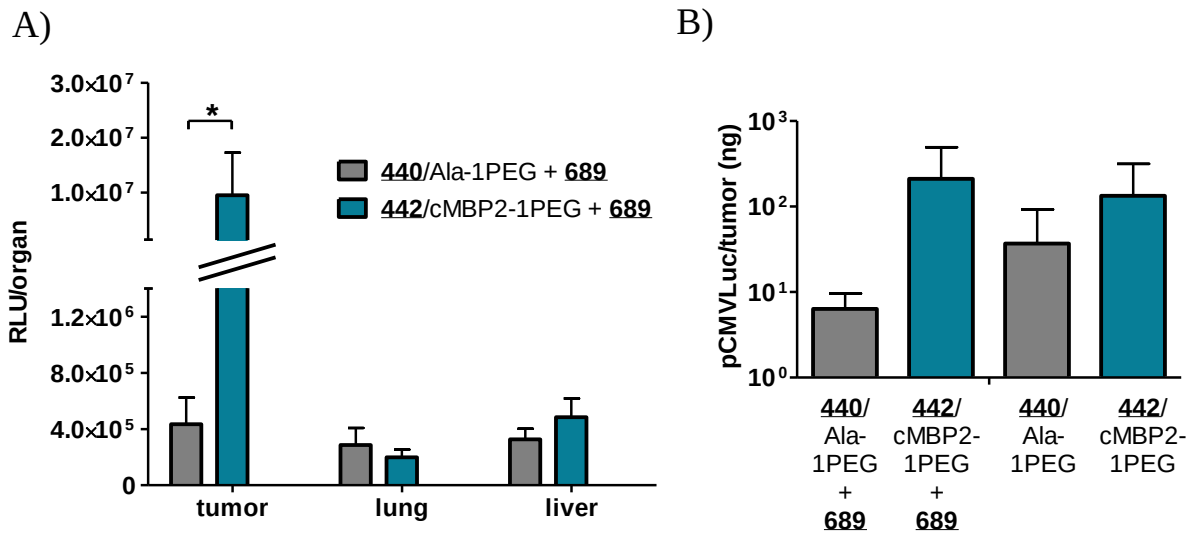

Figure 13: Gene transfer after intravenous administration of bi-polymeric particles. A) Luciferase gene expression in tumor, lung and liver 48 hours after intravenous administration of two-arm PEGylated cMBP2-targeted (**442**/cMBP2-1PEG) or alanine control (**440**/Ala-1PEG) polymers mixed with three-arm non-PEGylated polymer **689** into Huh7 tumor bearing mice. Luciferase gene expression is presented as relative light units per organ or tumor (RLU/organ). Lysis buffer RLU values were subtracted. Liver weight was around 1.6 g, lung weight around 230 mg and Huh7 tumor weight 452 ± 189 mg. Represented is the mean ± S.E.M. of five mice per group. B) Quantification of luciferase pDNA detected in tumors 4 hours after intravenous administration of either cMBP2-targeted or alanine control single - or bi-polymeric particles determined with qPCR. Represented is the mean ± S.E.M. of three mice per group. qPCR was performed by Petra Kos (PhD student, LMU Pharmaceutical Biotechnology). Significance of the results was evaluated by t-test (*$p<0.05$).

1.3.3.4. Co-addition of a non-shielded four-arm polymer to the initial two-arm polymer

To examine whether this beneficial effect after co-adding polymer **689** is specific or it can be achieved by the addition of any non-shielded polymer a different combination was investigated in their systemic transfection efficacy. Instead of three-arm polymer **689** a four-arm polymer with Sph building blocks (Scheme 1-II) was mixed in a ratio of 30:70 with the initial cMBP2-targeted two-arm polymer (**442**/cMBP2-1PEG) to reach an N/P ratio of 12. Polyplexes formed with cMBP2-targeted bi-polymeric particles (**442**/cMBP2-1PEG + **606**) or the corresponding untargeted alanine control (**440**/Ala-1PEG + **606**) were applied for systemic gene transfer studies in mice. Polyplexes containing 80 µg pDNA were injected intravenously into the tail vein of mice bearing subcutaneous Huh7 tumors. Mice were sacrificed 48 hours after administration, tumors and organs (lung and liver) were collected, homogenized in cell culture

lysis buffer and subsequently centrifuged. Luciferase activity determined in the supernatant yielded a significant cMBP2 tumor targeting effect, however with a lower luciferase expression in tumor and a remarkably increased expression in lung (Figure 14).

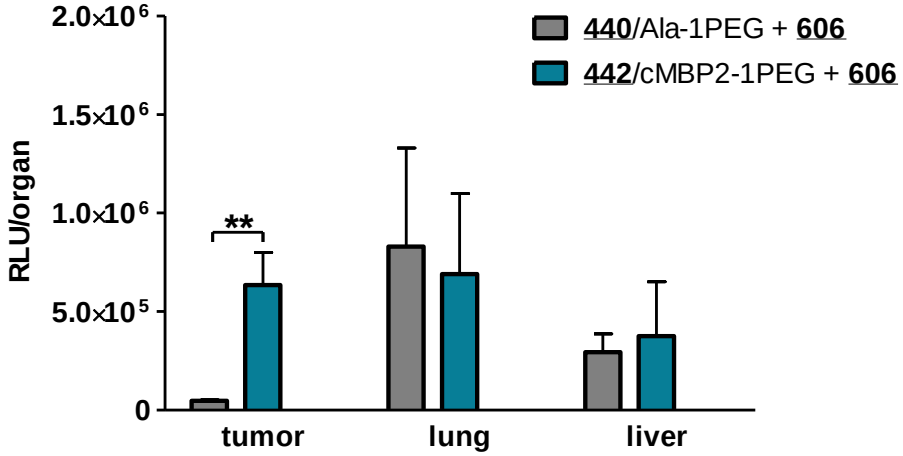

Figure 14: Systemic gene transfer after co-addition of a non-shielded four-arm polymer. Gene expression in tumor, lung and liver 48 hours after intravenous administration of two-arm PEGylated cMBP2-targeted (**442**/cMBP2-1PEG) or alanine control (**440**/Ala-1PEG) polymers combined with four-arm non-PEGylated polymer **606** into Huh7 tumor bearing mice. Luciferase gene expression is presented as relative light units per organ or tumor (RLU/organ). Lysis buffer RLU values were subtracted. Liver weight was around 1.5 g, lung weight around 210 mg and Huh7 tumor weight 438 ± 152 mg. Represented is the mean ± S.E.M. of five mice per group. Significance of the results was evaluated by t-test (**$p<0.01$).

2. Circumventing chemoresistance of cancer

In this chapter, two different approaches to circumvent chemoresistance of cancer were analyzed. First, the efficacy of the drug salinomycin against cancer cells and its ability to inhibit migration and metastasis was investigated *in vivo*. These experiments were performed together with Florian Kopp (PhD thesis 2013, LMU). The additive effect of salinomycin to the classical therapeutic drug doxorubicin was further investigated in a tumor mouse model. Secondly, packing of chemotherapeutic drugs inside mesoporous nanoparticles was investigated *in vivo* in terms of biodistribution, biocompatibility and tumor targeting. Stefan Niedermayer (PhD thesis 2014, LMU) and Stefan Datz (PhD student, LMU Physical Chemistry) synthesized these mesoporous nanoparticles (MSN).

2.1. Effects of doxorubicin upon increasing dosage

Regarding the effect of the classical chemotherapeutic drug doxorubicin on tumor growth and metastasis of 4T1-Luc breast tumors different dosages were evaluated in a preliminary dose-finding experiment for subsequent combinatorial treatment. BALB/c mice (n = 12) were divided into four groups, one control group (NaCl 0.9 %) and three treatment groups (2 mg/kg, 5 mg/kg, and 8 mg/kg doxorubicin). Luciferase expressing syngeneic 4T1 breast cancer cells were inoculated into the mammary fat pad. 24 hours later treatment started and was repeated every six days for three times. On day 18, after tumor cell inoculation, two mice treated with 8 mg/kg doxorubicin had to be euthanized due to severe weight loss (the third mouse of this group had to be euthanized already on day 7). The group treated with 5 mg/kg doxorubicin also lost weight initiating after one week of treatment compared to the control or lowest treatment group (2 mg/kg doxorubicin) which constantly gained weight. Figure 15 shows the weight loss-to-time diagram.

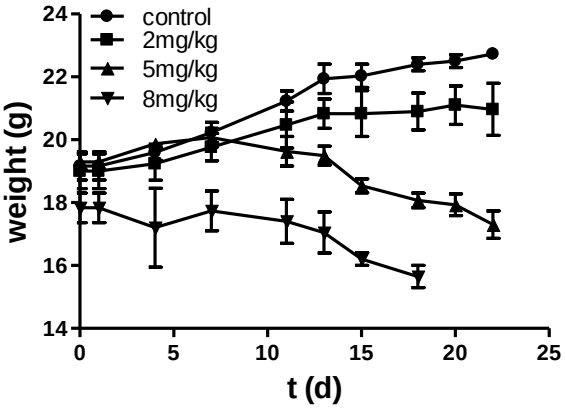

Figure 15: Weight loss-to-time diagram. Weight development of mice during systemic treatment with 2 mg/kg, 5 mg/kg, 8 mg/kg doxorubicin or control starting with 4T1-Luc breast cancer cell inoculation (day 0) and ending with euthanasia (day 22, day 18 for the 8 mg/kg group). Represented is the mean ± S.E.M. of three (two within the 8 mg/kg treatment group) mice per group over time.

Treatment with the lowest dosage (2 mg/kg doxorubicin) mediated no effect on hampering tumor growth but a similar increase in tumor volume as the control group visible in a tumor growth curve (Figure 16-A). Only treatment with 5 mg/kg doxorubicin led to a significant tumor growth inhibition without premature termination due to severe medical condition (Figure 16-B).

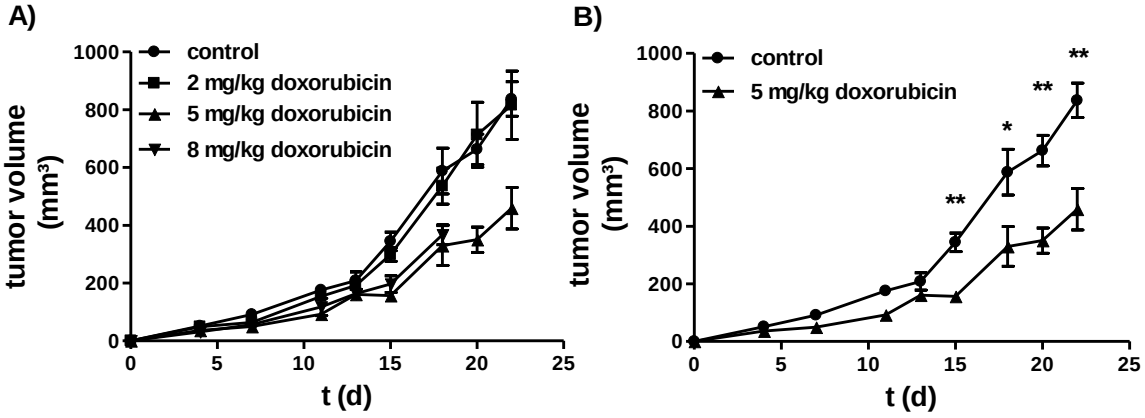

Figure 16: Tumor growth over time. Tumor volume of BALB/c mice bearing 4T1-Luc breast tumors in the mammary fat pad during three systemic treatments (day 1, 7 and 13) with 2 mg/kg, 5 mg/kg or 8 mg/kg doxorubicin or control (NaCl 0.9 %). Tumor growth was monitored for 22 days at indicated time points. A) Average tumor volumes of all four groups over time. B) Average tumor volumes of the group treated with 5 mg/kg doxorubicin compared to the control group. Significance of the results was evaluated by t-test (*$p<0.05$; **$p<0.01$). Represented is the mean ± S.E.M. of three mice per group.

At the end of the trial on day 22 (mice treated with 8 mg/kg doxorubicin on day 18) metastasis formation to the lungs was evaluated *via* bioluminescence imaging. For this purpose mice were anesthetized and injected with Na-luciferin intraperitoneally. After 15 minutes of distribution mice were euthanized through cervical dislocation, lungs were dissected and bioluminescence imaging was performed. For quantification of the tumor burden bioluminescent signals were counted as total flux/area (photons/second/cm^2). Figure 17-A represents the luminescent signal of 4T1-Luc tumors in lungs. The average luciferin signal in lungs of the group treated with the lowest dose of doxorubicin (2 mg/kg) was significantly higher than in the control group implying an enhanced metastasis formation upon low dosage treatment. Even higher dosage with 5 mg/kg doxorubicin led to a slightly increased tumor burden in the lungs compared to the control group. The highest dosage (8 mg/kg) of doxorubicin caused minor metastasis formation to the lungs. To visualize these findings, two pictures (ventral and dorsal side) were taken per lung (Figure 17-B). The group treated with 2 mg/kg doxorubicin had much higher luminescent signals than the other groups. As this experiment was performed for dose-finding, these results need to be validated by larger group numbers.

A)

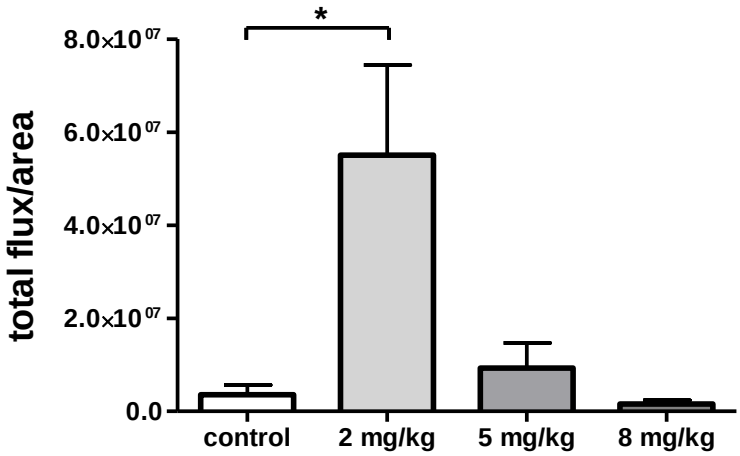

B)

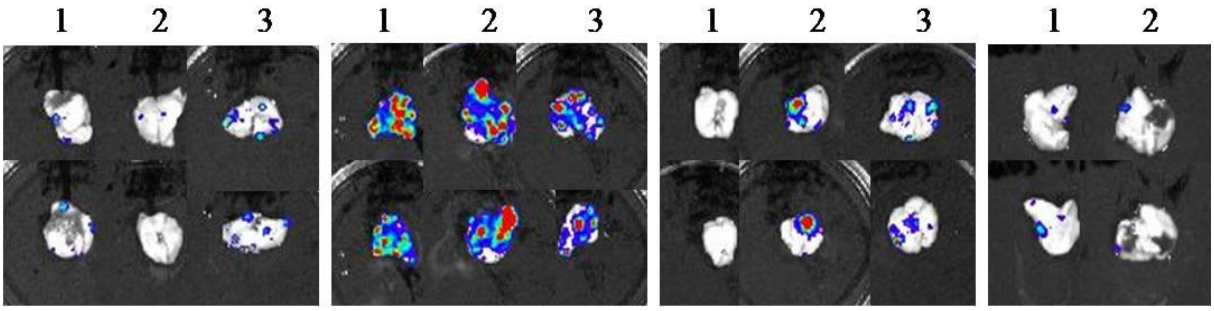

1 2 3 4

Figure 17: Quantification of tumor burden in the lungs. A) The luminescent signal of 4T1-Luc tumor formation to the lungs was counted as total flux/area (photons/second/cm^2). Represented is the mean ± S.E.M. of three mice per group. Significance of the results was evaluated by t-test (*$p<0.05$). B) Images of the harvested lungs. Panel no. 1 shows the tumor burden of the lungs of the control group, no. 2 of the group treated with 2 mg/kg doxorubicin, no. 3 of the group treated with 5 mg/kg doxorubicin and no. 4 of the group treated with 8 mg/kg doxorubicin. Each lung was pictured from dorsal and ventral side.

2.2. Influence of salinomycin on tumor growth

To evaluate the efficacy of the drug salinomycin to hamper tumor growth, luciferase expressing 4T1 breast cancer cells and syngeneic BALB/c mice were used in a subcutaneous tumor model. Subcutaneous tumor bearing mice were treated intraperitoneally with either salinomycin (5 mg/kg) or control (DMSO in phosphate buffered saline) for six times between day 3 and 15 after tumor implantation. Treatment with salinomycin mediated similar tumor size increase

over time to the control group visible in a tumor growth curve (Figure 18-A). Only a minor effect on tumor size could be observed for the final day (day 17) (Figure 18-B).

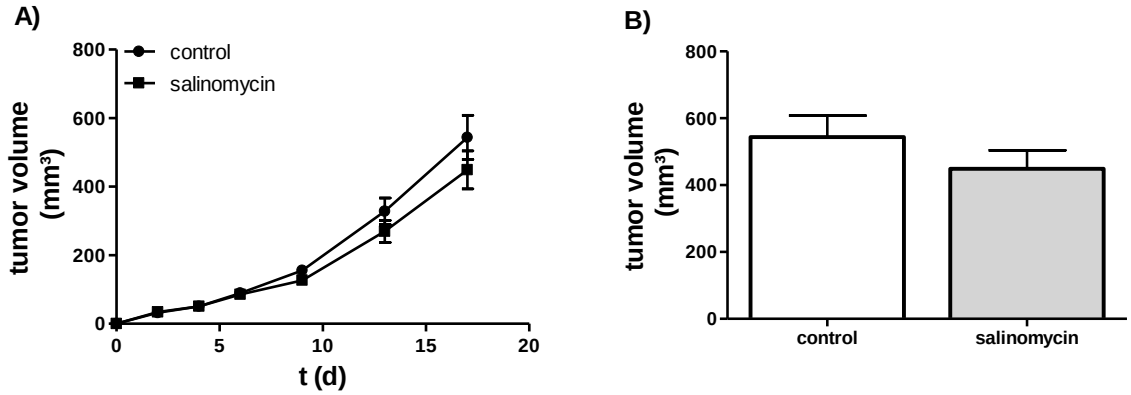

Figure 18: Tumor growth rate. Tumor volume of BALB/c mice bearing subcutaneous 4T1-Luc breast tumors during six intraperitoneal treatments (day 3, 6, 8, 10, 13 and 15) with 5 mg/kg salinomycin or control. A) Average tumor volumes of both groups over time. Tumor growth was monitored for 17 days at indicated time points. B) Average tumor volumes of the salinomycin treated group compared to the control group on the final day (day 17).
Represented is the mean ± S.E.M. of nine mice per group.

All mice were in good general condition during the experiment and both groups showed similar weight increase over time (Figure 19).

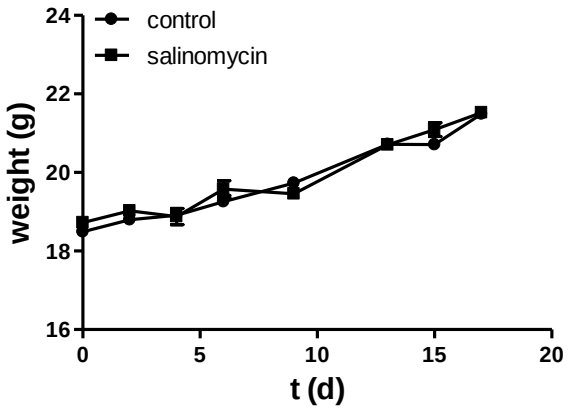

Figure 19: Weight loss-to-time diagram. Weight development of mice during intraperitoneal treatment with 5 mg/kg salinomycin or control starting with 4T1-Luc breast cancer cell inoculation (day 0) and ending with euthanasia (day 17). Represented is the mean ± S.E.M. of nine mice per group over time.

2.3. Influence of salinomycin on tumor colonization and migration

Besides the findings of salinomycin on hampering tumor growth we considered whether salinomycin is able to prevent metastasis formation *in vivo*. Hence, the effect of salinomycin on tumor cell colonization and migration was evaluated in a syngeneic 4T1-Luc mouse model. BALB/c mice (n = 20) were divided into two groups, one control group and one treatment group. Luciferase expressing syngeneic 4T1 breast cancer cells were injected intravenously *via* tail vein. 24 and 0.5 hours before tumor cell inoculation the treatment group was premedicated intraperitoneally with 5 mg/kg salinomycin. Treatment was repeated on day 3, 6 and 9 after tumor cell injection and tumor growth was monitored using bioluminescence imaging on day 3, 8 and at the end of the experiment (day 13). For this purpose mice were anesthetized and injected with Na-luciferin intraperitoneally. After 15 minutes of distribution bioluminescence imaging was performed. One mouse of the control group had to be sacrificed already earlier due to severe medical condition. Figure 20 shows the luminescent signals of the 4T1-Luc tumors in the lungs at the end of the trial (day 13).

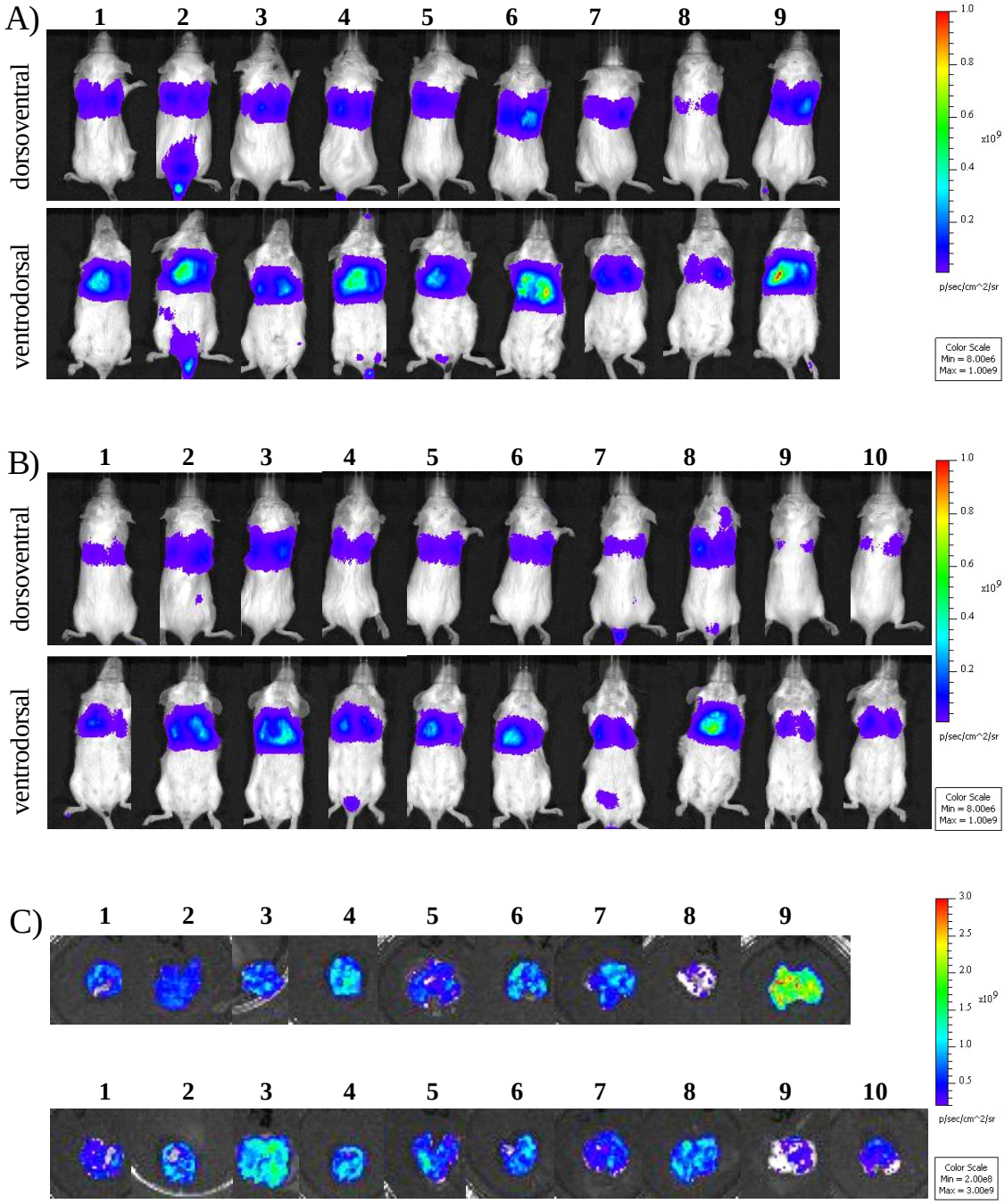

Figure 20: Bioluminescence Imaging. A) Images of mice with primary tumor formation in the lungs treated with control. The upper panel shows dorsoventral and the lower panel shows ventrodorsal images of mice. B) Images of mice with primary tumor formation in the lungs treated with 5 mg/kg salinomycin. The upper panel shows dorsoventral and the lower panel shows ventrodorsal images of mice. C) Images of dissected lungs. The upper panel shows tumor burden in the lungs of the control treated group and the lower panel shows tumor burden in the lungs of the salinomycin treated group.

All mice in both groups exhibited a thoracic luminescent signal reflecting the primary tumor burden in the lung of each mouse. A stronger signal could be observed in dorsal position of the mice (Figure 20-A+B lower panel). Mice treated with salinomycin showed similar signals in the lungs to the control mice. To localize the luminescent signal quite clearly lungs were dissected and imaged separately (Figure 20-C). The findings are in accordance with images of the living mice, salinomycin treated mice had similar signals in the lungs to control treated mice.

For quantification of the tumor burden over time bioluminescence imaging was performed on day 3, 8 and at the end of the trial (day 13). Signals were counted as total flux/area (photons/second/cm^2). Figure 21 represents the average luminescent signals over time. In line with the subcutaneous model, treatment with salinomycin did not yield a significant effect on primary tumor formation and growth over time.

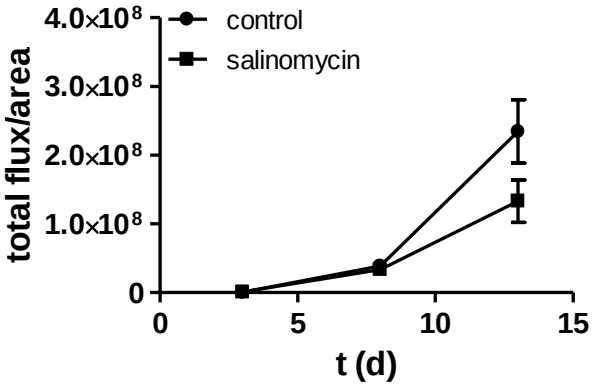

Figure 21: Quantification of tumor burden in the lungs. The luminescent signal of 4T1-Luc tumor formation in the lungs was counted as total flux/area (photons/second/cm^2). Represented is the mean ± S.E.M. of ten (treatment group) or nine (control group) mice over time.

To evaluate the effect of salinomycin on hampering migration, metastasis formation from primary tumor to secondary organs was analyzed subsequently. Therefore, mice were euthanized at the end of the trial (day 13) and organs (brain, spleen, kidneys and liver) were dissected for subsequent *ex vivo* luciferase measurements. Organs were homogenized in cell culture lysis buffer followed by centrifugation and determination of the luciferase activity in the supernatant. Remarkably, metastases in brain, spleen and kidneys were significantly reduced after treatment with salinomycin (Figure 22).

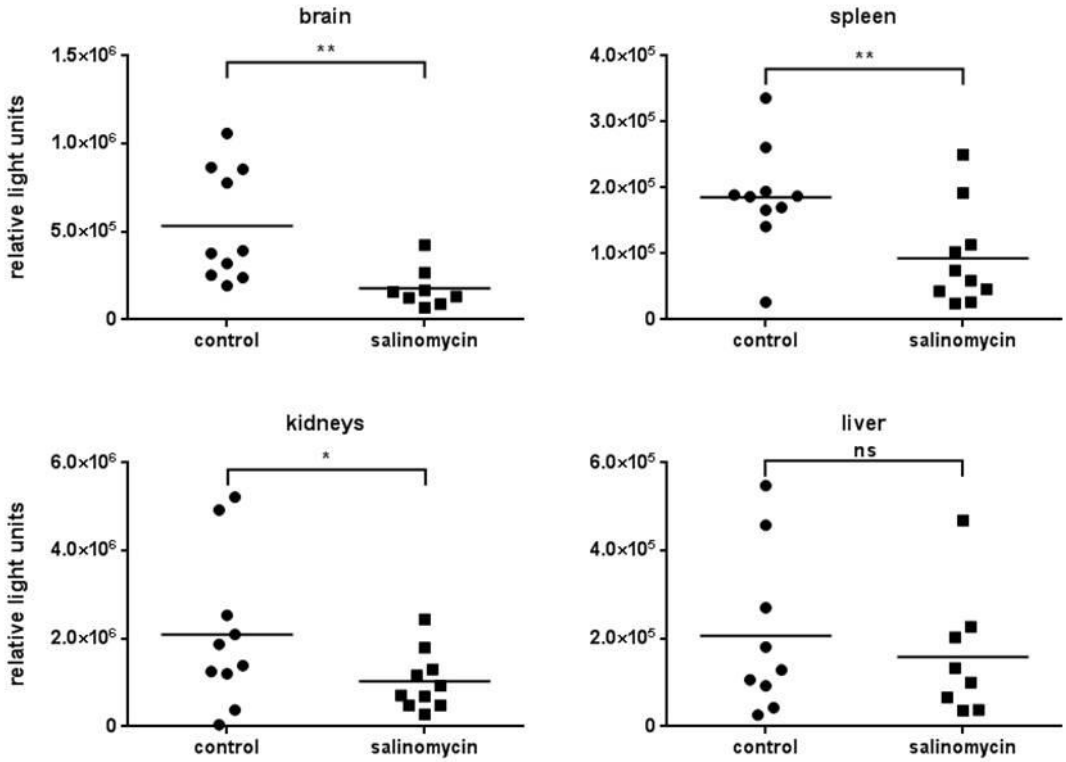

Figure 22: Metastasis formation in a syngeneic intravenous mouse tumor model. Metastasis in 4T1-Luc tumor bearing mice on day 13 after intraperitoneal treatment with 5 mg/kg salinomycin or control. Luciferase gene expression was analyzed in brain, spleen, kidneys and liver. Significance of the results was evaluated by t-test (*$p<0.05$; **$p<0.01$).

All mice were in good general condition at the beginning of the experiment. After one week they started to lose weight due to the tumor burden in the lungs and therefore the experiment had to be terminated at day 13. Both groups show similar body weight levels over time (Figure 23).

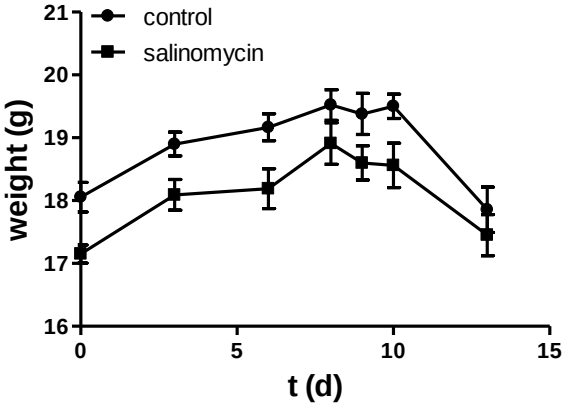

Figure 23: Weight loss-to-time diagram. Weight development of mice during intraperitoneal treatment with 5 mg/kg salinomycin or control starting with intravenous 4T1-Luc breast cancer cell inoculation (day 0) and ending with euthanasia (day 13). Represented is the mean ± S.E.M. of ten (treatment group) or nine (control group) mice over time.

2.4. Combinatorial effect of doxorubicin and salinomycin

Due to the positive effect of salinomycin on hampering migration but not on tumor growth reduction, it´s efficacy as an additive compound to the classical chemotherapeutic drug doxorubicin was investigated in a syngeneic tumor mouse model. BALB/c mice (n = 40) were divided into four groups, one control group and three treatment groups (single doxorubicin, single salinomycin and combined treatment). Luciferase expressing syngeneic 4T1 breast cancer cells were inoculated into the mammary fat pad. 24 hours later treatment with doxorubicin started. As the preliminary dose-finding experiment for doxorubicin revealed tumor growth inhibition but also severe weight loss of mice treated with 5 mg/kg and 8 mg/kg a lower dosage was inescapable (Figure 15 + 16). 2 mg/kg implied enhanced metastasis formation and mediated no tumor growth inhibition, thus, a compromise solution was found favourable. The doxorubicin and combinatorial group received 3.5 mg/kg weekly for three weeks intravenously. The salinomycin and combinatorial group received 5 mg/kg twice per week intraperitoneally. Treatment with salinomycin again mediated similar tumor size increase over time to the control group visible in a tumor growth curve (Figure 24-A). Only treatment with doxorubicin could reduce the tumor burden significantly whereas the combinatorial treatment could not yield any additional effect on tumor growth inhibition to single doxorubicin treatment. In Figure 24-B a detailed illustration of tumor size proportions at the end of the trial (day 21) is shown.

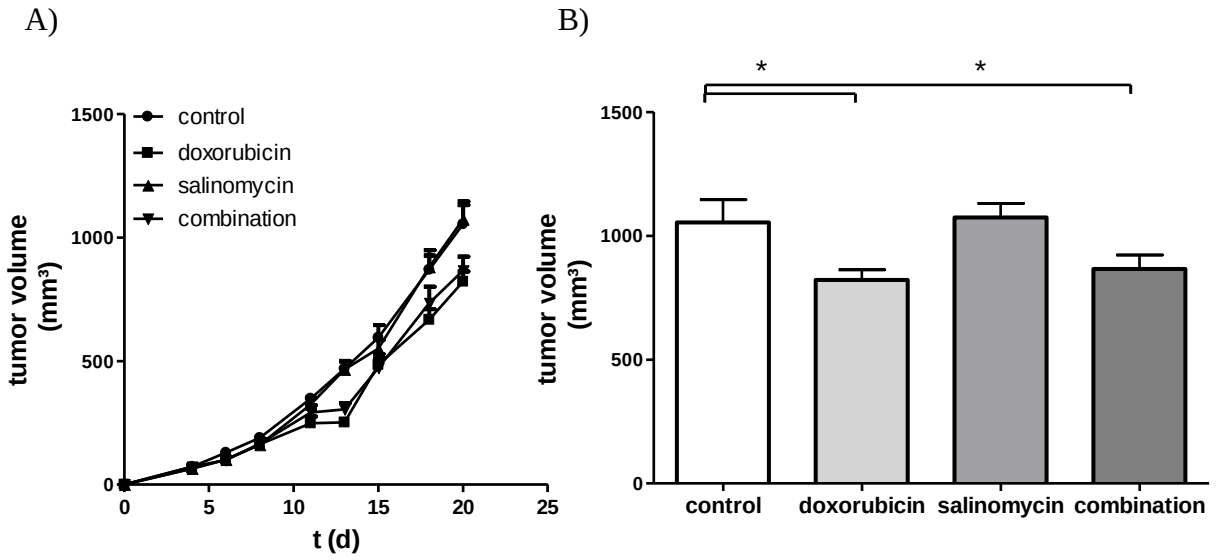

Figure 24: Tumor growth over time. Tumor volume of BALB/c mice bearing 4T1-Luc breast tumors in the mammary fat pad during either three systemic treatments (day 1, 8 and 15) with 3.5 mg/kg doxorubicin or six intraperitoneal treatments (day 4, 6, 11, 13, 18 and 20) with 5 mg/kg salinomycin or a combination of both. A) Average tumor volumes of all groups over time. Tumor growth was monitored for 21 days at indicated time points. B) Average tumor volumes of all treatment groups compared to the control group on the final day (day 21). Significance of the results was evaluated by t-test (*$p<0.05$).
Represented is the mean ± S.E.M. of ten mice per group.

At the end of the trial, on day 21 after tumor cell inoculation, metastasis formation to the lungs was evaluated using bioluminescence imaging. For this purpose mice were anesthetized and injected with Na-luciferin intraperitoneally. After 15 minutes of distribution mice were euthanized through cervical dislocation, lungs were dissected and bioluminescence imaging was performed. Figure 25-A shows the luminescent signals of the 4T1-Luc tumor burden in the lungs at the end of the trial (day 21). One mouse in the control group (number 9) and two in the doxorubicin treated group (number 5 and 9) did not develop metastasis formation to the lungs. For quantification of the tumor burden in the lungs bioluminescent signals were counted as total flux/area (photons/second/cm^2). Mice without metastases in the lungs were excluded as the experimental settings malfunctioned here. The control group yielded the highest amount of metastases in the lungs followed by the treatment groups (Figure 25-B). Within this experimental setting neither single nor combinatorial treatment were able to hamper metastasis formation significantly.

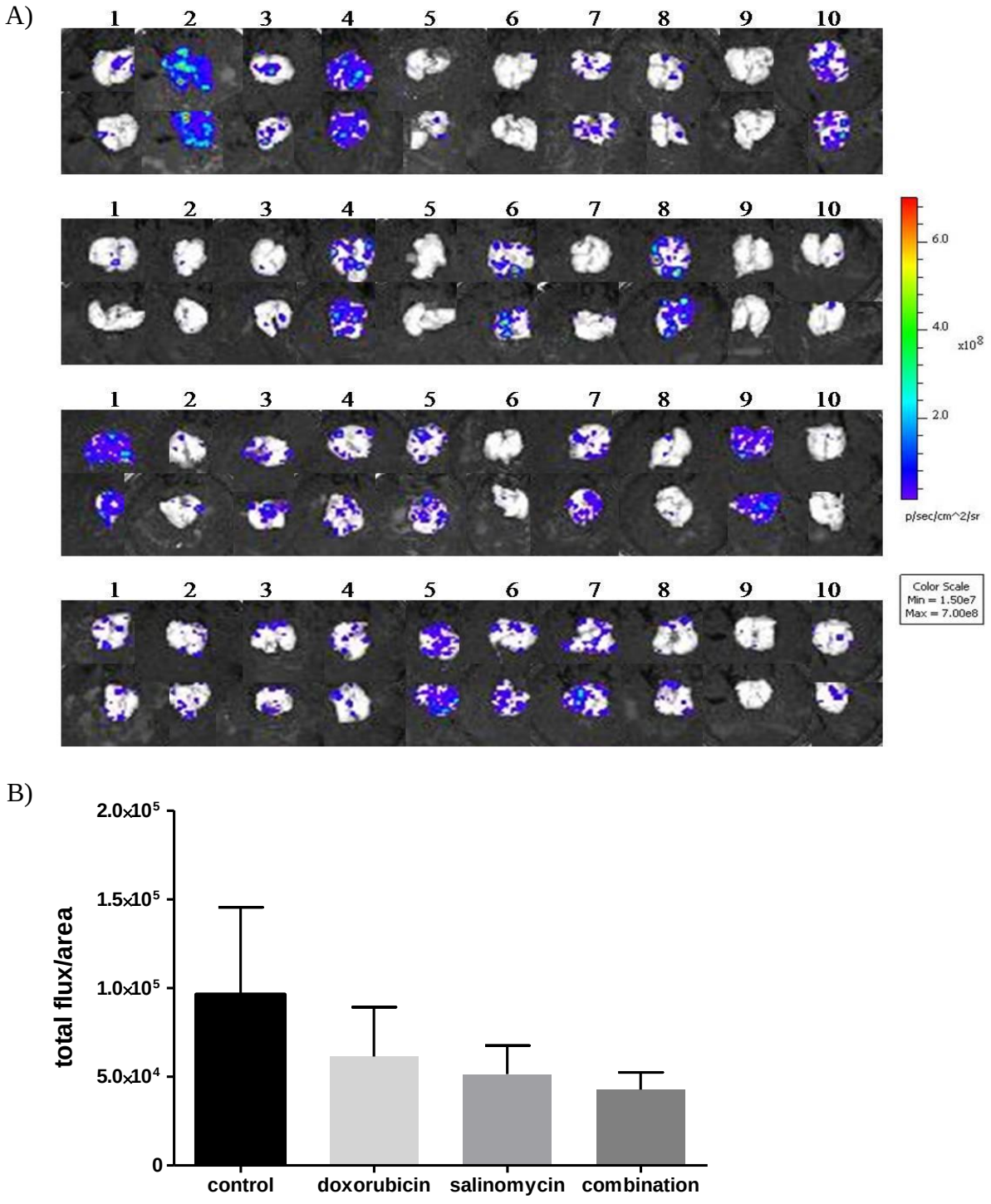

Figure 25: Metastasis formation to the lungs. A) Bioluminescence imaging of the dissected lungs. Panels (from top down) show the tumor burden in the lungs of the control, single doxorubicin, single salinomycin and combined treated mice. Each lung was pictured from dorsal and ventral side. B) The luminescent signal of 4T1-Luc tumor formation to the lungs was counted as total flux/area (photons/second/cm^2). Represented is the mean ± S.E.M. of ten mice per group.

All mice were in good general condition during the whole experiment, however the group treated with doxorubicin plus salinomycin showed minor weight increase over time compared to the other groups (Figure 26).

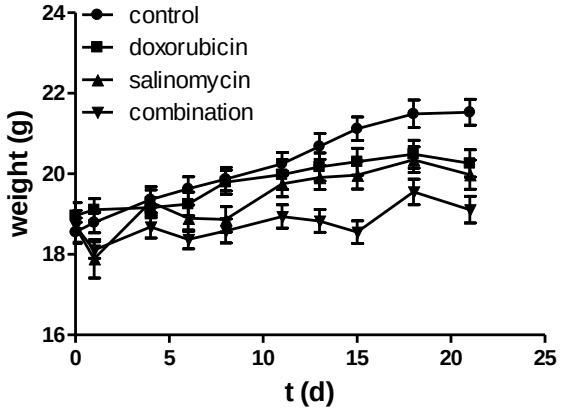

Figure 26: Weight loss-to-time diagram. Weight development of control, doxorubicin, salinomycin or combined treated mice starting with 4T1-Luc breast cancer cell inoculation (day 0) and ending with euthanasia (day 21). Represented is the mean ± S.E.M. of ten mice per group.

2.5. Mesoporous silica nanoparticles (MSN) for efficient drug delivery

Circumvention of resistance to a drug, to reduce its side effects or to protect it against body fluids can be achieved by encapsulating chemotherapeutics into drug delivery vehicles. Below, a multifunctional delivery vehicle based on mesoporous silica nanoparticles (MSN) with a pH-responsive coating is investigated *in vivo*. In previous *in vitro* experiments, MSN were characterized regarding physical and chemical properties and showed the successful delivery of several cargo into cells (Stefan Niedermayer, Veronika Weiss, PhD theses 2014, LMU).

2.5.1. Systemic biodistribution of MSN

In a first experiment, the biodistribution of functionalized polymer-coated and folic acid (FA) targeted MSN (MSN-PVP-PEG-NH_2-FA) was compared with unfunctionalized MSN (MSN-NH_2) and evaluated in tumor free mice. Anesthetized mice were injected intravenously into the tail vein with a 100 µg (5 mg/kg) dose of Cy7-labeled particles (Cy7 was covalently linked to amino-groups on the surface). Analysis using NIR imaging of the mice was done immediately after injection and repeated after 0.25, 0.5, 4, 24 and 48 hours. Figure 27 shows one representative mouse per group. Both particle types were well tolerated by the mice and both showed similar short circulation times. In ventral position of the mice (Figure 27 - upper panel)

a signal in the spleen could be observed on the left side of the body. The fluorescent signal cranial represents the lungs. In dorsal position (Figure 27 - lower panel) preferred liver accumulation could be observed. A signal in the bladder occurred 15 minutes after injection. In summary, both particle types showed similar biodistribution manners upon systemic administration.

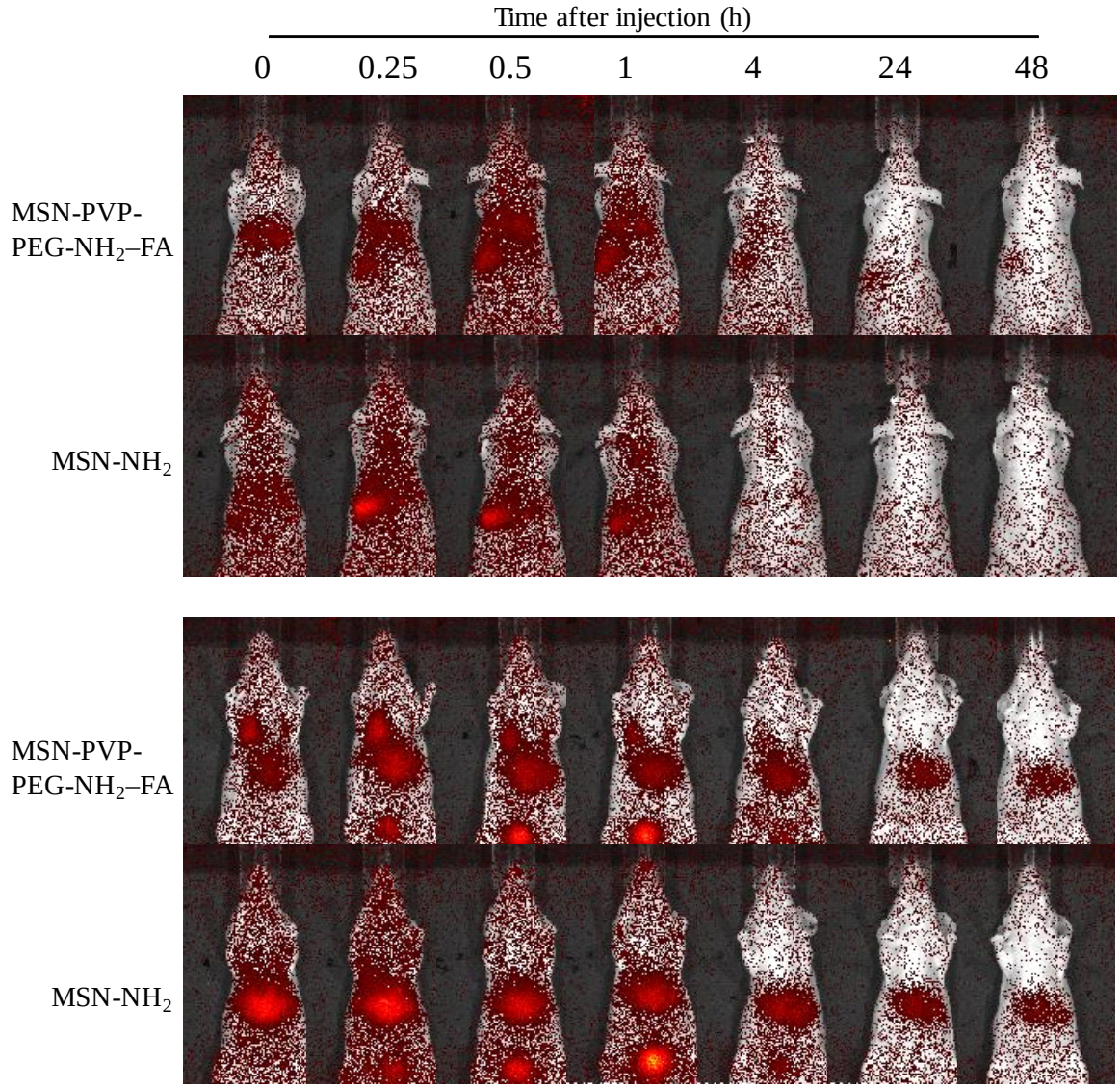

Figure 27: Biodistribution upon systemic administration. Cy7-labeled functionalized (MSN-PVP-PEG-NH_2-FA) and unfunctionalized (MSN-NH_2) particles were injected intravenously and NIR imaging was performed immediately. Time dependent distribution over 48 hours. The upper panel shows dorsoventral and the lower panel ventrodorsal images of mice. One representative mouse per group is shown. The color scale (efficiency) had a minimum of $1.2e^{-8}$ and a maximum of $1.0e^{-7}$ fluorescent photons/incident excitation photon.

To investigate the stability of particles and the attachment of the fluorescent dye due to the signal in the bladder, a second biodistribution experiment with Cy7 covalently linked to the inner surface of the particles was carried out. Anesthetized mice were injected intravenously into the tail vein with Cy7-loaded functionalized or unfunctionalized particles. Analysis using NIR imaging of the mice was done immediately after injection and repeated after 0.25, 0.5, 4, 24 and 48 hours. Figure 28 shows one representative mouse per group. Both particle types showed again similar short circulation times with a generally weaker fluorescent signal intensity compared to particles labeled on the outside of MSN. In dorsal position (Figure 28 - lower panel) preferred liver accumulation and a signal in the lung could be observed. Importantly, no signal in the bladder is visible implying a good particle stability and a stable attachment of dye to particles.

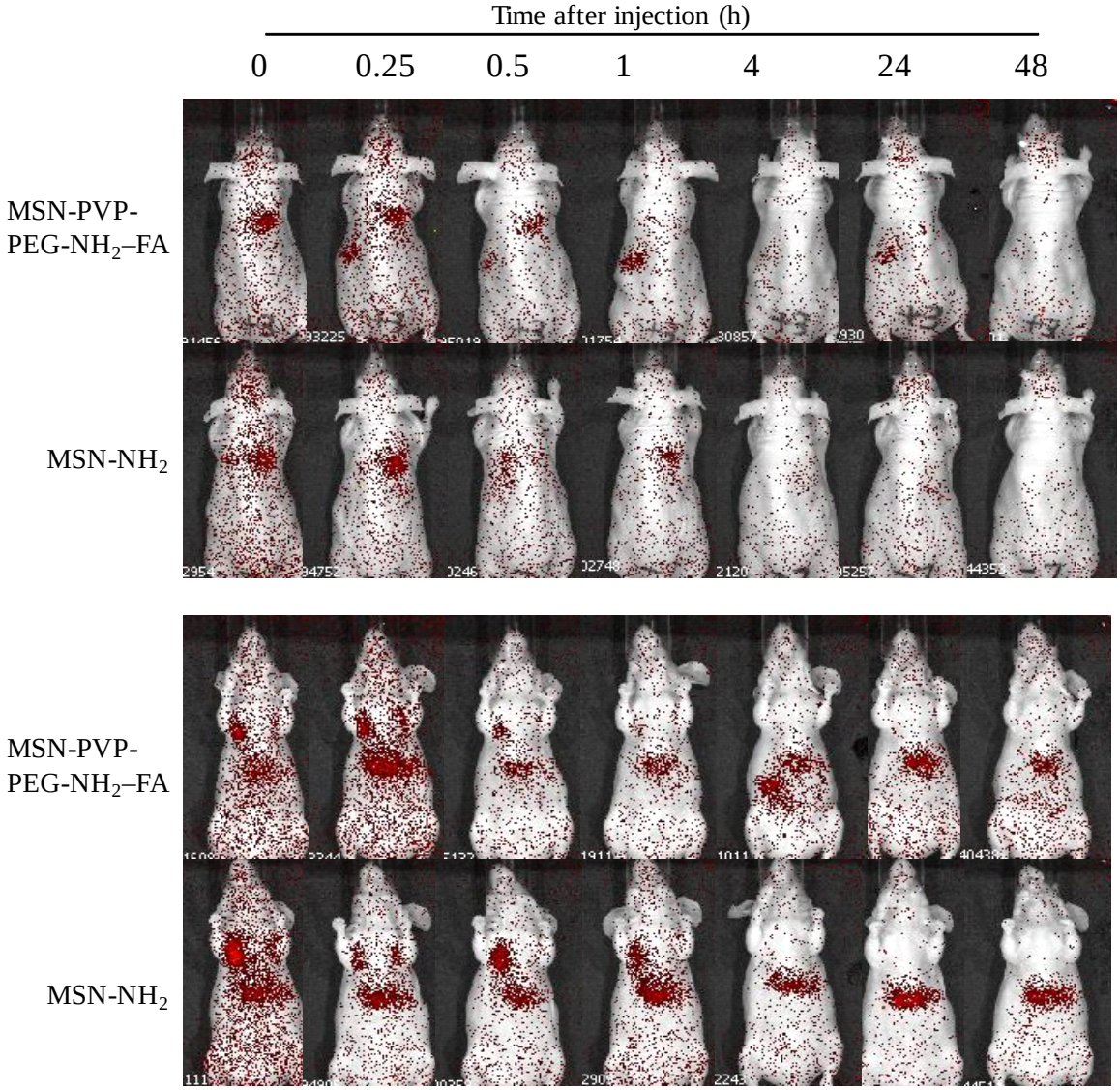

Figure 28: Biodistribution upon systemic administration. Cy7-loaded functionalized (MSN-PVP-PEG-NH_2-FA) and unfunctionalized (MSN-NH_2) particles were injected intravenously and NIR imaging was performed immediately. Time dependent distribution over 48 hours. The upper panel shows dorsoventral and the lower panel ventrodorsal images of mice. One representative mouse per group is shown. The color scale (efficiency) had a minimum of $1.3e^{-8}$ and a maximum of $6.0e^{-8}$ fluorescent photons/incident excitation photon.

2.5.2. Biocompatibility after systemic administration of MSN

To test the biocompatibility of mesoporous nanoparticles and to exclude the possibility of acute toxic effects after single dose application clinical chemistry parameters were analyzed. Tumor free NMRI nude mice (n = 9) were euthanized 48 hours after intravenous administration of a 100 µg (5 mg/kg) dose of functionalized (MSN-PVP-PEG-NH_2-FA) and unfunctionalized

(MSN-NH_2) particles or control (HEPES buffered glucose, HBG). Blood was collected in serum tubes. Serum parameters are shown in Table 1. Compared to the control group, treatment with both particle types showed no deviation of alanine transaminase (ALT) and aspartate transaminase (AST) levels implying intact liver function. Furthermore, serum creatinine levels and blood urea nitrogen (BUN) did not alter, proving that treatment did not compromise kidney function. Besides, histopathological examination of liver, lung, spleen and kidney were carried out. Organs were dissected, fixed in formalin, embedded into paraffin and stained with eosin and haematoxylin. Both particle types exhibited no histological disturbances compared to the HBG (control) treated group (Figure 29).

Table 1: Clinical chemistry parameters. Values shown: alanine transaminase (ALT); aspartate transaminase (AST); creatinine, blood urea nitrogen (BUN).

Treatment group	**ALT (U/l) ± SD**	**AST (U/l) ± SD**	**Creatinine (mg/dl) ± SD**	**BUN (mg/dl) ± SD**
control	33.9 ± 12.9	54.7 ± 14.1	0.3 ± 0.0	47.3 ± 8.5
MSN-PVP-PEG-NH_2–FA	43.2 ± 13.6	59.2 ± 12.1	0.3 ± 0.0	43.9 ± 6.7
MSN-NH_2	32.5 ± 2.5	51.9 ± 2.1	0.3 ± 0.0	47.4 ± 6.5

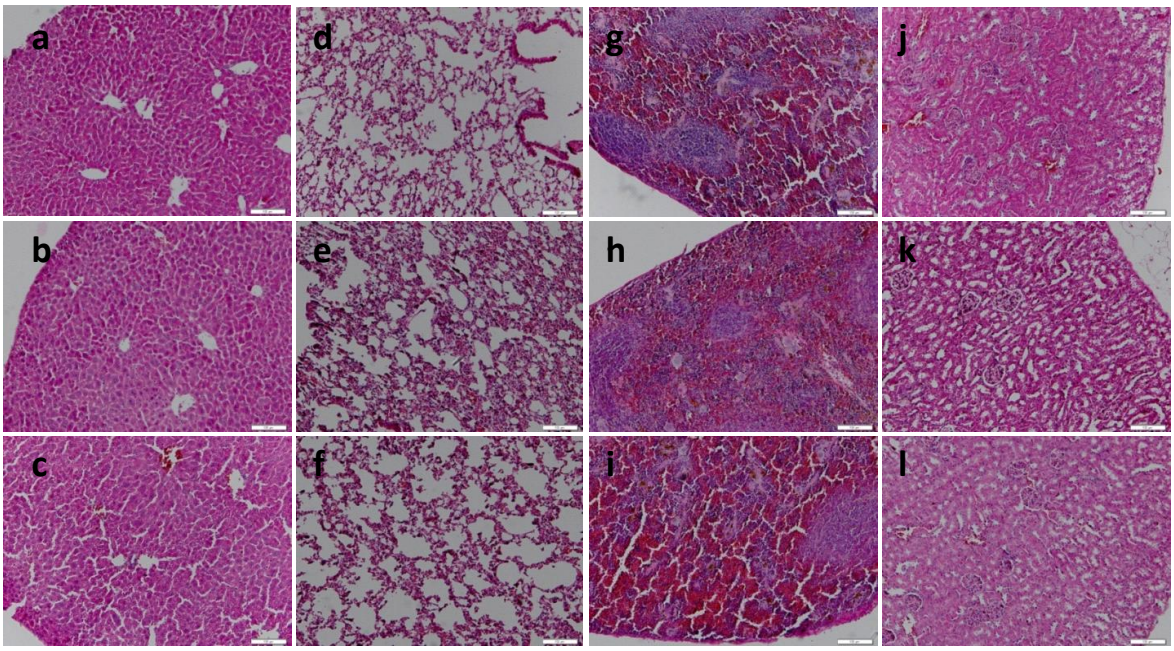

Figure 29: Histopathological sections 48 hours after systemic treatment with control (HBG), functionalized (MSN-PVP-PEG-NH_2-FA) and unfunctionalized (MSN-NH_2) particles. a) Liver after treatment with HBG, b) functionalized MSN and c) unfunctionalized MSN. d) Lung after treatment with HBG, e) functionalized MSN and f) unfunctionalized MSN. g) Spleen after treatment with HBG, h) functionalized MSN and i) unfunctionalized MSN. j) Kidney after treatment with HBG, k) functionalized MSN and l) unfunctionalized MSN. One representative image is shown. The scale bars represent 100 µm.

2.5.2.1. Biocompatibility with increased dosages of MSN

To test the biocompatibility of MSN with increased dosages a further experiment was carried out subsequently. Tumor free NMRI nude mice (n = 8) were divided into four groups and injected intravenously with a 1.6 mg (80 mg/kg) or 2 mg (100 mg/kg) dose of functionalized (MSN-PVP-PEG-NH_2-FA) and unfunctionalized (MSN-NH_2) particles. Intravenous administration of MSN was repeated after one week. Neither single nor second application of both dosages mediated any visual sign of toxicity.

2.5.3. Tumor-targeting after systemic injection of MSN

In a next step, biodistribution and tumor targeting upon systemic administration of MSN was investigated using confocal microscopy in a subcutaneous mouse tumor model with FA receptor overexpressing MDA MB 231 (breast adenocarcinoma) cells in NMRI nude mice (n = 9). Subcutaneous tumor bearing mice were injected intravenously *via* tail vein with functionalized but untargeted (MSN-PVP-PEG-NH_2) and FA targeted (MSN-PVP-PEG-NH_2-FA) particles

loaded with fluorescent dyes (calcein and covalently linked ATTO 633). The control group was injected with HBG. After 3 hours mice were euthanized, tumors and organs (liver, lung, spleen and kidneys) were dissected, prepared for cryosections and stained with DAPI. Figure 30 shows slices of cryosections analyzed *via* confocal microscopy. The highest accumulation of particles, visible as red dots (ATTO 633), can be seen in spleen followed by liver and lung but no particles can be seen in kidneys. Calcein loading was not detectable presumably due to the very weak signal and the high autofluorescence of the tissue in the region of calcein-detection (data not shown). Of note, both particles also accumulate passively in tumor. The active targeting abilities of FA targeted particles could not be evaluated within this experimental setting and have to be investigated further.

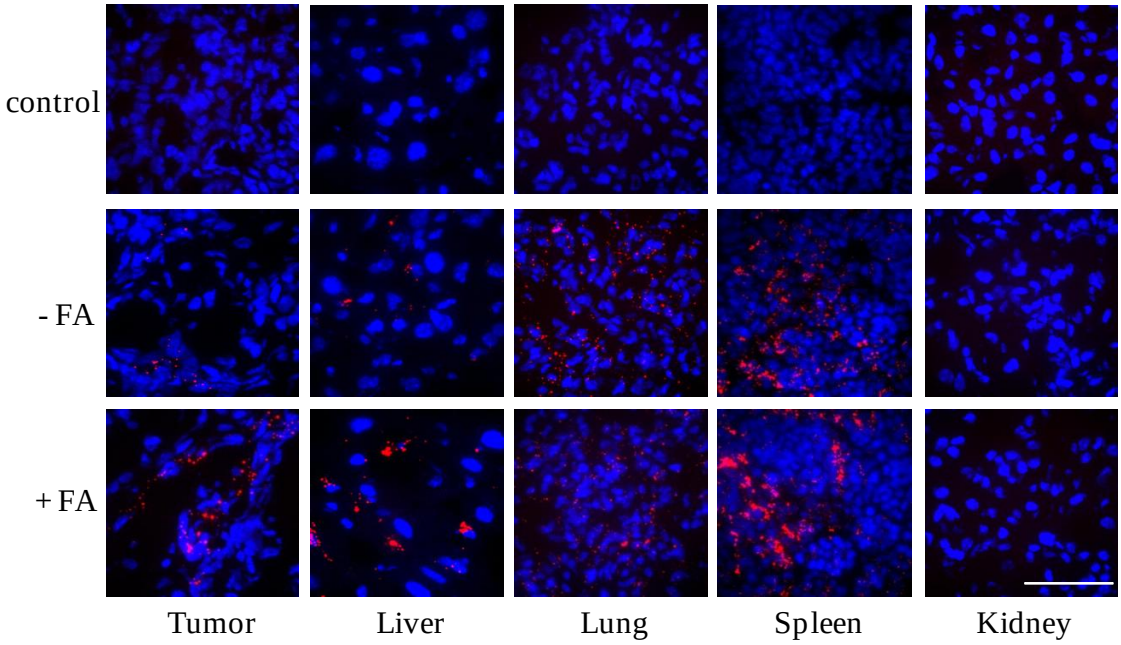

Figure 30: Distribution of MSN in a tumor mouse model. Passive tumor targeting of functionalized untargeted MSN-PVP-PEG-NH_2 and folic acid (FA) targeted MSN-PVP-PEG-NH_2-FA after systemic injection into MDA MB 231 tumor bearing mice. Cryosections of tumor, liver, lung, spleen and kidney 3 hours after injection. One representative mouse per group is shown, one mouse per horizontal row. Cell nuclei were stained with DAPI (blue) and particles with ATTO 633 (red). Images were taken with 63 x magnification. The scale bar represents 50 µm. Slices were analyzed by Veronika Weiss (PhD student, LMU, Department of Chemistry).

2.5.4. Retention of MSN in subcutaneous tumors

The retention efficacy of FA ligand containing MSN was investigated in a subcutaneous mouse tumor model with FA receptor overexpressing KB (human cervix carcinoma) cells in NMRI nude mice (n = 6) using NIR imaging. Subcutaneous tumor bearing mice were injected intratumorally with Cy7-labeled functionalized FA targeted (MSN-PVP-PEG-NH_2-FA) and untargeted (MSN-PVP-PEG-NH_2) MSN. Figure 31 shows total flux per tumor normalized to the initial value for one week after injection of MSN. Slightly increased retention for the FA modified particles could be observed within the first few hours compared to untargeted particles. Both particles displayed prolonged retention in tumors for more than one week (experiment had to be terminated as tumors became too big in size which is one of the human end points) compared to lower persistence upon systemic administration.

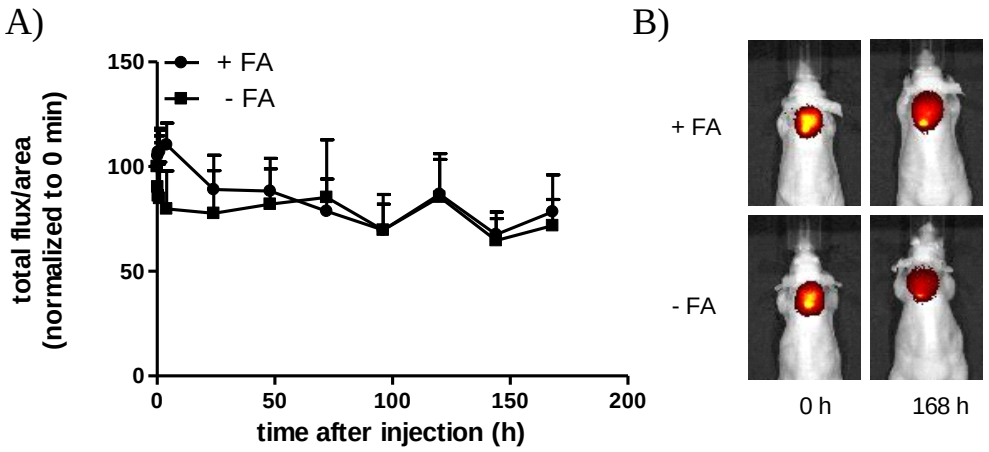

Figure 31: Retention of MSN in the tumor tissue. Folic acid (FA) targeted (MSN-PVP-PEG-NH_2-FA) and untargeted (MSN-PVP-PEG-NH_2) MSN labeled with Cy7 were injected intratumorally into KB tumor bearing mice. NIR imaging was performed for 7 days after application of MSN. A) Fluorescence signals of tumors were counted as total flux/area (photons/second/cm^2) and normalized to 0 minutes (min). Represented is the mean ± S.E.M. of three mice per group. B) Representative images of targeted (top) and untargeted (bottom) MSN in tumors.

IV. DISCUSSION

1. Polymeric nucleic acid carriers for tumor targeted gene delivery

1.1. In vivo evaluation of polypropylenimine dendrimers

In this chapter synthetic nucleic acid carriers based on the precise, symmetrical PPI dendrimer structure were evaluated in terms of their transfection efficacy. Modification of synthetic vectors while maintaining a defined structure reveals a great opportunity to overcome different obstacles in gene delivery. Increased molecular weight of the polymers can on the one hand improve transfection efficacy but on the other hand might result in increased cytotoxicity [88]. It is known that environment-triggered biodegradation can solve this problem [27, 89, 90]. Therefore, the octavalent polypropylenimine core (PPI G2) was attached with increasing units of small sequence-defined oligomers based on the oligoamino acid succinoyl-tetraethylene pentamine (Stp) [92]. Sequence-defined Stp polymers had been generated in precise form by solid-phase synthesis [92, 94, 162]. Biodegradability of Stp-linked PPI dendrimers results from reducible disulfide linkages through the incorporation of cysteines for which reason the Stp modified conjugates dissociate in the reducing cytosol environment (Figure 2).

In previous *in vitro* experiments the PPI conjugate with 5 Stp units (**536**/PPI-Stp5) revealed the most promising characteristics for *in vivo* application such as high transfection efficacy, good pDNA binding ability, low cytotoxicity and high endosomal buffering capacity and was subsequently chosen for systemic *in vivo* experiments. A higher luciferase gene expression in lung and liver was obtained with unmodified PPI G2 polyplexes (Figure 6). Aggregation of PPI G2 polyplexes into micrometer-sized structures could lead to their accumulation and entrapment in lung capillaries explaining the undesirable luciferase expression in this organ [163, 164]. Tang *et al*. also showed that DNA complexes of unmodified dendrimers generally appear as clusters in electron micrographs and have diameters in solutions larger than 1 µm [165]. In contrast, the modified conjugates are smaller (about 267 nm) and could therefore have a better systemic distribution and accumulation in the tumor tissue due to the so called enhanced permeability and retention (EPR) effect [50] explaining the significantly higher tumor luciferase expression of the **536**/PPI-Stp5 conjugates compared to the control PPI G2 polyplexes. This promising *in vivo* data illustrates the conversion of unmodified Stp which is ineffective [166] due to its small size into potent gene carriers upon attachment to PPI. This concept presents a platform of several modifications for future experiments such as better

stabilizing [95], targeted and shielded [70] sequence-defined oligomers to further improve gene delivery.

1.2. Effect on transfection efficacy *in vivo* upon incorporation of histidines

Next, precise, tunable structures with multiple functional domains were generated [167, 168] using solid-phase synthesis with Stp and succinoyl-pentaethylene hexamine (Sph). The Sph building block showed an improved nucleic acid compaction and gene transfer *in vitro* [162] which is in line with our preliminary *in vitro* experiments yielding the most promising results with this structure, thus it has undergone further investigations. A bottleneck in transfection process after cellular uptake is the escape of polyplexes from endolysosomes to reach the cytoplasm. The so called "proton sponge hypothesis" postulates improved transfection results by cationic delivery agents with high endosomal buffering capacity [48]. The endosomal escape is caused by chloride and water accumulation in the endosomes leading to osmotic pressure. Triggered by the concomitant increase of positive polymer charges in the endosomes, vesicles lyse consequently and release their content into the cytosol [47]. Histidine residues become cationized upon protonation of their imidazole rings, thus enhancing endosomal buffering capacity [49].

Polymers based on the building block Sph modified with histidines in the polycationic backbone (**606**/Sph-HC) and the histidine-free analog (**608**/Sph-AC) were compared with their transfection efficacy after intravenous administration into tumor bearing mice (Figure 8). The transgene expression in the Neuro2A tumor tissue 48 hours after injection was approximately 32-fold higher with the histidinylated polymers compared to its histidine free analog, implying a critical impact of histidines on gene transfer. Remarkably, gene expression levels in tumors were higher than in lung, liver, spleen, kidney and heart in the case of the histidinylated polymers. Which, in fact, is in accordance with the high density of blood vessels and low amount of infiltrating macrophages in Neuro2A tumors [169]. These characteristics cause on the one hand good DNA uptake into the tumor and on the other hand low DNA degradation and therefore facilitate high gene expression. Expression levels in lungs were 30-fold lower than in tumor compared to the high molecular weight linear polyethylenimine (LPEI), a cationic polymer also labeled as "gold standard" for pDNA delivery, which mediates 100-fold higher transfection levels in lungs than in Neuro2A tumors [170]. The good toleration of the polymers investigated in this experiment compared with LPEI 22 kDa [88, 170] and the far lower lung expression are in accordance with their lower molecular weight.

1.3. Evaluation of targeted c-Met-directed polymers for efficient gene transfer *in vivo*

Instead of passive targeting, another strategy to facilitate uptake of delivery agents into the tumor tissue is active targeting *via* targeting ligands. The c-Met/hepatocyte growth factor receptor (HGFR) is overexpressed in many tumors and hence displays an interesting target receptor in cancer therapy. The c-Met binding ligand cMBP2 with the amino acid sequence KSLSRHDHIHHH has previously been reported by Kim *et al*. In their study they showed targeting *in vitro* and *in vivo* with the radiolabeled (^{125}I) peptide here called cMBP2 [171] and proved its application as a specific optical imaging system [172]. Another c-Met binding peptide with the amino acid sequence YLFSVHWPPLKA was already tested as radioiodinated diagnostic agent for tumor imaging [173]. Yet, targeting c-Met has not been applied for gene delivery so far. Because its superiority over the other c-Met binding peptide (Petra Kos, PhD thesis 2014, LMU) the cMBP2 ligand was conjugated to sequence-defined oligomers composed of the artificial amino acid Stp for alleviation of gene delivery, histidines for increased buffering capacity as described before, terminal cysteines for increased polyplex stability and polyethylene glycol (PEG) units for surface shielding (Scheme 1). Targeted polyplexes were investigated *in vivo* in a xenograft tumor mouse model and compared to their untargeted control.

1.3.1. After intratumoral administration

In the first *in vivo* experiments, polyplexes were injected locally into subcutaneous c-Met overexpressing Huh7 tumors. Here, two-arm polymers with two different amounts of PEG_{24} units for surface shielding were investigated. Surface modification of delivery agents with PEG, a hydrophilic molecule, has been verified as a strategy to increase the solubility of hydrophobic drugs, prolong circulation times and reduce unspecific interactions with blood components like the complement system. By passive targeting it causes a higher accumulation at the tumor-site and can facilitate the incorporation of active targeting ligands additionally [174]. The PEG content has an influence on the polyplex biodistribution and the ligand accessibility but it can also reduce reporter gene expression [175-178].

We demonstrated that the cMBP2-targeted polymers, regardless of the amount of PEG shielding (**442**/cMBP2-1PEG and **694**/cMBP2-2PEG), showed much higher gene expression in tumor than their alanine control analogs (**440**/Ala-1PEG and **616**/Ala-2PEG) (Figure 9-A) favoring polymers with only 1 PEG_{24} chain. A proof for specificity of the targeting mechanism is given by the structural identity of both polyplexes apart from the cMBP2 ligand.

To investigate the retention capability in the tumor tissue, targeted and untargeted polyplexes were locally injected and their elution from the tumor was followed up for several days (Figure 10). Both particles remained in tumor over 72 hours, however, the non-targeted particles (**440**/Ala-1PEG) had a slightly shorter retention time as only a barely visible signal could be detected for the last time point. Moreover, a small part of these particles was immediately washed out of the tumor. Overall, a significantly different retention time could not be demonstrated within this experimental setting. One reason therefore might be the size of the polyplexes (approximately 200-400 nm) as they are more rigid once applied into the tumor tissue than smaller untargeted particles which - since unbound - can easier access the blood vessels and hence yield a significant retention effect [179].

1.3.2. After systemic administration

Although cMBP2-targeted polymers yielded a high gene expression upon local administration, in most cases an intratumoral application of therapeutics cannot be considered. Hence, for further investigations polyplexes were applied systemically. On its way to the tumor the cargo has to conquer several barriers. The complex has to be stable in the blood circulation, needs protection from unwanted interactions with other blood components and has to avoid activation of the complement system [180, 181]. Therefore, polymers were equipped with PEG shielding domains as described above.

In the first experiment the initial targeted and untargeted two-arm polymers were applied intravenously and transfection efficacy was measured after 48 hours (Figure 11). In contrast to the previous results upon local administration and although the amount of injected pDNA was increased for systemic administration, no cMBP2 targeting effect was obtained. Which, in fact, is underlining the special requirements and configurations of polyplexes for systemic delivery. Despite the application of polymers with one PEG_{24} chain and without disregarding the advantages of surface shielding, the PEG content is still very high because the polymers contain equal numbers of ethylene glycol units as protonatable Stp nitrogens. In a previous *in vitro* study this constitution resulted in insufficient pDNA condensation, presumably due to the interference with the PEG chains, and therefore form more loose structures [70]. Hence, polymers were designed towards the opposite direction to an augmented dimension of the polycationic part of the polymers. Adding extra polycationic arms has already previously been shown as favorable in the gene delivery process [94, 162]. Furthermore, the polycationic backbone of the polymers was rearranged from Stp to Sph building blocks. This replacement with the Sph building block was based on recent findings of improved gene transfer with this

novel building block [162]. Targeted and untargeted polymers now having four instead of two polycationic arms in the carrier backbone were applied intravenously. Although they did not show a beneficial effect upon *in vitro* transfections (Petra Kos, PhD thesis 2014, LMU), with these carriers a slight cMBP2 targeting effect in tumor was obtained. Tumor expression levels were similar to those in liver and lung (Figure 12).

To further enhance transfection efficacy and cMBP2 tumor-targeting upon systemic administration, another approach in the design of polymers was considered. This time polymers were not directly tuned in their chemical composition, but the desired features - pDNA compaction plus surface shielding with targeting - were spread to two unequal sequence-defined polymers, one with and one without PEG_{24} units. As mentioned above, PEG chains can shield the surface but are not advantageous invariably. They presumably interfere with the pDNA condensation process compared to PEG-free analogous polyplexes which form a compact shape of rod- or toroid-like structures unlike loose "spaghetti-type" structures which were formed by polyplexes with PEG units [70]. Thereupon, the initial targeted two-arm polymer (**442**/cMBP2-1PEG) was mixed with a non-shielded three-arm polymer (**689**) in a ratio of 70:30. This 30 percent co-addition of non-shielded polymers revealed change in shape to round-shaped particles compared to rather spaghetti-like structures obtained before (Dr. Petra Kos, Dr. Markus Döblinger, LMU, unpublished data not shown). These bi-polymeric particles greatly enhanced gene transfer in the tumor tissue in sharp contrast to mono-polymer **442**/cMBP2-1PEG polyplexes (Figure 13-A+B).

Despite these results we were interested whether this beneficial effect is specific to the co-added polymer **689** or whether it can be achieved by any non-shielded polymer. Instead of the three-arm polymer with Stp building blocks in the carrier backbone, now the four-arm polymer with Sph building blocks (**606**) was mixed with the initial shielded and targeted two-arm polymer (**442**/cMBP2-1PEG) in the same ratio as before (30:70) and was applied intravenously. This time, a significant tumor targeting effect was achieved again but was associated with an increased gene transfer in the lung (Figure 14) stating that non-shielded polymers cannot be added arbitrarily. To improve gene transfer polymers have to be carefully selected and refined for special requirements of systemic *in vivo* application which obviously cannot always be identified by sole *in vitro* testing.

2. Circumventing chemoresistance of cancer

2.1. Salinomycin as a potential additive compound to hamper metastasis

Chemoresistance of cancer is a major drawback in the successful treatment of cancer patients. An important mechanism of resistance formation to chemotherapeutic drugs are cancer stem cells (CSCs). These cells within a tumor are able to self-renew after chemotherapy and are therefore responsible for relapse [101, 102]. Salinomycin was recently found to selectively target CSCs [122]. In this work it was analyzed whether this novel anticancer drug has an influence on tumor growth and tumor metastasis *in vivo* in a syngeneic mouse model. Murine 4T1-Luc breast cancer cells originating from BALB/c mice are stably expressing luciferase which enables tracking of tumor growth and tumor cell dissemination *via* bioluminescence imaging.

First, a tumor mouse model using the classical drug doxorubicin was established for subsequent combinatorial treatment with salinomycin. Here, a dosage needed to be found that is high enough to mediate a cytotoxic effect but low enough to leave some expansion space for beneficial effects of a combinatorial treatment. Thus, three different dosages of doxorubicin (2 mg/kg, 5 mg/kg and 8 mg/kg) were evaluated regarding their compatibility, tumor growth and metastasis formation to a new tissue which was primarily the lungs (Figure 15, 16, 17). 4T1 breast cancer cells were inoculated orthotopically into the mammary fat pad of BALB/c mice within this tumor model and metastasis formation was monitored. The highest dosage led to severe weight loss therefore the mice had to be euthanized ahead of time. 5 mg/kg doxorubicin revealed tumor growth inhibition but also severe weight loss thus the dosage was still too high. The lowest dosage mediated no tumor size reduction but, of note, implied an enhanced metastasis formation to the lungs instead of an expected inhibition. However, these results have to be validated by larger group numbers. Doxorubicin is inducing cytostatic effects as well as dose dependent cancer cell migration by activating TGFβ signaling as shown by Bandyopadhyay *et al*. TGFβ signaling is known to induce epithelial to mesenchymal transition (EMT) [182]. EMT, a developmental program leading to invasive and migratory properties of cancer cells, is also able to generate stem cell-like cells resulting in resistance to chemotherapy [103, 104].

The CSCs targeting drug salinomycin was first tested regarding its effect on reducing tumor growth *in vivo*. Thus, a simplified setup with subcutaneous 4T1-Luc tumors in the flanks of the mice was used. Gupta *et al*. showed tumor size reduction of SUM159 human breast tumors in NOD/SCID mice with daily intraperitoneal injections of 5 mg/kg salinomycin for 5 weeks

[122]. In our tumor growth experiment treatment of 4T1-Luc tumors with salinomycin only mediated a minor effect on tumor size on the final day (Figure 18). We injected the same amount of salinomycin intraperitoneally but only for six times between day 3 and 15 after tumor implantation. 4T1-Luc tumors become necrotic after that short period although they were less than 600 mm^3 in size when the experiment had to be terminated to guarantee proper results for further *in vitro* experiments and to keep the mice in a good general condition. Dosage and treatment intervals were not increased as the mice turned out to be apathetic for a couple of hours after injection of salinomycin which could be based on the recently described neurotoxic side effects [183]. Another issue of 4T1-Luc tumors is their poor blood supply what could also explain the minor effect on tumor size reduction as only a smaller amount of salinomycin is able to reach the tumor. Subsequent *in vitro* investigation of tumors revealed increased apoptosis, an increased miR-200c expression, elevated E-cadherin protein levels and an epithelial-like tumor after salinomycin treatment. Hence, treatment led to an induction of mesenchymal to epithelial transition (MET) (Florian Kopp, PhD thesis 2013, LMU).

Based on these results and on encouraging preliminary *in vitro* experiments showing inhibitory effects of salinomycin on cell migration (Florian Kopp, PhD thesis 2013, LMU) we were also interested whether salinomycin was able to prevent metastasis *in vivo*. Because CSCs have been proposed to be in charge of colonization at secondary organs upon metastatic spreading [184] the question came up whether the inhibition of CSCs by salinomycin was accompanied by reduced metastasis formation *in vivo*. In this experiment 4T1-Luc cells were injected intravenously to specifically examine the final steps of metastasis, thus they form primary tumors almost without exception in the lungs. Mice were treated with salinomycin also before tumor cell inoculation to imitate a treated primary tumor aiming to prevent metastasis formation. This colonization experiment was terminated already on day 13 after tumor cell injection as mice started to lose weight due to the pulmonary tumor burden. Besides, this period was long enough to measure the luciferase signal through bioluminescence imaging (Figure 20, 23). One mouse of the control group had to be euthanized already earlier due to severe central nervous disorders what later turned out to be a matter of brain metastases. Primary tumor formation and growth in the lungs was not significantly affected with salinomycin treatment as also observed in the subcutaneous tumor growth model (Figure 21). In contrast, Gupta *et al.* showed a 4-fold reduction of lung tumor burden three weeks after intravenous injection of 4T1 cells into BALB/c mice. However, they pretreated 4T1 cells for four days *in vitro* with salinomycin compared to compound treatment of mice in our experiment, for which reason a direct comparison is very difficult [122]. Subsequent *in vitro* analysis of lung tumors revealed

considerably elevated miR-200c levels according to the subcutaneous 4T1-Luc tumors treated with salinomycin (Florian Kopp, PhD thesis 2013, LMU). Remarkably, metastases in brain, spleen and kidneys were significantly reduced after treatment with salinomycin determined by *ex vivo* luciferase measurements (Figure 22). These results suggest that salinomycin is capable to induce MET leading to significantly decreased metastasis formation to secondary organs. In summary, salinomycin treatment causes less migratory capacity of tumor cells, less metastasis and higher susceptibility to classical chemotherapy due to the induction of MET.

Therefore, salinomycin as a drug targeting CSCs might be an interesting candidate for combinatorial therapies together with agents targeting non-CSCs within tumors specifically as tumors contain different cellular phenotypes. Oak *et al*. demonstrated efficient killing of HER2 positive cells and CSCs upon treatment with the anti-HER2 monoclonal antibody trastuzumab and salinomycin opening an interesting possibility for further combinatorial treatments with salinomycin [185]. Kim *et al*. proposed an increased sensitivity of cancer cells to the apoptotic effects of doxorubicin associated with an increased DNA damage upon treatment with salinomycin *in vitro* [186]. Thus, the efficacy of salinomycin as an additive compound to the classical chemotherapeutic drug doxorubicin, an anthracycline antibiotic intercalating DNA, was investigated in the previously established syngeneic tumor mouse model. Based on those results of the dose finding experiment we decided to apply 3.5 mg/kg doxorubicin, the dosage of salinomycin was maintained with 5 mg/kg. 4T1-Luc cells were inoculated into the mammary fat pad and 24 hours later treatment with doxorubicin started and was repeated once a week compared to every six days in the preliminary experiment. These settings were changed with regard to the combinatorial treatment with salinomycin. Due to the slight toxic effect upon application of this drug we wanted the mice to recover completely before treatment with doxorubicin, thus the treatment intervals had always been the same. Combinatorial treatment with salinomycin and doxorubicin did not yield beneficial effects on tumor growth reduction. Only doxorubicin reduced the tumor burden significantly upon both single and combinatorial application (Figure 24). At the end of the trial metastasis formation to the lungs was again evaluated using bioluminescence imaging. Of note, some mice did not develop metastasis formation to the lungs implicating the problems of metastasis models. One reason could be an inhomogeneous inoculation of tumor cells into the mammary fat pad and into unequal areas more or less vascularized. On the contrary, intravenous injection of tumor cells led to a homogeneous colonization in the lungs within all mice implicating an advantage over the intramammary tumor model with spontaneous metastasis. Mice without metastases in the lungs were excluded from the analysis but this time neither single nor combinatorial treatment could

hamper metastasis formation significantly (Figure 25). However, different pharmacological parameters within the intramammary tumor model compared to the intravenous tumor model have to be considered. In future experiments the dosage of doxorubicin could be changed since this has a high impact on displaying beneficial effects with other compounds and the beginning of salinomycin treatment could be preponed to refine its effects. Despite these results salinomycin is still an interesting candidate for combinatorial treatments with other drugs. Besides, further *in vitro* processing still has to be performed. However, these findings illustrate once more the complexity of *in vivo* experiments and their implementation. Consequently, the experimental setups for further metastasis experiments should be revised and new tumor models should be considered such as further cancer cell lines.

2.2. Efficacy of mesoporous nanoparticles as tumor targeted delivery agents circumventing chemoresistance

A major drawback in the cure of cancer remains the multiple drug resistance (MDR) to free chemotherapeutic drugs and the severe toxic side effects of free chemotherapeutics to normal tissues due to the lack of tumor-selectivity [140]. Mesoporous nanoparticles are expected to overcome these obstacles by reversing MDR. Thus, a developed multifunctional drug delivery vehicle based on a mesoporous silica core with a pH-responsive polymer coating was investigated *in vivo* in terms of biodistribution, biocompatibility and tumor targeting.

First, the biodistribution of mesoporous silica nanoparticles (MSN) functionalized with the PVP/PEG coating and the folic acid (FA) ligand was evaluated and compared to unfunctionalized MSN without coating. Within the first trial the fluorescent dye Cy7 was covalently linked to the amino-groups on the outside of the particles. Near infrared fluorescence imaging revealed a sufficient signal with 5 mg/kg MSN and preferred accumulation of both particle types in liver and spleen (Figure 27). These results are in line with similar findings made by Wu *et al*., who investigated biodistribution of MSN for the first time by magnetic resonance imaging (MRI) and found an accumulation in liver and spleen [187]. This accumulation in healthy tissues can enhance side effects, should be substantially reduced and the accumulation in tumor maximized. Modification of the surface with PEG can reduce uptake of MSN by the reticuloendothelial system (RES) and increase the blood circulation time [188, 189]. Though this could not be observed within our experiment, dependance on amount, density and length of PEG has to be considered [190]. He *et al.* investigated *in vivo* biodistribution of MSN with several particle sizes (80 - 360 nm) and the effect of PEGylation and observed that MSN and PEG-MSN both mainly accumulate in liver and spleen and a minority in lung whereas

MSN in the size of 360 nm were easier captured by the organs [191]. The biodistribution of our PVP/PEG coated MSN are comparable with other studies published to date which mainly observe accumulation in spleen and liver. Although no clear effect upon PVP/PEG coating could be demonstrated within these experimental settings, particle size, shape and surface modification can affect biodistribution kinetics [191]. We could observe a signal in the bladder occurring 15 minutes after injection (Figure 27) what raised the question about the excretion of the particles. Degradation and elimination of MSN are investigated in many studies, but the wide variety not only of the particles itself but also of study designs and lack of standardization makes a comparison quite difficult. The porous structure and thus the large surface area of MSN are beneficial for accelerating degradation, but their chemical stability is generally higher than for organic particles [131] and the *in vivo* long-term effect of non-degraded particles is still unknown. Renal elimination of intact MSN through urine has been reported [192, 193] although their particle size is beyond the renal cut off limit of 4.5 - 5 nm [194], but the exact excretion process remained unclear in this case. Another elimination route of MSN is hepatobiliary excretion which has been shown by Lu *et al* [195]. This demonstrates the exceptional diversity of several MSN and their behavior meaning that unification could be beneficial for future experiments. Due to the bladder signal we wanted to investigate the stability of particles and the attachment of the fluorescent dye to the outer surface. Therefore, a second experiment was carried out with Cy7 linked to the inner surface of MSN. This time no bladder signal occurred implying a good particle stability in the blood circulation and a stable attachment of dye to particle although the signal intensity was lower compared to the attachment outside (Figure 28). To evaluate the biocompatibility of these MSN and to exclude the possibility of acute toxic effects after single dose application clinical chemistry parameters were analyzed. Compared to the control group, single treatment with functionalized (MSN-PVP-PEG-NH_2-FA) and unfunctionalized (MSN-NH_2) particles showed no deviations from liver and kidney parameters, (Table 1) and histopathological examinations showed no disturbances (Figure 29). Increased dosage with 80 and 100 mg/kg mediated no visual toxic effects. These findings are in accordance with He *et al*., they observed no tissue toxicity for MSN and PEG-MSN in one month [191]. Nevertheless, synthesis, particle size, morphology, surface modification, dosage and administration routes play an important role in hematological and histological biocompatibilities of MSN and have to be considered carefully. In addition, there are still many unknown issues that have to be addressed in the future like neuro-, brain- and reproductive toxicity or long term safety for up to one year [131].

Targeting of nanoparticles to the tumor can be achieved by the EPR effect as mentioned earlier and enhanced with specific interactions between the nanoparticle and the cancer cell *via* active targeting using specific targeting ligands. Folic acid (FA) is one of the most studied targeting ligands for active targeting by MSN *in vivo*. Many tumor types possess an overexpression of folate receptors [64, 196] but its expression on normal tissue is limited [65], therefore folate receptor targeting is a frequently used model. Mamaeva *et al*. showed active folate receptor targeting with MSN after intratumoral and intravenous administration [197] and Lu *et al*. demonstrated successful tumor growth inhibition of pancreatic tumors with camptothecin loaded and FA modified MSN [193]. Due to their pH-responsive polymer coating, which enables controlled drug release, biodistribution and tumor targeting upon systemic administration of MSN with and without FA ligand was investigated in a subcutaneous mouse tumor model with folate receptor overexpressing MDA MB 231 tumors. Confocal microscopy of cryosections 3 hours after intravenous administration revealed again high accumulation in spleen and liver but also an accumulation in tumor for both MSN, presumably due to the EPR effect in this tissue (Figure 30). The active targeting abilities of FA targeted particles have to be evaluated further with quantitative measurements or chemotherapeutic drug loaded MSN.

To evaluate the retention time of FA targeted and untargeted MSN, they were injected locally into subcutaneous KB tumors as these are highly overexpressing the folate receptor and were monitored for one week. The results display just a slightly increased retention time for the FA modified particles within the first few hours compared to untargeted particles (Figure 31). This could be due to the large size of the particles because they cannot be washed easily out of the tumor as it has been shown for smaller nanoparticles [179] in the same tumor model. Both particles showed prolonged retention times in tumor for more than one week compared to lower persistence upon systemic administration making them attractive also for local applications with constant release of drugs. The experiment had to be terminated as tumors became too big in size, which is one of the human end points, thus it could not be exactly defined how long the particles remained there.

In conclusion, the PVP/PEG coated MSN are promising particles for tumor targeted drug delivery but have to be refined concerning biodistribution and circulation times. Further experiments regarding the loading of drugs and their controlled release still have to be performed in the future.

V. SUMMARY

The high morbidity and mortality caused by cancer represents an urgent need to improve treatment of cancer patients. Insufficient success rates, side effects, therapy resistance and metastasis formation remain major drawbacks in the cure of cancer, despite of several treatment options. Therefore, we focused on two approaches to improve cancer treatment - tumor targeted nucleic acid delivery and prospects to circumvent chemoresistance.

Nucleic acid therapy shows great promise for the treatment of a broad range of genetically-based diseases. However, appropriate delivery of genes to target cells requires efficient delivery agents and displays a major challenge, hence three polymeric carriers were tested *in vivo*. First, the efficacy of biodegradable modified gene carriers was investigated. We could demonstrate that **536**/PPI-Stp5 carriers with a higher molecular weight led to enhanced transfection efficacy in tumor and reduced gene transfer in the healthy organs lung and liver compared to unmodified polypropylenimine dendrimers of the second generation (PPI G2). Secondly, escape from endosomes is a major challenge in gene delivery. Histidines are known to improve endosomal escape because they increase buffer capacity. Accordingly, *in vivo* transfection efficacy of polymers enriched with histidines was compared to a histidine free analog. This histidinylation led to an improved gene transfer in tumor which demonstrates the beneficial incorporation of such functional domains. Thirdly, active targeting *via* targeting ligands facilitates uptake of delivery agents into the tumor tissue. We demonstrated targeting of c-Met/hepatocyte growth factor receptor (HGFR), overexpressed in many tumors, using the c-Met binding peptide cMBP2 as targeting ligand. After intratumoral injection targeted polyplexes, regardless of the amount of PEG shielding, revealed high luciferase expression in tumor demonstrating the specificity of the targeting mechanism. For systemic application however, polymers with an augmented dimension of the polycationic part had to be formulated to mediate a slight targeting effect in distant tumors. A mixture of the targeted and shielded polymer with a non-shielded polymer, a new form of pDNA polyplex, resulted in successful systemic gene transfer. These results show that different requirements upon systemic application have to be fulfilled to obtain efficient gene carriers.

Acquisition of resistance to classical chemotherapeutics and formation of metastasis to secondary tissues remain enormous obstacles in the treatment of cancer. Cancer stem cells (CSCs) represent an important mechanism of chemoresistance and are known to be involved in tumor invasion and metastasis formation. Thus, the drug salinomycin, which was recently found to selectively target CSCs, is of particular importance for the search of new anticancer drugs.

Treatment with salinomycin resulted in significantly reduced metastatic tumor burden in a syngeneic mouse model. Concerning its effect on hampering tumor growth, salinomycin was not able to reduce the size of the tumor significantly. However, these findings suggest a combinatorial treatment with a classical chemotherapeutic drug. Therefore, we investigated the effect of treatment with doxorubicin and salinomycin on tumor growth and metastasis formation. Within our experimental settings we could not demonstrate a beneficial effect of salinomycin, yet we assume that the final outcome is associated with experimental setups.

Multiple drug resistance might be overcome by packing of drugs into nanoparticles. In this field mesoporous silica nanoparticles (MSN) are highly promising. Controlled drug release is a crucial point, therefore we evaluated pH-responsive coated MSN *in vivo* in terms of biodistribution, biocompatibility and tumor targeting. MSN, regardless of coating, revealed preferred liver and spleen accumulation but mediated no toxic side effects after single lower and repeated high dosage application. MSN accumulated passively in tumors to moderate extent after systemic injection and showed prolonged retention after local application.

In conclusion, this work deals with the *in vivo* evaluation of polymeric nanocarriers and strategies to circumvent chemoresistance. The results display encouraging options to improve cancer treatment which are a point of origin for further investigations.

VI. ZUSAMMENFASSUNG

Aufgrund der durch Krebs verursachten hohen Erkrankungshäufigkeit und Todesrate bedarf die Therapie von Krebspatienten einer dringenden Verbesserung. Unbefriedigende Erfolgsquoten, Nebenwirkungen, Therapieresistenzen und Metastasenbildung stellen trotz vielfältiger Therapiemöglichkeiten große Hindernissse im Kampf gegen den Krebs dar. Aus diesem Grund haben wir uns auf zwei Herangehensweisen konzentriert. Diese sind zum einen der zielgerichtete Transport therapeutischer Nukleinsäuren in den Tumor und zum anderen Aussichten die Bildung von Chemotherapeutika-Resistenzen zu umgehen.

Die Anwendung therapeutischer Nukleinsäuren ist sehr vielversprechend für eine große Anzahl an Krankheiten, die ihren Ursprung auf genetischer Ebene haben. Jedoch stellt der Transport von Genen in die Zielzellen eine der größten Herausforderungen dar. Hierfür werden effiziente Träger benötigt, weshalb wir drei verschiedene aus Polymeren bestehende Genfähren tierexperimentell getestet haben. Zuerst wurde die Wirksamkeit eines modifizierten, natürlich abbaubaren Trägers untersucht. Hierbei konnten wir zeigen, dass der Träger **536**/PPI-Stp5 mit einem erhöhten Molekulargewicht im Vergleich zu einem unmodifizierten Polypropylenimin aus der zweiten Generation (PPI G2) eine erhöhte Transfektionsrate in den Tumorzellen und einen reduzierten Gentransfer in den gesunden Organen Lunge und Leber bewirkte. Zweitens stellt das Entkommen der Genfähren aus dem Endosom eine weitere Herausforderung dar. Histidine sind bekannt dafür dieses Entweichen zu verbessern indem sie die Pufferkapazität erhöhen. Aus diesem Grund wurde die Wirksamkeit von mit Histidinen ausgestatteten Polymeren untersucht und mit Histidin-freien Analoga verglichen. Diese Histidinylierung führte zu einem verbesserten Gentransfer im Tumor, wodurch der Vorteil solch funktioneller Domänen dargestellt werden konnte. Drittens erleichtert aktives Ansteuern von Tumorzellen mithilfe von Liganden die Aufnahme der Genfähren. Unter Verwendung des Liganden c-Met-bindendes Peptid, cMBP2, steuerten wir den c-Met/Hepatozyten Wachstumsfaktor Rezeptor (HGFR) an, welcher in vielen Tumoren überexprimiert ist. Die Injektion der zielgerichteten Polyplexe in den Tumor führte ungeachtet der Höhe an Abschirmung mit PEG zu einer hohen Expression an Luciferase, wodurch die spezifische Wirkungsweise bewiesen werden konnte. Um einen zumindest leichten zielgerichteten Effekt nach systemischer Verabreichung zu erhalten wurden jedoch Polymere mit erhöhtem polykationischen Anteil benötigt. Erst eine Mischung aus zielgerichtetem abgeschirmten und nicht abgeschirmten Polymer, also eine neue

Art von pDNA Polyplex, führte zum Erfolg. Diese Ergebnisse machen die unterschiedlichen Anforderungen an eine Genfähre für die systemische Verabreichung deutlich.

Der Erwerb von Resistenzen gegenüber klassischen Chemotherapeutika und die Metastasierung in sekundäre Organe stellen immer noch gewaltige Hürden im Kampf gegen den Krebs dar. Krebsstammzellen verkörpern einen wichtigen Mechanismus der Chemoresistenz- Bildung und sind an Tumorinvasion und Metastasierung beteiligt. Aus diesem Grund ist Salinomycin, ein Medikament welches neulich als Krebsstammzell-spezifisch entdeckt wurde, von großem Interesse für die Suche nach neuen Krebstherapeutika. Die Behandlung mit Salinomycin führte zu einer erheblich reduzierten Tumor-Metastasierung in einem gen-identischen Mausmodell, ohne einen wesentlichen Einfluss auf das Tumorwachstum zu haben. Diese Erkenntnisse rechtfertigten eine kombinatorische Behandlungsstrategie mit einem klassischen Chemotherapeutikum. Daraufhin haben wir die Auswirkungen auf Tumorwachstum und Metastasierung nach kombinatorischer Behandlung mit Doxorubicin und Salinomycin untersucht. Wir konnten allerdings keine vorteilhafte Wirkung durch Salinomycin erreichen. Jedoch vermuten wir, dass das Ergebnis mit den Versuchsbedingungen zusammenhängt.

Die Mehrfachresistenz kann möglicherweise mithilfe der Verpackung von Medikamenten in Nanopartikel überwunden werden. Mesoporöse Nanopartikel aus Siliziumdioxid haben sich als sehr vielversprechend erwiesen. Die kontrollierte Medikamentenfreisetzung ist entscheidend, deshalb haben wir Partikel mit einer pH-abhängigen Hülle bezüglich ihrer Biodistribution, Verträglichkeit und Tumor-Ansteuerung getestet. Die Partikel zeigten unabhängig von ihrer Hülle eine bevorzugte Ansammlung in Leber und Milz und verursachten keine Nebenwirkungen sowohl nach einmaliger niedriger und zweimaliger Verabreichung einer höheren Dosis. Außerdem häuften sie sich nach systemischer Verabreichung in moderatem Umfang passiv im Tumor an und verweilten nach lokaler Verabreichung für längere Zeit im Tumor.

Zusammenfassend handelt diese Arbeit von der *in vivo* Testung von auf Polymeren basierenden Genfähren und Strategien zur Umgehung von Chemoresistenzen. Die Ergebnisse zeigen vielversprechende Ansätze zur Verbesserung der Krebstherapie auf, welche Ausgangspunkte für fortführende Untersuchungen darstellen.

VII. REFERENCES

1. Ferlay, J., Soerjomataram, I., Ervik, M., Dikshit, R., et al. *GLOBOCAN 2012 v1.0, Cancer Incidence and Mortality Worldwide: IARC CancerBase No. 11 [Internet]. Lyon, France: International Agency for Research on Cancer*. 2013; http://globocan.iarc.fr, accessed on 23/august/2014.
2. Ferlay, J., Shin, H.R., Bray, F., Forman, D., et al., *Estimates of worldwide burden of cancer in 2008: GLOBOCAN 2008.* Int J Cancer, 2010. **127**(12): p. 2893-917.
3. Bray, F., Jemal, A., Grey, N., Ferlay, J., et al., *Global cancer transitions according to the Human Development Index (2008-2030): a population-based study.* The Lancet Oncology, 2012. **13**(8): p. 790-801.
4. Wagner, E., *Functional Polymer Conjugates for Medicinal Nucleic Acid Delivery.* Adv. Polymer Sci., 2012. **247**: p. 1-30.
5. http://www.wiley.com//legacy/wileychi/genmed/clinical/.
6. Kircheis, R., Ostermann, E., Wolschek, M.F., Lichtenberger, C., et al., *Tumor-targeted gene delivery of tumor necrosis factor-alpha induces tumor necrosis and tumor regression without systemic toxicity.* Cancer Gene Ther, 2002. **9**(8): p. 673-680.
7. Raty, J.K., Pikkarainen, J.T., Wirth, T., and Yla-Herttuala, S., *Gene therapy: the first approved gene-based medicines, molecular mechanisms and clinical indications.* Curr Mol Pharmacol, 2008. **1**(1): p. 13-23.
8. Scott, D.W. and Lozier, J.N., *Gene therapy for haemophilia: prospects and challenges to prevent or reverse inhibitor formation.* Br J Haematol, 2012. **156**(3): p. 295-302.
9. Blaese, R.M., Culver, K.W., Miller, A.D., Carter, C.S., et al., *T lymphocyte-directed gene therapy for ADA- SCID: initial trial results after 4 years.* Science, 1995. **270**(5235): p. 475-480.
10. Verma, I.M. and Somia, N., *Gene therapy -- promises, problems and prospects.* Nature, 1997. **389**(6648): p. 239-42.
11. Zhang, G., Budker, V., and Wolff, J.A., *High levels of foreign gene expression in hepatocytes after tail vein injections of naked plasmid DNA.* Hum.Gene Ther., 1999. **10**(10): p. 1735-1737.
12. Liu, F., Song, Y., and Liu, D., *Hydrodynamics-based transfection in animals by systemic administration of plasmid DNA.* Gene Ther., 1999. **6**(7): p. 1258-1266.
13. Houk, B.E., Hochhaus, G., and Hughes, J.A., *Kinetic modeling of plasmid DNA degradation in rat plasma.* AAPS.PharmSci., 1999. **1**(3): p. E9.
14. Burke, R.S. and Pun, S.H., *Extracellular Barriers to in Vivo PEI and PEGylated PEI Polyplex-Mediated Gene Delivery to the Liver.* Bioconjug Chem, 2008. **19**(3): p. 693-704.
15. Xiang, S., Tong, H., Shi, Q., Fernandes, J.C., et al., *Uptake mechanisms of non-viral gene delivery.* J Control Release, 2012. **158**(3): p. 371-8.
16. Deng, Y., Wang, C.C., Choy, K.W., Du, Q., et al., *Therapeutic potentials of gene silencing by RNA interference: Principles, challenges, and new strategies.* Gene, 2014. **538**(2): p. 217-227.
17. Dauty, E. and Verkman, A.S., *Actin cytoskeleton as the principal determinant of size-dependent DNA mobility in cytoplasm: a new barrier for non-viral gene delivery.* J.Biol Chem, 2005. **280**(9): p. 7823-7828.
18. Lukacs, G.L., Haggie, P., Seksek, O., Lechardeur, D., et al., *Size-dependent DNA mobility in cytoplasm and nucleus.* J.Biol Chem, 2000. **275**(3): p. 1625-1629.

19. Brunner, S., Sauer, T., Carotta, S., Cotten, M., et al., *Cell cycle dependence of gene transfer by lipoplex, polyplex and recombinant adenovirus.* Gene Ther, 2000. **7**(5): p. 401-407.
20. Brunner, S., Furtbauer, E., Sauer, T., Kursa, M., et al., *Overcoming the nuclear barrier: cell cycle independent nonviral gene transfer with linear polyethylenimine or electroporation.* Mol.Ther., 2002. **5**(1): p. 80-86.
21. Li, S.D. and Huang, L., *Non-viral is superior to viral gene delivery.* J.Control Release, 2007. **123**(3): p. 181-183.
22. Gao, K. and Huang, L., *Nonviral methods for siRNA delivery.* Mol Pharm, 2009. **6**(3): p. 651-8.
23. Wagner, E., *Polymers for siRNA Delivery: Inspired by Viruses to be Targeted, Dynamic, and Precise.* Acc Chem Res, 2012. **45**(7): p. 1005-13.
24. Hughes, J., Yadava, P., and Mesaros, R., *Liposomal siRNA delivery.* Methods Mol Biol, 2010. **605**: p. 445-59.
25. Parker, A.L., Newman, C., Briggs, S., Seymour, L., et al., *Nonviral gene delivery: techniques and implications for molecular medicine.* Expert.Rev.Mol.Med., 2003. **5**: p. 1-15.
26. Felgner, P.L., Barenholz, Y., Behr, J.P., Cheng, S.H., et al., *Nomenclature for synthetic gene delivery systems.* Hum Gene Ther, 1997. **8**(5): p. 511-2.
27. Scholz, C. and Wagner, E., *Therapeutic plasmid DNA versus siRNA delivery: Common and different tasks for synthetic carriers.* J Control Release, 2012. **161**(2): p. 554-65.
28. Spagnou, S., Miller, A.D., and Keller, M., *Lipidic carriers of siRNA: differences in the formulation, cellular uptake, and delivery with plasmid DNA.* Biochemistry, 2004. **43**(42): p. 13348-56.
29. Wagner, E., Ogris, M., and Zauner, W., *Polylysine-based transfection systems utilizing receptor-mediated delivery.* Adv.Drug Deliv.Rev., 1998. **30**(1-3): p. 97-113.
30. Baker, A., Saltik, M., Lehrmann, H., Killisch, I., et al., *Polyethylenimine (PEI) is a simple, inexpensive and effective reagent for condensing and linking plasmid DNA to adenovirus for gene delivery.* Gene Ther., 1997. **4**(8): p. 773-782.
31. Zintchenko, A., Philipp, A., Dehshahri, A., and Wagner, E., *Simple Modifications of Branched PEI Lead to Highly Efficient siRNA Carriers with Low Toxicity.* Bioconjug Chem, 2008. **19**(7): p. 1448-1455.
32. Dufes, C., Uchegbu, I.F., and Schatzlein, A.G., *Dendrimers in gene delivery.* Adv Drug Deliv.Rev., 2005. **57**(15): p. 2177-2202.
33. Ogris, M., Steinlein, P., Carotta, S., Brunner, S., et al., *DNA/polyethylenimine transfection particles: Influence of ligands, polymer size, and PEGylation on internalization and gene expression.* AAPS.PharmSci., 2001. **3**(3): p. E21.
34. Boussif, O., Lezoualc'h, F., Zanta, M.A., Mergny, M.D., et al., *A versatile vector for gene and oligonucleotide transfer into cells in culture and in vivo: polyethylenimine.* Proc.Natl.Acad.Sci.U.S.A, 1995. **92**(16): p. 7297-7301.
35. Kircheis, R., Wightman, L., and Wagner, E., *Design and gene delivery activity of modified polyethylenimines.* Adv.Drug Deliv.Rev., 2001. **53**(3): p. 341-358.
36. Fischer, D., Li, Y., Ahlemeyer, B., Krieglstein, J., et al., *In vitro cytotoxicity testing of polycations: influence of polymer structure on cell viability and hemolysis.* Biomaterials, 2003. **24**(7): p. 1121-1131.
37. Wang, C.Y. and Huang, L., *pH-sensitive immunoliposomes mediate target-cell-specific delivery and controlled expression of a foreign gene in mouse 86.* Proc.Natl.Acad.Sci.U.S.A., 1987. **84**(0027-8424): p. 7851-7855.
38. Damen, M., Aarbiou, J., van Dongen, S.F., Buijs-Offerman, R.M., et al., *Delivery of DNA and siRNA by novel gemini-like amphiphilic peptides.* J Control Release, 2010. **145**(1): p. 33-9.

39. Kuo, W.T., Huang, H.Y., and Huang, Y.Y., *Polymeric micelles comprising stearic acid-grafted polyethyleneimine as nonviral gene carriers.* J Nanosci Nanotechnol, 2010. **10**(9): p. 5540-7.
40. Lehto, T., Abes, R., Oskolkov, N., Suhorutsenko, J., et al., *Delivery of nucleic acids with a stearylated (RxR)4 peptide using a non-covalent co-incubation strategy.* J Control Release, 2010. **141**(1): p. 42-51.
41. Tonges, L., Lingor, P., Egle, R., Dietz, G.P., et al., *Stearylated octaarginine and artificial virus-like particles for transfection of siRNA into primary rat neurons.* RNA, 2006. **12**(7): p. 1431-8.
42. Wang, D.A., Narang, A.S., Kotb, M., Gaber, A.O., et al., *Novel branched poly(ethylenimine)-cholesterol water-soluble lipopolymers for gene delivery.* Biomacromolecules., 2002. **3**(6): p. 1197-1207.
43. Oba, M., Miyata, K., Osada, K., Christie, R.J., et al., *Polyplex micelles prepared from omega-cholesteryl PEG-polycation block copolymers for systemic gene delivery.* Biomaterials, 2011. **32**(2): p. 652-63.
44. Doms, R.W., Helenius, A., and White, J., *Membrane fusion activity of the influenza virus hemagglutinin. The low pH-induced conformational change.* The Journal of biological chemistry, 1985. **260**(5): p. 2973-81.
45. Raghuraman, H. and Chattopadhyay, A., *Melittin: a membrane-active peptide with diverse functions.* Biosci Rep, 2007. **27**(4-5): p. 189-223.
46. Akinc, A., Thomas, M., Klibanov, A.M., and Langer, R., *Exploring polyethylenimine-mediated DNA transfection and the proton sponge hypothesis.* J Gene Med, 2005. **7**(5): p. 657-663.
47. Sonawane, N.D., Szoka, F.C., Jr., and Verkman, A.S., *Chloride Accumulation and Swelling in Endosomes Enhances DNA Transfer by Polyamine-DNA Polyplexes.* J.Biol.Chem., 2003. **278**(45): p. 44826-44831.
48. Behr, J.P., *The proton sponge: A trick to enter cells the viruses did not exploit.* Chimia, 1997. **51**(1-2): p. 34-36.
49. Midoux, P. and Monsigny, M., *Efficient gene transfer by histidylated polylysine/pDNA complexes.* Bioconjug.Chem., 1999. **10**(3): p. 406-411.
50. Maeda, H., *The enhanced permeability and retention (EPR) effect in tumor vasculature: the key role of tumor-selective macromolecular drug targeting.* Adv Enzyme Regul, 2001. **41**: p. 189-207.
51. Folkman, J., *Angiogenesis in cancer, vascular, rheumatoid and other disease.* Nat.Med., 1995. **1**(1): p. 27-31.
52. Maeda, H., Bharate, G.Y., and Daruwalla, J., *Polymeric drugs for efficient tumor-targeted drug delivery based on EPR-effect.* Eur. J. Pharm. Biopharm., 2009. **71**(3): p. 409-419.
53. Wagner, E., Cotten, M., Foisner, R., and Birnstiel, M.L., *Transferrin-polycation-DNA complexes: the effect of polycations on the structure of the complex and DNA delivery to cells.* Proc.Natl.Acad.Sci.U.S.A, 1991. **88**(10): p. 4255-4259.
54. Huang, R.Q., Qu, Y.H., Ke, W.L., Zhu, J.H., et al., *Efficient gene delivery targeted to the brain using a transferrin-conjugated polyethyleneglycol-modified polyamidoamine dendrimer.* FASEB J, 2007. **21**(4): p. 1117-25.
55. Chan, C.K. and Jans, D.A., *Enhancement of polylysine-mediated transferrinfection by nuclear localization sequences: polylysine does not function as a nuclear localization sequence 804.* Hum.Gene Ther., 1999. **10**(10): p. 1695-1702.
56. Liang, K.W., Hoffman, E.P., and Huang, L., *Targeted delivery of plasmid DNA to myogenic cells via transferrin-conjugated peptide nucleic acid.* Mol Ther, 2000. **1**(3): p. 236-43.

57. Harbottle, R.P., Cooper, R.G., Hart, S.L., Ladhoff, A., et al., *An RGD-oligolysine peptide: a prototype construct for integrin-mediated gene delivery.* Hum.Gene Ther, 1998. **9**(7): p. 1037-1047.
58. Desgrosellier, J.S. and Cheresh, D.A., *Integrins in cancer: biological implications and therapeutic opportunities.* Nat Rev Cancer, 2010. **10**(1): p. 9-22.
59. Oba, M., Fukushima, S., Kanayama, N., Aoyagi, K., et al., *Cyclic RGD peptide-conjugated polyplex micelles as a targetable gene delivery system directed to cells possessing alphavbeta3 and alphavbeta5 integrins.* Bioconjug Chem, 2007. **18**(5): p. 1415-1423.
60. Shir, A., Ogris, M., Wagner, E., and Levitzki, A., *EGF receptor-targeted synthetic double-stranded RNA eliminates glioblastoma, breast cancer, and adenocarcinoma tumors in mice.* PLoS Med, 2006. **3**(1): p. e6.
61. Li, Z., Zhao, R., Wu, X., Sun, Y., et al., *Identification and characterization of a novel peptide ligand of epidermal growth factor receptor for targeted delivery of therapeutics.* Faseb J, 2005. **19**(14): p. 1978-1985.
62. Blessing, T., Kursa, M., Holzhauser, R., Kircheis, R., et al., *Different strategies for formation of pegylated EGF-conjugated PEI/DNA complexes for targeted gene delivery.* Bioconjug Chem, 2001. **12**(4): p. 529-537.
63. Mickler, F.M., Mockl, L., Ruthardt, N., Ogris, M., et al., *Tuning nanoparticle uptake: live-cell imaging reveals two distinct endocytosis mechanisms mediated by natural and artificial EGFR targeting ligand.* Nano Lett, 2012. **12**(7): p. 3417-23.
64. Toffoli, G., Cernigoi, C., Russo, A., Gallo, A., et al., *Overexpression of folate binding protein in ovarian cancers.* Int J Cancer, 1997. **74**(2): p. 193-8.
65. Weitman, S.D., Lark, R.H., Coney, L.R., Fort, D.W., et al., *Distribution of the folate receptor GP38 in normal and malignant cell lines and tissues.* Cancer Res, 1992. **52**(12): p. 3396-401.
66. Merdan, T., Callahan, J., Petersen, H., Kunath, K., et al., *Pegylated polyethylenimine-fab' antibody fragment conjugates for targeted gene delivery to human ovarian carcinoma cells.* Bioconjug.Chem., 2003. **14**(5): p. 989-996.
67. Wang, L., Su, W., Liu, Z., Zhou, M., et al., *CD44 antibody-targeted liposomal nanoparticles for molecular imaging and therapy of hepatocellular carcinoma.* Biomaterials, 2012. **33**(20): p. 5107-14.
68. Kim, E.M., Jeong, H.J., Park, I.K., Cho, C.S., et al., *Asialoglycoprotein receptor targeted gene delivery using galactosylated polyethylenimine-graft-poly(ethylene glycol): in vitro and in vivo studies.* J Control Release, 2005. **108**(2-3): p. 557-567.
69. Lee, T.Y., Lin, C.T., Kuo, S.Y., Chang, D.K., et al., *Peptide-mediated targeting to tumor blood vessels of lung cancer for drug delivery.* Cancer Res, 2007. **67**(22): p. 10958-65.
70. Martin, I., Dohmen, C., Mas-Moruno, C., Troiber, C., et al., *Solid-phase-assisted synthesis of targeting peptide-PEG-oligo(ethane amino)amides for receptor-mediated gene delivery.* Org Biomol Chem, 2012. **10**(16): p. 3258-68.
71. Weissleder, R., Kelly, K., Sun, E.Y., Shtatland, T., et al., *Cell-specific targeting of nanoparticles by multivalent attachment of small molecules.* Nat Biotechnol, 2005. **23**(11): p. 1418-23.
72. Zarnegar, R., *Regulation of HGF and HGFR gene expression.* Exs, 1995. **74**: p. 33-49.
73. Martin, T.A. and Jiang, W.G., *Hepatocyte growth factor and its receptor signalling complex as targets in cancer therapy.* Anticancer Agents Med Chem, 2010. **10**(1): p. 2-6.
74. Peruzzi, B. and Bottaro, D.P., *Targeting the c-Met signaling pathway in cancer.* Clin Cancer Res, 2006. **12**(12): p. 3657-60.

75. Lu, R.M., Chang, Y.L., Chen, M.S., and Wu, H.C., *Single chain anti-c-Met antibody conjugated nanoparticles for in vivo tumor-targeted imaging and drug delivery.* Biomaterials, 2011. **32**(12): p. 3265-74.
76. Vosjan, M.J., Vercammen, J., Kolkman, J.A., Stigter-van Walsum, M., et al., *Nanobodies targeting the hepatocyte growth factor: potential new drugs for molecular cancer therapy.* Mol Cancer Ther, 2012. **11**(4): p. 1017-25.
77. Mittra, E.S., Fan-Minogue, H., Lin, F.I., Karamchandani, J., et al., *Preclinical efficacy of the anti-hepatocyte growth factor antibody ficlatuzumab in a mouse brain orthotopic glioma model evaluated by bioluminescence, PET, and MRI.* Clin Cancer Res, 2013. **19**(20): p. 5711-21.
78. Chen, X., Ding, G., Gao, Q., Sun, J., et al., *A human anti-c-Met Fab fragment conjugated with doxorubicin as targeted chemotherapy for hepatocellular carcinoma.* PLoS One, 2013. **8**(5): p. e63093.
79. Sideratou, Z., Kontoyianni, C., Drossopoulou, G.I., and Paleos, C.M., *Synthesis of a folate functionalized PEGylated poly(propylene imine) dendrimer as prospective targeted drug delivery system.* Bioorg Med Chem Lett, 2010. **20**(22): p. 6513-7.
80. Koppu, S., Oh, Y.J., Edrada-Ebel, R., Blatchford, D.R., et al., *Tumor regression after systemic administration of a novel tumor-targeted gene delivery system carrying a therapeutic plasmid DNA.* J Control Release, 2010. **143**(2): p. 215-21.
81. Santos, J.L., Oliveira, H., Pandita, D., Rodrigues, J., et al., *Functionalization of poly(amidoamine) dendrimers with hydrophobic chains for improved gene delivery in mesenchymal stem cells.* Journal of Controlled Release, 2010. **144**(1): p. 55-64.
82. Jevprasesphant, R., Penny, J., Attwood, D., McKeown, N.B., et al., *Engineering of dendrimer surfaces to enhance transepithelial transport and reduce cytotoxicity.* Pharm Res, 2003. **20**(10): p. 1543-50.
83. Wang, X., He, Y., Wu, J., Gao, C., et al., *Synthesis and evaluation of phenylalanine-modified hyperbranched poly(amido amine)s as promising gene carriers.* Biomacromolecules, 2010. **11**(1): p. 245-51.
84. Kim, T.I., Baek, J.U., Zhe, B.C., and Park, J.S., *Arginine-conjugated polypropylenimine dendrimer as a non-toxic and efficient gene delivery carrier.* Biomaterials, 2007. **28**(11): p. 2061-2067.
85. Choi, J.S., Nam, K., Park, J.Y., Kim, J.B., et al., *Enhanced transfection efficiency of PAMAM dendrimer by surface modification with l-arginine.* J Control Release, 2004. **99**(3): p. 445-456.
86. Yu, G.S., Bae, Y.M., Choi, H., Kong, B., et al., *Synthesis of PAMAM dendrimer derivatives with enhanced buffering capacity and remarkable gene transfection efficiency.* Bioconjug Chem, 2011. **22**(6): p. 1046-55.
87. Ward, C.M., Read, M.L., and Seymour, L.W., *Systemic circulation of poly(L-lysine)/DNA vectors is influenced by polycation molecular weight and type of DNA: differential circulation in mice and rats and the implications for human gene therapy 1.* Blood, 2001. **97**(8): p. 2221-2229.
88. Moghimi, S.M., Symonds, P., Murray, J.C., Hunter, A.C., et al., *A two-stage poly(ethylenimine)-mediated cytotoxicity: implications for gene transfer/therapy.* Mol Ther, 2005. **11**(6): p. 990-995.
89. Schatzlein, A.G., *Targeting of Synthetic Gene Delivery Systems.* J Biomed.Biotechnol., 2003. **2003**(2): p. 149-158.
90. Wagner, E., *Strategies to improve DNA polyplexes for in vivo gene transfer: will "artificial viruses" be the answer?* Pharm.Res., 2004. **21**(1): p. 8-14.
91. Zinselmeyer, B.H., Mackay, S.P., Schatzlein, A.G., and Uchegbu, I.F., *The lower-generation polypropylenimine dendrimers are effective gene-transfer agents.* Pharm.Res., 2002. **19**(7): p. 960-967.

92. Schaffert, D., Badgujar, N., and Wagner, E., *Novel Fmoc-polyamino acids for solid-phase synthesis of defined polyamidoamines.* Org Lett, 2011. **13**(7): p. 1586-9.
93. Hartmann, L., Krause, E., Antonietti, M., and Borner, H.G., *Solid-phase supported polymer synthesis of sequence-defined, multifunctional poly(amidoamines).* Biomacromolecules., 2006. **7**(4): p. 1239-1244.
94. Schaffert, D., Troiber, C., Salcher, E.E., Frohlich, T., et al., *Solid-phase synthesis of sequence-defined T-, i-, and U-shape polymers for pDNA and siRNA delivery.* Angew Chem Int Ed Engl, 2011. **50**(38): p. 8986-9.
95. Troiber, C., Edinger, D., Kos, P., Schreiner, L., et al., *Stabilizing effect of tyrosine trimers on pDNA and siRNA polyplexes.* Biomaterials, 2013. **34**(5): p. 1624-33.
96. Frohlich, T., Edinger, D., Klager, R., Troiber, C., et al., *Structure-activity relationships of siRNA carriers based on sequence-defined oligo (ethane amino) amides.* J Control Release, 2012. **160**(3): p. 532-41.
97. Scholz, C., Kos, P., and Wagner, E., *Comb-like oligoaminoethane carriers: change in topology improves pDNA delivery.* Bioconjug Chem, 2014. **25**(2): p. 251-61.
98. Longley, D.B. and Johnston, P.G., *Molecular mechanisms of drug resistance.* J Pathol, 2005. **205**(2): p. 275-92.
99. Gatti, L. and Zunino, F., *Overview of tumor cell chemoresistance mechanisms.* Methods Mol Med, 2005. **111**: p. 127-48.
100. Chien, A.J. and Moasser, M.M., *Cellular mechanisms of resistance to anthracyclines and taxanes in cancer: intrinsic and acquired.* Semin Oncol, 2008. **35**(2 Suppl 2): p. S1-S14; quiz S39.
101. Chuthapisith, S., Eremin, J., El-Sheemey, M., and Eremin, O., *Breast cancer chemoresistance: emerging importance of cancer stem cells.* Surg Oncol, 2010. **19**(1): p. 27-32.
102. Dean, M., Fojo, T., and Bates, S., *Tumour stem cells and drug resistance.* Nat Rev Cancer, 2005. **5**(4): p. 275-84.
103. Mani, S.A., Guo, W., Liao, M.J., Eaton, E.N., et al., *The epithelial-mesenchymal transition generates cells with properties of stem cells.* Cell, 2008. **133**(4): p. 704-15.
104. Polyak, K. and Weinberg, R.A., *Transitions between epithelial and mesenchymal states: acquisition of malignant and stem cell traits.* Nat Rev Cancer, 2009. **9**(4): p. 265-73.
105. Dykxhoorn, D.M., Wu, Y., Xie, H., Yu, F., et al., *miR-200 Enhances Mouse Breast Cancer Cell Colonization to Form Distant Metastases.* PLoS ONE, 2009. **4**(9): p. e7181.
106. Bartel, D.P., *MicroRNAs: genomics, biogenesis, mechanism, and function.* Cell, 2004. **116**(2): p. 281-97.
107. Garzon, R., Marcucci, G., and Croce, C.M., *Targeting microRNAs in cancer: rationale, strategies and challenges.* Nat Rev Drug Discov, 2010. **9**(10): p. 775-89.
108. Croce, C.M., *Causes and consequences of microRNA dysregulation in cancer.* Nat Rev Genet, 2009. **10**(10): p. 704-14.
109. Iorio, M.V. and Croce, C.M., *MicroRNA dysregulation in cancer: diagnostics, monitoring and therapeutics. A comprehensive review.* EMBO Mol Med, 2012. **4**(3): p. 143-59.
110. Inui, M., Martello, G., and Piccolo, S., *MicroRNA control of signal transduction.* Nat Rev Mol Cell Biol, 2010. **11**(4): p. 252-263.
111. Blower, P.E., Chung, J.H., Verducci, J.S., Lin, S., et al., *MicroRNAs modulate the chemosensitivity of tumor cells.* Mol Cancer Ther, 2008. **7**(1): p. 1-9.
112. Kovalchuk, O., Filkowski, J., Meservy, J., Ilnytskyy, Y., et al., *Involvement of microRNA-451 in resistance of the MCF-7 breast cancer cells to chemotherapeutic drug doxorubicin.* Mol Cancer Ther, 2008. **7**(7): p. 2152-9.

113. Sarkar, F.H., Li, Y., Wang, Z., Kong, D., et al., *Implication of microRNAs in drug resistance for designing novel cancer therapy.* Drug Resistance Updates, 2010. **13**(3): p. 57-66.
114. Bao, L., Hazari, S., Mehra, S., Kaushal, D., et al., *Increased expression of P-glycoprotein and doxorubicin chemoresistance of metastatic breast cancer is regulated by miR-298.* Am J Pathol, 2012. **180**(6): p. 2490-503.
115. Gregory, P.A., Bert, A.G., Paterson, E.L., Barry, S.C., et al., *The miR-200 family and miR-205 regulate epithelial to mesenchymal transition by targeting ZEB1 and SIP1*. Nat Cell Biol, 2008. **10**(5): p. 593-601.
116. Park, S.M., Gaur, A.B., Lengyel, E., and Peter, M.E., *The miR-200 family determines the epithelial phenotype of cancer cells by targeting the E-cadherin repressors ZEB1 and ZEB2.* Genes Dev, 2008. **22**(7): p. 894-907.
117. Hurteau, G.J., Carlson, J.A., Roos, E., and Brock, G.J., *Stable expression of miR-200c alone is sufficient to regulate TCF8 (ZEB1) and restore E-cadherin expression.* Cell Cycle, 2009. **8**(13): p. 2064-9.
118. Korpal, M., Lee, E.S., Hu, G., and Kang, Y., *The miR-200 family inhibits epithelial-mesenchymal transition and cancer cell migration by direct targeting of E-cadherin transcriptional repressors ZEB1 and ZEB2.* J Biol Chem, 2008. **283**(22): p. 14910-4.
119. Howe, E.N., Cochrane, D.R., and Richer, J.K., *Targets of miR-200c mediate suppression of cell motility and anoikis resistance.* Breast Cancer Res, 2011. **13**(2): p. R45.
120. Burk, U., Schubert, J., Wellner, U., Schmalhofer, O., et al., *A reciprocal repression between ZEB1 and members of the miR-200 family promotes EMT and invasion in cancer cells.* EMBO Rep, 2008. **9**(6): p. 582-9.
121. Gibbons, D.L., Lin, W., Creighton, C.J., Rizvi, Z.H., et al., *Contextual extracellular cues promote tumor cell EMT and metastasis by regulating miR-200 family expression.* Genes Dev, 2009. **23**(18): p. 2140-51.
122. Gupta, P.B., Onder, T.T., Jiang, G., Tao, K., et al., *Identification of selective inhibitors of cancer stem cells by high-throughput screening.* Cell, 2009. **138**(4): p. 645-59.
123. Miyazaki, Y., Shibuya, M., Sugawara, H., Kawaguchi, O., et al., *Salinomycin, a new polyether antibiotic.* J Antibiot (Tokyo), 1974. **27**(11): p. 814-21.
124. DANFORTH, H.D., RUFF, M.D., REID, W.M., and MILLER, R.L., *Anticoccidial Activity of Salinomycin in Battery Raised Broiler Chickens.* Poultry Science, 1977. **56**(3): p. 926-932.
125. Naujokat, C. and Steinhart, R., *Salinomycin as a drug for targeting human cancer stem cells.* J Biomed Biotechnol, 2012. **2012**: p. 950658.
126. Dong, T.T., Zhou, H.M., Wang, L.L., Feng, B., et al., *Salinomycin selectively targets 'CD133+' cell subpopulations and decreases malignant traits in colorectal cancer lines.* Ann Surg Oncol, 2011. **18**(6): p. 1797-804.
127. Ketola, K., Hilvo, M., Hyotylainen, T., Vuoristo, A., et al., *Salinomycin inhibits prostate cancer growth and migration via induction of oxidative stress.* Br J Cancer, 2012. **106**(1): p. 99-106.
128. Fojo, A., Hamilton, T.C., Young, R.C., and Ozols, R.F., *Multidrug resistance in ovarian cancer.* Cancer, 2011. **60**(1987): p. 2075-2080.
129. Wu, Q., Yang, Z., Nie, Y., Shi, Y., et al., *Multi-drug resistance in cancer chemotherapeutics: mechanisms and lab approaches.* Cancer Lett, 2014. **347**(2): p. 159-66.
130. Dong, X. and Mumper, R.J., *Nanomedicinal strategies to treat multidrug-resistant tumors: current progress.* Nanomedicine (Lond), 2010. **5**(4): p. 597-615.

131. Chen, Y., Chen, H., and Shi, J., *In Vivo Bio-Safety Evaluations and Diagnostic/Therapeutic Applications of Chemically Designed Mesoporous Silica Nanoparticles.* Advanced Materials, 2013. **25**(23): p. 3144-3176.
132. Wagner, V., Dullaart, A., Bock, A.-K., and Zweck, A., *The emerging nanomedicine landscape.* Nat Biotech, 2006. **24**(10): p. 1211-1217.
133. Peer, D., Karp, J.M., Hong, S., Farokhzad, O.C., et al., *Nanocarriers as an emerging platform for cancer therapy.* Nat Nano, 2007. **2**(12): p. 751-760.
134. Laurent, S., Forge, D., Port, M., Roch, A., et al., *Magnetic iron oxide nanoparticles: synthesis, stabilization, vectorization, physicochemical characterizations, and biological applications.* Chem Rev, 2008. **108**(6): p. 2064-110.
135. Patra, C.R., Bhattacharya, R., Mukhopadhyay, D., and Mukherjee, P., *Fabrication of gold nanoparticles for targeted therapy in pancreatic cancer.* Adv Drug Deliv Rev, 2010. **62**(3): p. 346-61.
136. Liu, Z., Robinson, J.T., Tabakman, S.M., Yang, K., et al., *Carbon materials for drug delivery & cancer therapy.* Materials Today, 2011. **14**(7–8): p. 316-323.
137. Benezra, M., Penate-Medina, O., Zanzonico, P.B., Schaer, D., et al., *Multimodal silica nanoparticles are effective cancer-targeted probes in a model of human melanoma.* J Clin Invest, 2011. **121**(7): p. 2768-80.
138. Ruiz-Hernandez, E., Baeza, A., and Vallet-Regi, M., *Smart drug delivery through DNA/magnetic nanoparticle gates.* ACS Nano, 2011. **5**(2): p. 1259-66.
139. Schlossbauer, A., Warncke, S., Gramlich, P.M.E., Kecht, J., et al., *A Programmable DNA-Based Molecular Valve for Colloidal Mesoporous Silica.* Angewandte Chemie International Edition, 2010. **49**(28): p. 4734-4737.
140. He, Q. and Shi, J., *MSN anti-cancer nanomedicines: chemotherapy enhancement, overcoming of drug resistance, and metastasis inhibition.* Adv Mater, 2014. **26**(3): p. 391-411.
141. He, Q., Gao, Y., Zhang, L., Zhang, Z., et al., *A pH-responsive mesoporous silica nanoparticles-based multi-drug delivery system for overcoming multi-drug resistance.* Biomaterials, 2011. **32**(30): p. 7711-20.
142. Chen, A.M., Zhang, M., Wei, D., Stueber, D., et al., *Co-delivery of doxorubicin and Bcl-2 siRNA by mesoporous silica nanoparticles enhances the efficacy of chemotherapy in multidrug-resistant cancer cells.* Small, 2009. **5**(23): p. 2673-7.
143. Meng, H., Liong, M., Xia, T., Li, Z., et al., *Engineered design of mesoporous silica nanoparticles to deliver doxorubicin and P-glycoprotein siRNA to overcome drug resistance in a cancer cell line.* ACS Nano, 2010. **4**(8): p. 4539-50.
144. Pan, L., Liu, J., He, Q., Wang, L., et al., *Overcoming multidrug resistance of cancer cells by direct intranuclear drug delivery using TAT-conjugated mesoporous silica nanoparticles.* Biomaterials, 2013. **34**(11): p. 2719-2730.
145. Fan, W., Shen, B., Bu, W., Chen, F., et al., *Rattle-structured multifunctional nanotheranostics for synergetic chemo-/radiotherapy and simultaneous magnetic/luminescent dual-mode imaging.* J Am Chem Soc, 2013. **135**(17): p. 6494-503.
146. Cauda, V., Schlossbauer, A., Kecht, J., Zürner, A., et al., *Multiple Core−Shell Functionalized Colloidal Mesoporous Silica Nanoparticles.* Journal of the American Chemical Society, 2009. **131**(32): p. 11361-11370.
147. Strassert, C.A., Otter, M., Albuquerque, R.Q., Höne, A., et al., *Photoactive Hybrid Nanomaterial for Targeting, Labeling, and Killing Antibiotic-Resistant Bacteria.* Angewandte Chemie International Edition, 2009. **48**(42): p. 7928-7931.
148. Liu, R., Liao, P., Liu, J., and Feng, P., *Responsive Polymer-Coated Mesoporous Silica as a pH-Sensitive Nanocarrier for Controlled Release.* Langmuir, 2011. **27**(6): p. 3095-3099.

149. Tarn, D., Xue, M., and Zink, J.I., *pH-responsive dual cargo delivery from mesoporous silica nanoparticles with a metal-latched nanogate.* Inorg Chem, 2013. **52**(4): p. 2044-9.
150. Ashley, C.E., Carnes, E.C., Phillips, G.K., Padilla, D., et al., *The targeted delivery of multicomponent cargos to cancer cells by nanoporous particle-supported lipid bilayers.* Nat Mater, 2011. **10**(5): p. 389-397.
151. Cauda, V., Engelke, H., Sauer, A., Arcizet, D., et al., *Colchicine-Loaded Lipid Bilayer-Coated 50 nm Mesoporous Nanoparticles Efficiently Induce Microtubule Depolymerization upon Cell Uptake.* Nano Letters, 2010. **10**(7): p. 2484-2492.
152. Mackowiak, S.A., Schmidt, A., Weiss, V., Argyo, C., et al., *Targeted Drug Delivery in Cancer Cells with Red-Light Photoactivated Mesoporous Silica Nanoparticles.* Nano Letters, 2013. **13**(6): p. 2576-2583.
153. Vivero-Escoto, J.L., Slowing, I.I., Wu, C.-W., and Lin, V.S.Y., *Photoinduced Intracellular Controlled Release Drug Delivery in Human Cells by Gold-Capped Mesoporous Silica Nanosphere.* Journal of the American Chemical Society, 2009. **131**(10): p. 3462-3463.
154. Slowing, I.I., Vivero-Escoto, J.L., Wu, C.W., and Lin, V.S., *Mesoporous silica nanoparticles as controlled release drug delivery and gene transfection carriers.* Adv Drug Deliv Rev, 2008. **60**(11): p. 1278-88.
155. Croissant, J. and Zink, J.I., *Nanovalve-controlled cargo release activated by plasmonic heating.* J Am Chem Soc, 2012. **134**(18): p. 7628-31.
156. Schlossbauer, A., Dohmen, C., Schaffert, D., Wagner, E., et al., *pH-responsive release of acetal-linked melittin from SBA-15 mesoporous silica.* Angew Chem Int Ed Engl, 2011. **50**(30): p. 6828-30.
157. Brewer, E., Coleman, J., and Lowman, A., *Emerging technologies of polymeric nanoparticles in cancer drug delivery.* J. Nanomaterials, 2011. **2011**: p. 1-10.
158. Shu, J.Y., Panganiban, B., and Xu, T., *Peptide-polymer conjugates: from fundamental science to application.* Annu Rev Phys Chem, 2013. **64**: p. 631-57.
159. Hong, C.-Y., Li, X., and Pan, C.-Y., *Fabrication of smart nanocontainers with a mesoporous core and a pH-responsive shell for controlled uptake and release.* Journal of Materials Chemistry, 2009. **19**(29): p. 5155-5160.
160. Sun, J.-T., Hong, C.-Y., and Pan, C.-Y., *Fabrication of PDEAEMA-Coated Mesoporous Silica Nanoparticles and pH-Responsive Controlled Release.* The Journal of Physical Chemistry C, 2010. **114**(29): p. 12481-12486.
161. Synytska, A., Stamm, M., Diez, S., and Ionov, L., *Simple and fast method for the fabrication of switchable bicomponent micropatterned polymer surfaces.* Langmuir, 2007. **23**(9): p. 5205-9.
162. Salcher, E.E., Kos, P., Frohlich, T., Badgujar, N., et al., *Sequence-defined four-arm oligo(ethanamino)amides for pDNA and siRNA delivery: Impact of building blocks on efficacy.* J Control Release, 2012. **164**(3): p. 380-6.
163. Li, S.D. and Huang, L., *Gene therapy progress and prospects: non-viral gene therapy by systemic delivery.* Gene Ther, 2006. **13**(18): p. 1313-1319.
164. Chollet, P., Favrot, M.C., Hurbin, A., and Coll, J.L., *Side-effects of a systemic injection of linear polyethylenimine-DNA complexes.* J Gene Med, 2002. **4**(1): p. 84-91.
165. Tang, M.X. and Szoka, F.C., *The influence of polymer structure on the interactions of cationic polymers with DNA and morphology of the resulting complexes.* Gene Ther, 1997. **4**: p. 823-832.
166. Schaffert, D., Troiber, C., and Wagner, E., *New Sequence-Defined Polyaminoamides with Tailored Endosomolytic Properties for Plasmid DNA Delivery.* Bioconjug Chem, 2012. **23**(6): p. 1157-1165.

167. Hartmann, L. and Börner, H.G., *Precision Polymers: Monodisperse, Monomer-Sequence-Defined Segments to Target Future Demands of Polymers in Medicine.* Advanced Materials, 2009. **21**(32-33): p. 3425-3431.
168. Kos, P. and Wagner, E., *Polymers for siRNA Delivery: Combining precision with multifunctionality.* Chimica Oggi - Chemistry Today 2013. **31**(2): p. 6-10.
169. Smrekar, B., Wightman, L., Wolschek, M.F., Lichtenberger, C., et al., *Tissue-dependent factors affect gene delivery to tumors in vivo.* Gene Ther, 2003. **10**(13): p. 1079-88.
170. Russ, V., Elfberg, H., Thoma, C., Kloeckner, J., et al., *Novel degradable oligoethylenimine acrylate ester-based pseudodendrimers for in vitro and in vivo gene transfer.* Gene Ther, 2008. **15**(1): p. 18-29.
171. Kim, E.M., Park, E.H., Cheong, S.J., Lee, C.M., et al., *Characterization, biodistribution and small-animal SPECT of I-125-labeled c-Met binding peptide in mice bearing c-Met receptor tyrosine kinase-positive tumor xenografts.* Nucl Med Biol, 2009. **36**(4): p. 371-8.
172. Kim, E.M., Park, E.H., Cheong, S.J., Lee, C.M., et al., *In vivo imaging of mesenchymal-epithelial transition factor (c-Met) expression using an optical imaging system.* Bioconjug Chem, 2009. **20**(7): p. 1299-306.
173. Zhao, P., Grabinski, T., Gao, C., Skinner, R.S., et al., *Identification of a met-binding peptide from a phage display library.* Clin Cancer Res, 2007. **13**(20): p. 6049-55.
174. van Vlerken, L.E., Vyas, T.K., and Amiji, M.M., *Poly(ethylene glycol)-modified nanocarriers for tumor-targeted and intracellular delivery.* Pharm.Res., 2007. **24**(8): p. 1405-1414.
175. Mishra, S., Webster, P., and Davis, M.E., *PEGylation significantly affects cellular uptake and intracellular trafficking of non-viral gene delivery particles.* Eur.J Cell Biol., 2004. **83**(3): p. 97-111.
176. Hamidi, M., Azadi, A., and Rafiei, P., *Pharmacokinetic consequences of pegylation.* Drug Deliv., 2006. **13**(6): p. 399-409.
177. Khargharia, S., Kizzire, K., Ericson, M.D., Baumhover, N.J., et al., *PEG length and chemical linkage controls polyacridine peptide DNA polyplex pharmacokinetics, biodistribution, metabolic stability and in vivo gene expression.* J Control Release, 2013. **170**(3): p. 325-33.
178. Nelson, C.E., Kintzing, J.R., Hanna, A., Shannon, J.M., et al., *Balancing cationic and hydrophobic content of PEGylated siRNA polyplexes enhances endosome escape, stability, blood circulation time, and bioactivity in vivo.* ACS Nano, 2013. **7**(10): p. 8870-80.
179. Dohmen, C., Edinger, D., Frohlich, T., Schreiner, L., et al., *Nanosized Multifunctional Polyplexes for Receptor-Mediated SiRNA Delivery.* ACS nano, 2012. **6**(6): p. 5198-208.
180. Plank, C., Mechtler, K., Szoka, F.C., Jr., and Wagner, E., *Activation of the complement system by synthetic DNA complexes: a potential barrier for intravenous gene delivery.* Hum.Gene Ther, 1996. **7**(12): p. 1437-1446.
181. Owens, D.E., 3rd and Peppas, N.A., *Opsonization, biodistribution, and pharmacokinetics of polymeric nanoparticles.* Int J Pharm, 2006. **307**(1): p. 93-102.
182. Bandyopadhyay, A., Wang, L., Agyin, J., Tang, Y., et al., *Doxorubicin in combination with a small TGFbeta inhibitor: a potential novel therapy for metastatic breast cancer in mouse models.* PLoS One, 2010. **5**(4): p. e10365.
183. Boehmerle, W., Muenzfeld, H., Springer, A., Huehnchen, P., et al., *Specific targeting of neurotoxic side effects and pharmacological profile of the novel cancer stem cell drug salinomycin in mice.* J Mol Med (Berl), 2014. **92**(8): p. 889-900.
184. Croker, A.K. and Allan, A.L., *Cancer stem cells: implications for the progression and treatment of metastatic disease.* J Cell Mol Med, 2008. **12**(2): p. 374-90.

185. Oak, P.S., Kopp, F., Thakur, C., Ellwart, J.W., et al., *Combinatorial treatment of mammospheres with trastuzumab and salinomycin efficiently targets HER2-positive cancer cells and cancer stem cells.* Int J Cancer, 2012. **131**(12): p. 2808-19.
186. Kim, J.H., Chae, M., Kim, W.K., Kim, Y.J., et al., *Salinomycin sensitizes cancer cells to the effects of doxorubicin and etoposide treatment by increasing DNA damage and reducing p21 protein.* Br J Pharmacol, 2011. **162**(3): p. 773-84.
187. Wu, S.H., Lin, Y.S., Hung, Y., Chou, Y.H., et al., *Multifunctional mesoporous silica nanoparticles for intracellular labeling and animal magnetic resonance imaging studies.* Chembiochem, 2008. **9**(1): p. 53-7.
188. Meng, H., Xue, M., Xia, T., Ji, Z., et al., *Use of size and a copolymer design feature to improve the biodistribution and the enhanced permeability and retention effect of doxorubicin-loaded mesoporous silica nanoparticles in a murine xenograft tumor model.* ACS Nano, 2011. **5**(5): p. 4131-44.
189. He, Q., Zhang, J., Shi, J., Zhu, Z., et al., *The effect of PEGylation of mesoporous silica nanoparticles on nonspecific binding of serum proteins and cellular responses.* Biomaterials, 2010. **31**(6): p. 1085-92.
190. Knop, K., Hoogenboom, R., Fischer, D., and Schubert, U.S., *Poly(ethylene glycol) in Drug Delivery: Pros and Cons as Well as Potential Alternatives.* Angewandte Chemie International Edition, 2010. **49**(36): p. 6288-6308.
191. He, Q., Zhang, Z., Gao, F., Li, Y., et al., *In vivo biodistribution and urinary excretion of mesoporous silica nanoparticles: effects of particle size and PEGylation.* Small, 2011. **7**(2): p. 271-80.
192. Huang, X., Li, L., Liu, T., Hao, N., et al., *The shape effect of mesoporous silica nanoparticles on biodistribution, clearance, and biocompatibility in vivo.* ACS Nano, 2011. **5**(7): p. 5390-9.
193. Lu, J., Li, Z., Zink, J.I., and Tamanoi, F., *In vivo tumor suppression efficacy of mesoporous silica nanoparticles-based drug-delivery system: enhanced efficacy by folate modification.* Nanomedicine, 2012. **8**(2): p. 212-20.
194. Longmire, M., Choyke, P.L., and Kobayashi, H., *Clearance properties of nano-sized particles and molecules as imaging agents: considerations and caveats.* Nanomedicine (Lond), 2008. **3**(5): p. 703-17.
195. Lu, J., Liong, M., Li, Z., Zink, J.I., et al., *Biocompatibility, Biodistribution, and Drug-Delivery Efficiency of Mesoporous Silica Nanoparticles for Cancer Therapy in Animals.* Small, 2010. **6**(16): p. 1794-1805.
196. Hartmann, L.C., Keeney, G.L., Lingle, W.L., Christianson, T.J., et al., *Folate receptor overexpression is associated with poor outcome in breast cancer.* Int J Cancer, 2007. **121**(5): p. 938-42.
197. Mamaeva, V., Rosenholm, J.M., Bate-Eya, L.T., Bergman, L., et al., *Mesoporous silica nanoparticles as drug delivery systems for targeted inhibition of Notch signaling in cancer.* Mol Ther, 2011. **19**(8): p. 1538-46.

VIII. APPENDIX

1. Abbreviations

ABC	Adenosine triphosphate (ATP) binding cassette
Ala	Alanine
ALT	Alanine transaminase
AST	Aspartate transaminase
BCRP	Breast cancer resistance protein
BUN	Blood urea nitrogen
CCD	Charge-coupled device
cMBP2	c-Met binding peptide 2
CMV	Cytomegalovirus
CSCs	Cancer stem cells
Cy7	Cyanine 7
DAPI	4`,6-diamidino-2-phenylindole
DMSO	Dimethyl sulfoxide
DNA	Deoxyribonucleic acid
e.g.	exempli gratia (for example)
EDTA	Ethylenediamine tetraacetic acid
EGF	Epidermal growth factor
EMT	Epithelial to mesenchymal transition
EPR effect	Enhanced permeability and retention effect
FA	Folic acid
FCS	Fetal calf serum
FDA	Food and drug administration
FELASA	Federation of European laboratory animal science associations
h	hours
HA2	Hemagglutinin subunit 2
HBG	HEPES buffered glucose
HEPES	N-(2-hydroxyethyl) piperazine-N`-(2-ethanesulfonic acid)
HER2	Human epidermal growth factor 2
HGF	Hepatocyte growth factor
HGFR	Hepatocyte growth factor receptor

LPEI	Linear polyethylenimine
Luc	Luciferase
MDR	Multiple drug resistance
MET	Mesenchymal to epithelial transition
min	minutes
miR-200c	micro RNA 200c
miRNA	micro RNA
MRI	Magnetic resonance imaging
mRNA	Messenger RNA
MRP1	MDR-associated protein 1
MSN	Mesoporous silica nanoparticles
Mw	Molecular weight
N/P	Polymer nitrogen to nucleic acid phosphate ratio
NaCl	Sodium chloride
NIR	Near infrared
NLS	Nuclear localization signal
no.	Number
NPC	Nuclear pore complex
PAMAM	Polyamidoamine
PBS	Phosphate buffered saline
pCMVLuc	Plasmid encoding firefly luciferase under the control of CMV promotor
pDNA	Plasmid DNA
PEG	Polyethylene glycol
PEG_{24}	Polyethylene glycol with 24 ethylene glycol units
PEI	Polyethylenimine
P-glycoprotein	Permeability glycoprotein
PLL	Polylysine
PPI G2	Polypropylenimine of the second generation
PPI	Polypropylenimine
PVP	Poly(vinylpyridine)
RES	Reticuloendothelial system
RISC	RNA-induced silencing complex
RLU	Relative light units

RNA	Ribonucleic acid
ROI	Region of interest
RT-PCR	Reverse transcription polymerase chain reaction
S.D.	Standard deviation
S.E.M.	Standard error of the mean
SCID	Severe combined immune deficiency
siRNA	Small interfering RNA
Sph	Succinoyl-pentaethylene hexamine
Stp	Succinoyl-tetraethylene pentamine
TAT peptide	Transactivator of transcription of human immunodeficiency virus, a cell-penetrating peptide
TGFβ	Transforming growth factor beta
Wnt	Wingless-related integration site

2. Publications

2.1. Original articles

Petra Kos, Ulrich Lächelt, Annika Herrmann, Markus Döblinger, Dongsheng He, Ernst Wagner, *Compacted cMet-Directed Polyplexes for Tumor-targeted Gene Transfer in vivo.* Manuscript prepared.

Florian Kopp, Adam Hermawan, Prajakta Shirish Oak, Vijay Kumar Ulaganathan, Annika Herrmann, Nefertiti Elnikhely, Chitra Thakur, Zhiguang Xiao, Pjotr Knyazev, Beyhan Ataseven, Ulf R Rapp, Rajkumar Savai, Ernst Wagner and Andreas Roidl, *Sequential salinomycin treatment results in resistance formation through clonal selection of epithelial-like tumor cells in vitro and in vivo.* Translational Oncology. Manuscript in revision.

Stefan Niedermayer, Veronika Weiss, Annika Herrmann, Alexandra Schmidt, Stefan Datz, Ernst Wagner, Christoph Bräuchle, Thomas Bein, *Multifunctional Polymer-Capped Mesoporous Silica Nanoparticles for pH-Responsive Targeted Drug Delivery*. Manuscript submitted.

Kopp, F., Hermawan, A., Oak, P.S., Herrmann, A., Wagner, E., Roidl, A., *Salinomycin treatment reduces metastatic tumor burden by hampering cancer cell migration.* Mol Cancer, 2014. **13**: article 16.

Lächelt, U., Kos, P., Mickler, F.M., Herrmann, A., Salcher, E.E., Rödl, W., Badgujar, N., Bräuchle, C., Wagner, E., *Fine-tuning of proton sponges by precise diaminoethanes and histidines in pDNA polyplexes.* Nanomedicine NBM, 2014. **10**(1): p. 35-44.

Kos, P., Scholz, C., Salcher, E.E., Herrmann, A., Wagner, E., *Gene Transfer with Sequence-Defined Oligo(ethanamino)amides Bioreducibly Attached to a Propylenimine Dendrimer Core.* Pharmaceutical Nanotechnology, 2013. **1**(4): p. 269-281.

Bogomilova, A., Höhn, M., Günther, M., Herrmann, A., Troev, K., Wagner, E., Schreiner, L., *A polyphosphoester conjugate of melphalan as antitumoral agent.* Eur J Pharm Sci, 2013. **50**(3-4): p. 410-9.

Troiber, C., Edinger, D., Kos, P., Schreiner, L., Kläger R., Herrmann, A., Wagner E., *Stabilizing effect of tyrosine trimers on pDNA and siRNA polyplexes.* Biomaterials, 2013. **34**(5): p. 1624-33.

2.2. Abstracts

Kos, P., Lächelt, U., Herrmann, A., He, D., Wagner, E., *Sequence-defined nanocarriers for c-Met receptor-directed gene transfer in vitro and in vivo.* 17th Annual Meeting of the American Society of Gene & Cell Therapy, Washington, USA (May 2014).

Kos, P., Lächelt, U., Mickler, F.M., Herrmann, A., Wagner, E., *Aiming at the bullseye: Pursuing the tumor-addressed gene delivery with sequence-defined nanocarriers comprising novel protein and peptidic targeting ligands.* XIX. Annual Meeting of German Society for Gene Therapy, Ulm, Germany (March 2014).

Lächelt, U., Kos, P., Herrmann, A., Wagner, E., *Proton sponge mechanism revisited and revised: Precise polymer DNA complexes for tumor-directed gene transfer*. XIX. Annual Meeting of German Society for Gene Therapy, Hamburg, Germany (February/March 2013).

2.3. Poster

Sommer, A.K., Hermawan, A., Mickler, F.M., Herrmann, A., Bräuchle, C., Wagner, E., Knyazev, P., Ullrich, A., Roidl, A., *Tamoxifen resistance can be overcome by salinomycin treatment.* 23rd Biennial Congress of the European Association for Cancer Research, Munich, Germany (July 2014).

IX. ACKNOWLEDGEMENTS

First of all I would like to thank Prof. Dr. Ernst Wagner for giving me the opportunity to perform this work in his laboratories under his supervision. Thanks for the professional support over the last years and the trust in both experimental and organizational tasks.

I would like to thank Prof. Dr. Eckhard Wolf for being my veterinary supervisor and for accepting this thesis at the veterinary faculty.

Thanks to Dr. Andreas Roidl for the excellent scientific support and supervision concerning the salinomycin project.

I would also like to thank my collaboration partners concerning the MSN project, Prof. Dr. Thomas Bein and Prof. Dr. Christoph Bräuchle. Furthermore, I would like to thank Stefan Datz and Dr. Stefan Niedermayer for providing me with uncountable samples and Dr. Veronika Weiss for her excellent work on the microscope and patience with numerous slices.

My gratitude goes to Wolfgang Rödl for solving all technical problems in the lab, animal facility and with my PC. Thanks for your support and patience no matter which time of the day.

Thanks a lot to Miriam Höhn for her great scientific support in the lab and also for handling all administrative stuff. I would like to thank Dr. Martina Rüffer for organizing the practical courses and Ursula Biebl and Anna Kulinyak for their work in the lab.

My special thanks go to all colleagues in the animal facility, Dr. Laura Schreiner, Johanna Busse, Dr. Rebekka Kubisch-Dohmen, Dr. Florian Kopp, Dr. Daniel Edinger and Eva Kessel. Thanks for your help, excellent teamwork and a great atmosphere. I would especially like to thank Dr. Petra Kos for the great collaboration during numerous animal experiments. Thanks to Markus Kovac for taking care of the animals and for his support in the animal facility.

I want to thank Ulrich Lächelt, Dongsheng He and Dr. Edith Salcher for synthesizing the polymers.

My gratitude goes to Linda Beckert for an amazing time in our “violent female” office, for discussing scientific and non-scientific problems and for carefully proofreading this thesis. It was great having you as a colleague, stay “breathless” as you use to be!

I would like to express my deepest gratitude to my family. Thank you for your support, encouragement and trust in every period of my life.

Thank you, Tommy, for always being at my side and accepting me as I am. Thank you for supporting my decision to go to Munich.

Last but not least I would like to remind of my dear friend Maarit who suffered from a severe cancer disease just during this work. I admire your incredible strength, your positivity in every situation and your faith. I miss you.